

Automated, Efficient, and Practical Extreme Value Analysis with Environmental Applications

Brian M. Bader, Ph.D.
University of Connecticut, 2022

ABSTRACT

Although the fundamental probabilistic theory of extremes has been well developed, there are many practical considerations that must be addressed in application. The contribution of this thesis is four-fold. The first concerns the choice of r in the r largest order statistics modeling of extremes. Practical concern lies in choosing the value of r ; a larger value necessarily reduces variance of the estimates, however there is a trade-off in that it may also introduce bias. Current model diagnostics are somewhat restrictive, either involving prior knowledge about the domain of the distribution or using visual tools. We propose a pair of formal goodness-of-fit tests, which can be carried out in a sequential manner to select r . A recently developed adjustment for multiplicity in the ordered, sequential setting is applied to provide error control. It is shown via simulation that both tests hold their size and have adequate power to detect deviations from the null model.

The second contribution pertains to threshold selection in the peaks-over-threshold

approach. Existing methods for threshold selection in practice are informal as in visual diagnostics or rules of thumb, computationally expensive, or do not account for the multiple testing issue. We take a methodological approach, modifying existing goodness-of-fit tests combined with appropriate error control for multiplicity to provide an efficient, automated procedure for threshold selection in large scale problems.

The third combines a theoretical and methodological approach to improve estimation within non-stationary regional frequency models of extremal data. Two alternative methods of estimation to maximum likelihood (ML), maximum product spacing (MPS) and a hybrid L-moment / likelihood approach are incorporated in this framework. In addition to having desirable theoretical properties compared to ML, it is shown through simulation that these alternative estimators are more efficient in short record lengths.

The methodology developed is demonstrated with climate based applications. Last, an overview of computational issues for extremes is provided, along with a brief tutorial of the R package `eva`, which improves the functionality of existing extreme value software, as well as contributing new implementations.

Automated, Efficient, and Practical Extreme Value Analysis with Environmental Applications

Brian M. Bader

B.A., Mathematics, Stony Brook University, NY, USA, 2009

M.A., Statistics, Columbia University, NY, USA, 2011

A Dissertation
Submitted in Partial Fulfillment of the
Requirements for the Degree of
Doctor of Philosophy
at the
University of Connecticut

2022

Copyright by

Brian M. Bader

2022

APPROVAL PAGE

Doctor of Philosophy Dissertation

**Automated, Efficient, and Practical Extreme Value
Analysis with Environmental Applications**

Presented by

Brian M. Bader, B.A. Mathematics, M.A. Statistics

Major Advisor

Jun Yan

Associate Advisor

Kun Chen

Associate Advisor

Dipak K. Dey

Associate Advisor

Xuebin Zhang

University of Connecticut

2022

Acknowledgements

“On this life that we call home, the years go fast and the days go so slow.” — Modest Mouse

This is sound advice for anyone considering to pursue a PhD. It’s hard to believe this chapter of my life is coming to an end — the past four years have gone so fast, yet at times I thought it would never come soon enough. It has been full of ups and downs, but at the lowest of times, the only thing to do was continue on. I’ve made many new friends (who will hopefully turn into old), mentors, and gained precious knowledge that I think will benefit me throughout the rest of my life.

I’d like to thank Dr. Ming-Hui Chen for guiding me through the qualifying exam process and allowing me to thrive in the Statistical Consulting Service. I’ve gained valuable experience from participating in this group. I appreciate Dr. Dipak Dey for taking time out of his busy schedule as a dean to give me advice, recommendations, and to be on this committee. The same appreciation goes to Dr. Kun Chen for agreeing to be on my committee. Suggestions by Dr. Vartan Choulakian and Dr. Zhiyi Chi helped improve some of the methodology and data analysis in this research.

Dr. Jun Yan, my major advisor, has guided me throughout the research process and pushed me along to make sure I completed all the necessary milestones in a timely manner. I must admit that I was slightly intimidated of him at first, but I now believe

that he is most likely the best choice of advisor (for me) and I am glad things fell into place as such. He is truly a kind person and has always been understanding of any problems I have had over the past two years. Although I am not pursuing the academic route at the moment, I appreciate his enthusiastic nudge for me to go in that direction.

Additionally, Dr. Xuebin Zhang has graciously spent his time and energy into conversations with myself and Dr. Yan to improve our manuscripts and our knowledge of environmental extremes. Of course I am thankful of the support he and Environment and Climate Change Canada gave by funding some of this research.

The journey would not have been the same with a different cohort — I am grateful to all their support and friendship during such trying times. I have to acknowledge my family for encouraging me to follow my academic pursuits even if it meant not seeing me as often as they'd like during these four years. The same goes for all my friends back home.

Last, but not least, I wouldn't have made it through without the full support of my wife Deirdre and two cats Eva and Cuddlemonkey (who joined our family as a result of all this). I cannot express my total love and gratitude for them in words.

This research was partially supported by an NSF grant (DMS 1521730), a University of Connecticut Research Excellence Program grant, and Environment and Climate Change Canada.

Contents

| | |
|---|------------|
| Acknowledgements | iii |
| 1 Introduction | 1 |
| 1.1 Overview of Extreme Value Analysis | 1 |
| 1.1.1 Block Maxima / GEV_r Distribution | 3 |
| 1.1.2 Peaks Over Threshold (POT) Approach | 6 |
| 1.1.3 Non-stationary Regional Frequency Analysis (RFA) | 8 |
| 1.2 Motivation | 9 |
| 1.2.1 Choice of r in the r Largest Order Statistics Model | 10 |
| 1.2.2 Selection of Threshold in the POT Approach | 12 |
| 1.2.3 Estimation in Non-stationary RFA | 15 |
| 1.3 Outline of Thesis | 16 |
| 2 Automated Selection of r in the r Largest Order Statistics Model | 19 |
| 2.1 Introduction | 19 |
| 2.2 Model and Data Setup | 23 |
| 2.3 Score Test | 24 |
| 2.3.1 Parametric Bootstrap | 26 |
| 2.3.2 Multiplier Bootstrap | 27 |

| | | |
|----------|--|-----------|
| 2.4 | Entropy Difference Test | 29 |
| 2.5 | Simulation Results | 31 |
| 2.5.1 | Size | 31 |
| 2.5.2 | Power | 36 |
| 2.6 | Automated Sequential Testing Procedure | 38 |
| 2.7 | Illustrations | 46 |
| 2.7.1 | Lowestoft Sea Levels | 46 |
| 2.7.2 | Annual Maximum Precipitation: Atlantic City, NJ | 50 |
| 2.8 | Discussion | 52 |
| 3 | Automated Threshold Selection in the POT Approach | 55 |
| 3.1 | Introduction | 55 |
| 3.2 | Automated Sequential Testing Procedure | 60 |
| 3.3 | The Tests | 63 |
| 3.3.1 | Anderson–Darling and Cramér–von Mises Tests | 64 |
| 3.3.2 | Moran’s Test | 66 |
| 3.3.3 | Rao’s Score Test | 68 |
| 3.3.4 | A Power Study | 69 |
| 3.4 | Simulation Study of the Automated Procedures | 71 |
| 3.5 | Application to Return Level Mapping of Extreme Precipitation | 78 |
| 3.6 | Discussion | 83 |

| | | |
|----------|--|------------|
| 4 | Robust and Efficient Estimation in Non-Stationary RFA | 87 |
| 4.1 | Introduction | 87 |
| 4.2 | Non-Stationary Homogeneous Region Model | 91 |
| 4.2.1 | Existing Estimation Methods | 94 |
| 4.3 | New Methods | 96 |
| 4.3.1 | Hybrid Likelihood / L-moment Approach | 96 |
| 4.3.2 | Maximum Product Spacing | 98 |
| 4.4 | Simulation Study | 100 |
| 4.5 | California Annual Daily Maximum Winter Precipitation | 107 |
| 4.6 | Discussion | 114 |
| 5 | An R Package for Extreme Value Analysis: eva | 117 |
| 5.1 | Introduction | 117 |
| 5.2 | Efficient handling of near-zero shape parameter | 119 |
| 5.3 | The GEV_r distribution | 120 |
| 5.3.1 | Goodness-of-fit testing | 121 |
| 5.3.2 | Profile likelihood | 122 |
| 5.3.3 | Fitting the GEV_r distribution | 124 |
| 5.4 | Summary | 130 |
| 6 | Conclusion | 132 |
| 6.1 | Future Work | 135 |

| | | |
|----------|--|------------|
| A | Appendix | 139 |
| A.1 | Data Generation from the GEV_r Distribution | 139 |
| A.2 | Asymptotic Distribution of $T_n^{(r)}(\theta)$ | 141 |
| A.3 | Semi-Parametric Bootstrap Resampling in RFA | 143 |
| | Bibliography | 144 |

List of Tables

| | | |
|-----|---|----|
| 2.1 | Empirical size (in %) for the parametric bootstrap score test under the null distribution GEV_r , with $\mu = 0$ and $\sigma = 1$ based on 1000 samples, each with bootstrap sample size $L = 1000$ | 33 |
| 2.2 | Empirical size (in %) for multiplier bootstrap score test under the null distribution GEV_r , with $\mu = 0$ and $\sigma = 1$. 1000 samples, each with bootstrap sample size $L = 1000$ were used. Although not shown, the empirical size for $r = 1$ and $\xi = -0.25$ becomes acceptable when sample size is 1000. | 34 |
| 2.3 | Empirical size (in %) for the entropy difference (ED) test under the null distribution GEV_r , with $\mu = 0$ and $\sigma = 1$ based on 10,000 samples. . . . | 35 |
| 2.4 | Empirical rejection rate (in %) of the multiplier score test and the ED test in the first data generating scheme in Section 2.5.2 from 1000 replicates. | 37 |
| 2.5 | Empirical rejection rate (in %) of the multiplier score test and the ED test in the second data generating scheme in Section 2.5.2 from 1000 replicates. | 38 |

| | | |
|-----|---|-----|
| 2.6 | Percentage of choice of r using the ForwardStop and StrongStop rules at various significance levels or FDRs, under ED, parametric bootstrap (PB) score, and multiplier bootstrap (MB) score tests, with $n = 100$ and $\xi = 0.25$ for the simulation setting described in Section 2.6. Correct choice is $r = 4$ | 45 |
| 3.1 | Empirical rejection rates of four goodness-of-fit tests for GPD under various data generation schemes described in Section 3.3.4 with nominal size 0.05. GPDMix(a, b) refers to a 50/50 mixture of GPD(1, a) and GPD(1, b). | 70 |
| 4.1 | Failure rate (%) in optimization for the three estimation methods in the combined 12 settings of number of sites, observations, and dependence levels within each spatial dependence structure (SC, SM, and GC) out of 10,000 replicates. The setup is described in detail in Section 4.4. | 103 |

List of Figures

| | | |
|-----|--|----|
| 1.1 | The density function of the Generalized Extreme Value distribution for shape parameter values of -0.5 , 0 , and 0.5 with location and scale parameters fixed at zero and one, respectively. | 5 |
| 1.2 | A comparison of extremes selected via the peaks over threshold (left) versus block maxima approach for example time series data. | 6 |
| 1.3 | Mean Residual Life plot of Fort Collins daily precipitation data found in R package extRemes | 13 |
| 1.4 | Threshold stability plot for the shape parameter of the Fort Collins daily precipitation data found in R package extRemes | 14 |
| 1.5 | Hill plot of the Fort Collins daily precipitation data found in R package extRemes | 14 |
| 2.1 | Comparisons of the empirical vs. $\chi^2(3)$ distribution (solid curve) based on 5000 replicates of the score test statistic under the null GEV_r distribution. The number of blocks used is $n = 5000$ with parameters $\mu = 0$, $\sigma = 1$, and $\xi \in (-0.25, 0.25)$ | 26 |

- 2.2 Observed FWER for the ED, parametric bootstrap (PB) score, and multiplier bootstrap (MB) score tests (using No Adjustment and StrongStop) versus expected FWER at various nominal levels. The 45 degree line indicates agreement between the observed and expected rates under H_0 42
- 2.3 Observed FDR (from ForwardStop) and observed FWER (from StrongStop) versus expected FDR and FWER, respectively, at various nominal levels. This is for the simulation setting described in Section 2.6, using the ED, parametric bootstrap (PB) score, and multiplier bootstrap (MB) score tests. The 45 degree line indicates agreement between the observed and expected rates. 43
- 2.4 Adjusted p-values using ForwardStop, StrongStop, and raw (unadjusted) p-values for the ED and PB Score tests applied to the Lowestoft sea level data. The horizontal dashed line represents the 0.05 possible cutoff value. 48
- 2.5 Location, scale, and shape parameter estimates, with 95% delta confidence intervals for $r = 1, \dots, 40$ for the Lowestoft sea level data. Also included are the estimates and 95% profile likelihood confidence intervals for the 50, 100, and 200 year return levels. The vertical dashed line represents the recommended cutoff value of r from the analysis in Section 2.7.1. 49

| | | |
|-----|---|----|
| 2.6 | Adjusted p-values using ForwardStop, StrongStop, and raw (unadjusted) p-values for the ED and PB Score tests applied to the Atlantic City precipitation data. The horizontal dashed line represents the 0.05 possible cutoff value. | 51 |
| 2.7 | Location, scale, and shape parameter estimates, with 95% delta confidence intervals for $r = 1$ through $r = 10$ for the Atlantic City precipitation data. Also included are the estimates and 95% profile likelihood confidence intervals for the 50, 100, and 200 year return levels. The vertical dashed line represents the recommended cutoff value of r from the analysis in Section 2.7.2. | 52 |
| 3.1 | Observed FWER for the Anderson–Darling test (using StrongStop and no adjustment) versus expected FWER at various nominal levels under the null GPD at ten thresholds for 10,000 replicates in each setting as described in Section 3.4. The 45 degree line indicates agreement between the observed and expected rates under H_0 | 72 |
| 3.2 | Plot of the (scaled) density of the mixture distribution used to generate misspecification of H_0 for the simulation in Section 3.4. The vertical line indicates the continuity point of the two underlying distributions. | 73 |

| | | |
|-----|--|----|
| 3.3 | Frequency distribution (out of 1000 simulations) of the number of rejections for the Anderson–Darling test and various stopping rules (ForwardStop, StrongStop, and no adjustment), at the 5% nominal level, for the misspecified distribution sequential simulation setting described in Section 3.4. 50 thresholds are tested, with the 34th being the true threshold. | 75 |
| 3.4 | Observed FDR (using ForwardStop) and observed FWER (using StrongStop) versus expected FDR and FWER respectively using the Anderson–Darling test, at various nominal levels. This is for the sequential simulation setting under misspecification described in Section 3.4. The 45 degree line indicates agreement between the observed and expected rates. | 76 |
| 3.5 | Average performance comparison of the three stopping rules in the simulation study under misspecification in Section 3.4, using the Anderson–Darling test for various parameters. Shown are the relative frequencies of the average value of each metric (bias, squared error, and coverage) for each stopping rule and parameter of interest. For each parameter of interest and metric, the sum of average values for the three stopping rules equates to 100%. RL refers to return level. | 77 |
| 3.6 | Distribution of chosen percentiles (thresholds) for the 720 western US coastal sites, as selected by each stopping rule. Note that this does not include sites where all thresholds were rejected by the stopping rule. . . . | 81 |

| | | |
|-----|--|-----|
| 3.7 | Map of US west coast sites for which all thresholds were rejected (black / circle) and for which a threshold was selected (grey / triangle), by stopping rule. | 82 |
| 3.8 | Comparison of return level estimates (50, 100, 250, 500 year) based on the chosen threshold for ForwardStop vs. StrongStop for the US west coast sites. The 45 degree line indicates agreement between the two estimates. This is only for the sites in which both stopping rules did not reject all thresholds. | 83 |
| 3.9 | Map of US west coast sites with 50, 100, and 250 year return level estimates for the threshold chosen using ForwardStop and the Anderson–Darling test. This is only for the sites in which a threshold was selected. | 84 |
| 4.1 | Schlather model root mean squared error of the parameters for each estimation method, from 1000 replicates of each setting discussed in Section 4.4. W, M, S refers to weak, medium, and strong dependence, with m being the number of sites and n , the number of observations within each site. | 104 |
| 4.2 | Smith model root mean squared error of the parameters for each estimation method, from 1000 replicates of each setting discussed in Section 4.4. W, M, S refers to weak, medium, and strong dependence, with m being the number of sites and n , the number of observations within each site. . | 105 |

| | | |
|-----|--|-----|
| 4.3 | Gaussian copula model root mean squared error of the parameters for each estimation method, from 1000 replicates of each setting discussed in Section 4.4. W, M, S refers to weak, medium, and strong dependence, with m being the number of sites and n , the number of observations within each site. | 106 |
| 4.4 | Locations of the 27 California sites used in the non-stationary regional frequency analysis of annual daily maximum winter precipitation events. | 108 |
| 4.5 | Scatterplot of Spearman correlations by euclidean distance between each pair of the 27 California sites used in the non-stationary regional frequency analysis of annual daily maximum winter precipitation events. | 109 |
| 4.6 | Estimates and 95% semi-parametric bootstrap confidence intervals of the location parameter covariates (positive and negative SOI piecewise terms), proportionality, and shape parameters for the three methods of estimation in the non-stationary RFA of the 27 California site annual winter maximum precipitation events. | 110 |
| 4.7 | Estimates and 95% semi-parametric bootstrap confidence intervals of the marginal site-specific location means for the three estimation methods in the non-stationary RFA of the 27 California site annual winter maximum precipitation events. | 111 |

| | | |
|-----|--|-----|
| 4.8 | Estimates and 95% semi-parametric bootstrap confidence intervals of the shape parameter by the three estimation methods, for the full 53 year and 18 year subset sample of California annual winter precipitation extremes. The horizontal dashed line corresponds to the shape parameter estimate of each method for the subset sample. | 112 |
| 4.9 | Left: 50 year return level estimates (using MPS) at the 27 sites, conditioned on the mean sample SOI value (-0.40). Right: Estimated percent increase in magnitude of the 50 year event at the sample minimum SOI (-28.30) versus the mean SOI value. | 113 |
| 5.1 | Plot of GEV cumulative distribution function with $x = 1$, $\mu = 0$ and $\sigma = 1$, with ξ ranging from -0.0001 to 0.0001 on the cubic scale. The naive implementation is represented by the solid red line, with the implementation in R package <code>eva</code> as the dashed blue line. | 121 |
| 5.2 | Estimates and 95% profile likelihood confidence intervals for the 250 year return level of the LoweStoft sea level dataset, for $r = 1$ through $r = 10$. | 123 |
| 5.3 | Estimates and 95% delta method confidence intervals for the 250 year return level of the LoweStoft sea level dataset, for $r = 1$ through $r = 10$. | 124 |

| | | |
|-----|--|-----|
| 5.4 | Plot of the largest order statistic (block maxima) from a GEV_{10} distribution with shape parameter parameter $\xi = 0$. The location and scale have an intercept of 100 and 1, with positive trends of 0.02 and 0.01, respectively. The indices (1 to 100) are used as the corresponding trend coefficients. | 126 |
|-----|--|-----|

Chapter 1

Introduction

1.1 Overview of Extreme Value Analysis

Both statistical modeling and theoretical results of extremes remain a subject of active research. Extreme value theory provides a solid statistical framework to handle atypical, or heavy-tailed phenomena. There are many important applications that require modeling of extreme events. In hydrology, a government or developer may want an estimate of the maximum flood event that is expected to occur every 100 years, say, in order to determine the needs of a structure. In climatology, extreme value theory is used to determine if the magnitude of extremal events are time-dependent or not. Similarly, in finance, market risk assessment can be approached from an extremes standpoint. See Coles (2001); Tsay (2005); Dey and Yan (2016) for more specific examples.

Further, the study of extremes in a spatial context has been an area of interest for many researchers. In an environmental setting, one may want to know if certain geographic and/or climate features have an effect on extremes of precipitation, temperature, wave height, etc. Recently, many explicit models for spatial extremes have been developed. For an overview, see Davison, Padoan, Ribatet, et al. (2012). Another approach in

the same context, regional frequency analysis (RFA), allows one to ‘trade space for time’ in order to improve the efficiency of certain parameter estimates. Roughly speaking, after estimating site-specific parameters, data are transformed onto the same scale and pooled in order to estimate the shared parameters. This approach offers two particular advantages over fully-specified multivariate models. First, only the marginal distributions at each site need to be explicitly chosen – the dependence between sites can be handled by appropriate semi-parametric procedures and second, it can handle very short record lengths. See Hosking and Wallis (2005) or Wang, Yan, and Zhang (2014) for a thorough review.

A major quantity of interest in extremes is the t -period return level. This can be thought of as the maximum event that will occur on average every t periods and can be used in various applications such as value at risk in finance and flood zone predictions. Thus, it is quite important to obtain accurate estimates of this quantity and in some cases, determine if it is non-stationary. Given some specified extremal distribution, the stationary t -period return level z_t can be expressed in terms of its upper quantile

$$z_t = Q(1 - 1/t)$$

where $Q(p)$ is the quantile function of this distribution.

Within the extreme value framework, there are several different approaches to modeling extremes. In the following, the various approaches will be discussed and a data

example of extreme daily precipitation events in California is used to motivate the content of this thesis.

1.1.1 Block Maxima / GEV_r Distribution

The block maxima approach to extremes involves splitting the data into mutually exclusive blocks and selecting the top order statistic from within each block. Typically blocks can be chosen naturally; for example, for daily precipitation data over n years, a possible block size B could be $B = 365$, with the block maxima referring to the largest annual daily precipitation event. To clarify ideas, here the underlying data is of size $365 \times n$ and the sample of extremes is size n , the number of available blocks. There is a requirement that the block size be ‘large enough’ to ensure adequate convergence in the limiting distribution of the block maxima; further discussion of this topic will be delegated to later sections.

It has been shown (e.g. Leadbetter, Lindgren, and Rootzén, 2012; De Haan and Ferreira, 2007; Coles, 2001) that the only non-degenerate limiting distribution of the block maxima of a sample of size B i.i.d. random variables, when appropriately normalized and as $B \rightarrow \infty$, must be the Generalized Extreme Value (GEV) distribution. The GEV distribution has cumulative distribution function given by

$$F(y|\mu, \sigma, \xi) = \begin{cases} \exp \left[- \left(1 + \xi \frac{y-\mu}{\sigma} \right)^{-\frac{1}{\xi}} \right], & \xi \neq 0, \\ \exp \left[- \exp \left(- \frac{y-\mu}{\sigma} \right) \right], & \xi = 0, \end{cases} \quad (1.1)$$

with location parameter μ , scale parameter $\sigma > 0$, shape parameter ξ , and $1 + \xi(y - \mu)/\sigma > 0$. By taking the first derivative with respect to y the probability density function is obtained as

$$f(y|\mu, \sigma, \xi) = \begin{cases} \frac{1}{\sigma} \left(1 + \xi \frac{y-\mu}{\sigma}\right)^{-(\frac{1}{\xi}+1)} \exp \left[- \left(1 + \xi \frac{y-\mu}{\sigma}\right)^{-\frac{1}{\xi}} \right], & \xi \neq 0, \\ \frac{1}{\sigma} \exp \left(- \frac{y-\mu}{\sigma} \right) \exp \left[- \exp \left(- \frac{y-\mu}{\sigma} \right) \right], & \xi = 0. \end{cases} \quad (1.2)$$

Denote this distribution as $\text{GEV}(\mu, \sigma, \xi)$. The shape parameter ξ controls the tail of the distribution. When $\xi > 0$, the GEV distribution has a heavy, unbounded upper tail. When $\xi = 0$, this is commonly referred to as the Gumbel distribution and has a lighter tail. Figure 1.1 shows the GEV density for various shape parameter values.

Weissman (1978) generalized this result further, showing that the limiting joint distribution of the r largest order statistics of a random sample of size B as $B \rightarrow \infty$ (denoted here as the GEV_r distribution) has probability density function

$$f_r(y_1, y_2, \dots, y_r|\mu, \sigma, \xi) = \sigma^{-r} \exp \left\{ - (1 + \xi z_r)^{-\frac{1}{\xi}} - \left(\frac{1}{\xi} + 1 \right) \sum_{j=1}^r \log(1 + \xi z_j) \right\} \quad (1.3)$$

for location parameter μ , scale parameter $\sigma > 0$ and shape parameter ξ , where $y_1 > \dots > y_r$, $z_j = (y_j - \mu)/\sigma$, and $1 + \xi z_j > 0$ for $j = 1, \dots, r$. The joint distribution for $\xi = 0$ can be found by taking the limit $\xi \rightarrow 0$ in conjunction with the Dominated Convergence Theorem and the shape parameter controls the tails of this distribution as discussed in the univariate GEV case. When $r = 1$, this distribution is exactly the GEV

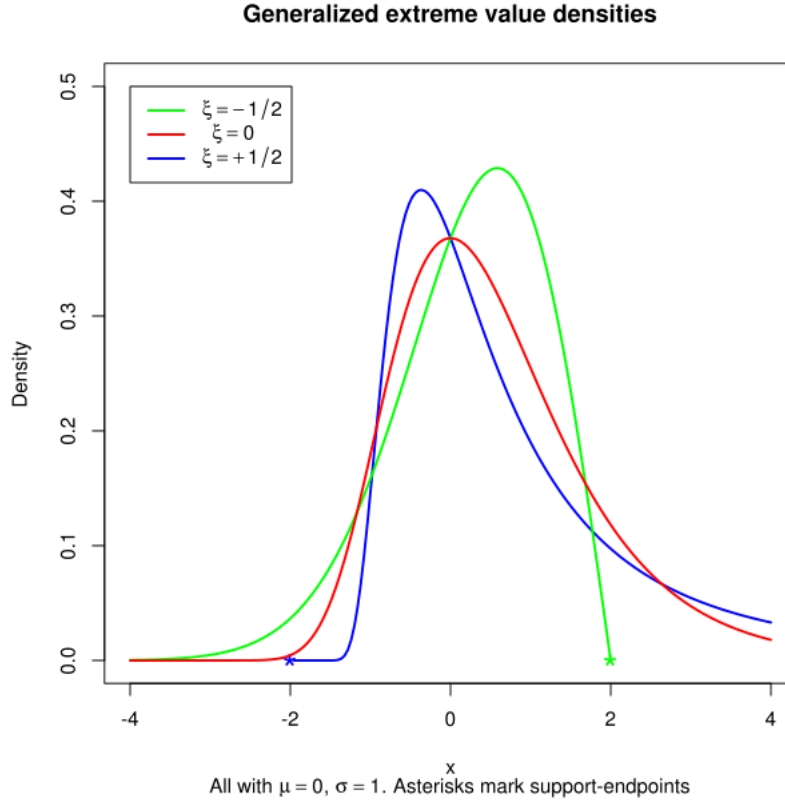


Figure 1.1: The density function of the Generalized Extreme Value distribution for shape parameter values of -0.5 , 0 , and 0.5 with location and scale parameters fixed at zero and one, respectively.

distribution. The parameters $\theta = (\mu, \sigma, \xi)^\top$ remain the same for $j = 1, \dots, r$, $r \ll B$, but the convergence rate to the limit distribution reduces sharply as r increases. The conditional distribution of the r th component given the top $r - 1$ variables in (1.3) is the GEV distribution right truncated by y_{r-1} , which facilitates simulation from the GEV_r distribution; see Appendix A.1.

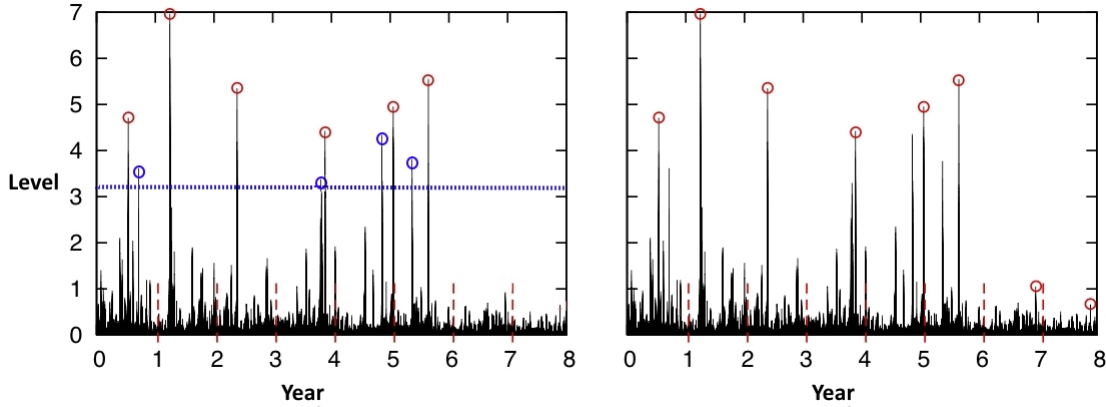


Figure 1.2: A comparison of extremes selected via the peaks over threshold (left) versus block maxima approach for example time series data.

1.1.2 Peaks Over Threshold (POT) Approach

Another approach to modeling extremes is the peaks over threshold method (POT). Instead of breaking up the underlying data into blocks and extracting the top observations from each block, POT sets some high threshold and uses only the observations above the threshold. Thus, POT is only concerned with the relevant observations, regardless of temporal ordering. Figure 1.2 displays the differences between the POT and block maxima approaches.

Extreme value theory (McNeil and Saladin, 1997) says that given a suitably high threshold, data above the threshold will follow the Generalized Pareto (GPD) distribution. Under general regularity conditions, the only possible non-degenerate limiting distribution of properly rescaled exceedances of a threshold u is the GPD as $u \rightarrow \infty$ (e.g.,

Pickands, 1975). The GPD has cumulative distribution function

$$F(y|\theta) = \begin{cases} 1 - \left[1 + \frac{\xi y}{\sigma_u}\right]^{-1/\xi} & \xi \neq 0, \quad y > 0, \quad 1 + \frac{\xi y}{\sigma_u} > 0, \\ 1 - \exp\left[-\frac{y}{\sigma_u}\right] & \xi = 0, \quad y > 0, \end{cases} \quad (1.4)$$

where $\theta = (\sigma_u, \xi)$, ξ is a shape parameter, and $\sigma_u > 0$ is a threshold-dependent scale parameter. The GPD also has the property that for some threshold $v > u$, the excesses follow a GPD with the same shape parameter, but a modified scale $\sigma_v = \sigma_u + \xi(v - u)$. Let X_1, \dots, X_n be a random sample of size n . If u is sufficiently high, the exceedances $Y_i = X_i - u$ for all i such that $X_i > u$ are approximately a random sample from a GPD.

The GPD has the probability density function given by

$$f(y|\sigma_u, \xi) = \begin{cases} \frac{1}{\sigma_u} \left[1 + \frac{\xi y}{\sigma_u}\right]^{-(\frac{1}{\xi}+1)}, & \xi \neq 0, \\ \frac{1}{\sigma_u} \exp\left[-\frac{y}{\sigma_u}\right], & \xi = 0. \end{cases} \quad (1.5)$$

defined on $y \geq 0$ when $\xi \geq 0$ and $0 \leq y \leq -\sigma_u/\xi$ when $\xi < 0$.

Both the block or threshold approach are justified in theory, but choice in application depends on the context or availability of data. For instance, it may be the case that only the block maxima or top order statistics from each period are available. The block maxima / r largest approach provides a natural framework in which to retain temporal structure, while the POT requires additional care. This may be important if interest is in modeling non-stationary extremes. Ferreira, de Haan, et al. (2015) provide an

overview of practical considerations when choosing between the two methods.

1.1.3 Non-stationary Regional Frequency Analysis (RFA)

Regional frequency analysis (RFA) is commonly used when historical records are short, but observations are available at multiple sites within a homogeneous region. A common difficulty with extremes is that, by definition, data is uncommon and thus short record length may make the estimation of parameters questionable. Regional frequency analysis resolves this problem by ‘trading space for time’; data from several sites are used in estimating event frequencies at any one site (Hosking and Wallis, 2005). Essentially, certain parameters are assumed to be shared across sites, which increases the efficiency in estimation of those parameters.

In RFA, only the marginal distribution at each location needs to be specified. To set ideas, assume a region consists of m sites over n periods. Thus, observation t at site s can be denoted as Y_{st} . A common assumption is that data within each site are independent between periods; however, within each period t , it is typically the case that there is correlation between sites. For example, sites within close geographic distance cannot have events assumed to be independent. Fully specified multivariate models generally require this dependence structure to be explicitly defined and it is clear that the dependence cannot be ignored. As noted by authors Stedinger (1983) and Hosking and Wallis (1988), intersite dependence can have a dramatic effect on the variance of these estimators.

There are a number of techniques available to adjust the estimator variances accordingly without directly specifying the dependence structure. Some examples are combined score equations (Wang, 2015), pairwise likelihood (Wang et al., 2014; Shang, Yan, Zhang, et al., 2015), semi-parametric bootstrap (Heffernan and Tawn, 2004), and composite likelihood (Chandler and Bate, 2007).

1.2 Motivation

This thesis focuses on developing sound statistical methodology and theory to address practical concerns in extreme value applications. A common theme across the various methods developed here is automation, efficiency, and utility. There is a wide literature available of theoretical results and although recently the statistical modeling of extremes in application has gained in popularity, there are still methodological improvements that can be made. One of the major complications when modeling extremes in practice is deciding “what is extreme?”. The block maxima approach simplifies this idea somewhat, but for the POT approach, the threshold must be chosen. Similarly, if one wants to use the r largest order statistics from each block (to improve efficiency of the estimates), how is r chosen? Again, most of the current approaches do not address all three aspects mentioned earlier - automation, efficiency, and utility. For example, visual diagnostics cannot be easily automated, while certain resampling approaches are not scalable (efficiency), and many of the existing theoretical results may require some prior knowledge

about the domain of attraction of the limiting distribution and/or require computational methods in finite samples.

As data continues to grow, there is a need for automation and efficiency / scalability. Climate summaries are currently available for tens of thousands of surface sites around the world via the Global Historical Climatology Network (GHCN) (Menne, Durre, Vose, Gleason, and Houston, 2012), ranging in length from 175 years to just hours. Other sources of large scale climate information are the National Oceanic and Atmospheric Administration (NOAA), United States Geological Survey (USGS), National Centers for Environmental Information (NCEI), Environment and Climate Change Canada, etc.

One particular motivating example is creating a return level map of extreme precipitation for sites across the western United States. Climate researchers may want to know how return levels of extreme precipitation vary across a geographical region and if these levels are affected by some external force such as the El Niño–Southern Oscillation (ENSO). In California alone, there are over 2,500 stations with some daily precipitation records available. Either using a jointly estimated model such as regional frequency analysis or analyzing data site-wise, appropriate methods are needed to accommodate modeling a large number of sites.

1.2.1 Choice of r in the r Largest Order Statistics Model

While the theoretical framework of extreme value theory is sound, there are many practical problems that arise in applications. One such issue is the choice of r in the GEV_r

distribution. Since r is not explicitly a parameter in the distribution (1.3), the usual model selection techniques (i.e. likelihood-ratio testing, AIC, BIC) are not available. A bias-variance trade-off exists when selecting r . As r increases, the variance decreases because more data is used, but if r is chosen too high such that the approximation of the data to the GEV_r distribution no longer holds, bias may occur. It has been shown that the POT method is more efficient than block maxima in small samples (Caires, 2009) and thus it is often recommended to use that method over block maxima.

It appears that in application, the GEV_r distribution is often not considered because of the issues surrounding the selection of r and that simply using the block maxima or POT approach are more straightforward. To the author's knowledge, no comparison between efficiency of the GEV_r distribution and POT method has been carried out in finite samples. In practice (An and Pandey, 2007; Smith, 1986) the recommendation for the choice of r is sometimes based on the amount of reduction in standard errors of the estimates.

Smith (1986) and Tawn (1988) used probability plots for the marginal distributions of the r th order statistic to assess goodness of fit. Note that this can only diagnose poor model fit at the marginal level – it does not consider the full joint distribution. Tawn (1988) suggested an alternative test of fit using a spacings result in Weissman (1978), however this requires prior knowledge about the domain of attraction of the limiting distribution. These issues become even more apparent when it is desired to fit the GEV_r distribution to more than just one sample. This is carried out for 30 stations

in the Province of Ontario on extreme wind speeds (An and Pandey, 2007) but the value of $r = 5$ is fixed across all sites.

1.2.2 Selection of Threshold in the POT Approach

A similar, but distinct problem is threshold selection when modeling with the Generalized Pareto distribution. In practice, the threshold must be chosen, yet it cannot be chosen using traditional model selection tests since it is not a parameter in the distribution. This has been studied thoroughly in the literature. Various graphical procedures exist. The mean residual life (MRL) plot, introduced by Davison and Smith (1990) uses the expectation of GPD excesses; for $v > u$, $E[X - v | X > v]$ is linear in v when the GPD fits the data above u . The idea is to choose the smallest value of u such that the plot is linear above this point. The Hill estimator (Hill, 1975) for the tail index ξ is based on a sum of the log spacings of the top $k + 1$ order statistics. Drees, De Haan, and Resnick (2000) discuss the Hill plot, which plots the Hill estimator against the top k order statistics. The value of k is chosen as the largest (i.e. lowest threshold) such that the Hill estimator has become stable. A similar figure, referred to as the threshold stability plot, compares the estimates of the GPD parameters at various thresholds and the idea is to choose a threshold such that the parameters at this threshold and higher are stable.

It is clear that visual diagnostics cannot be scaled effectively. Even in the one sample case can be quite difficult to interpret, with the Hill plot being referred to as the ‘Hill

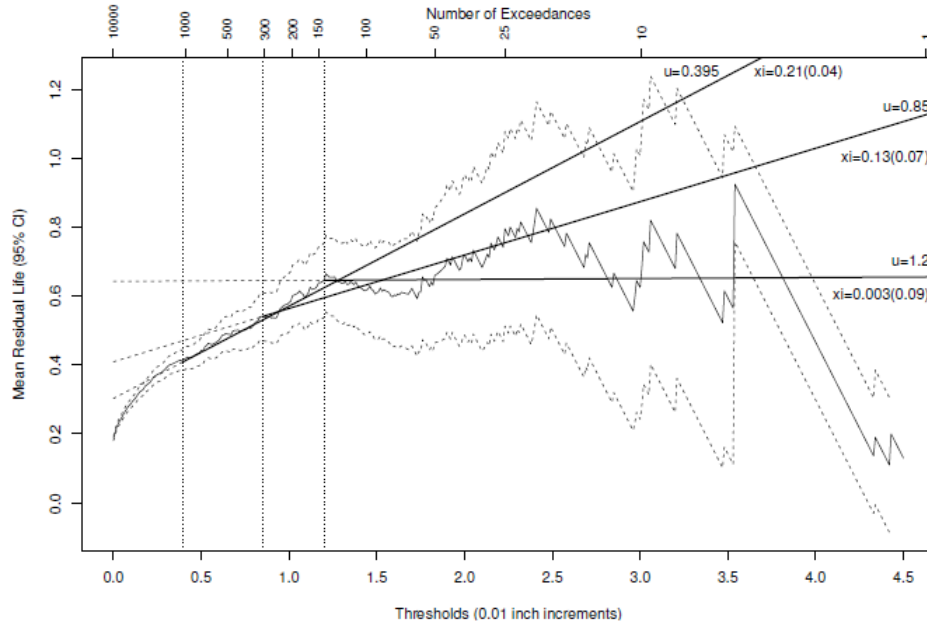


Figure 1.3: Mean Residual Life plot of Fort Collins daily precipitation data found in R package `extRemes`.

Horror Plot’. Figures 1.3, 1.4, and 1.5 are examples of the mentioned plots applied to the Fort Collins daily precipitation data in R package `extRemes` (Gilleland and Katz, 2011a).

Some practitioners suggest various ‘rules of thumb’, which involve selecting the threshold based on some predetermined fraction of the data or it can involve complicated resampling techniques. There is also the idea of using a mixture distribution, which involves specifying a ‘bulk’ distribution for the data below the threshold and using the GPD to model data above the threshold. In this way, the threshold can be explicitly modeled as a parameter. There are some drawbacks to this approach however – the ‘bulk’ distribution must be specified, and care is needed to ensure that the two densities

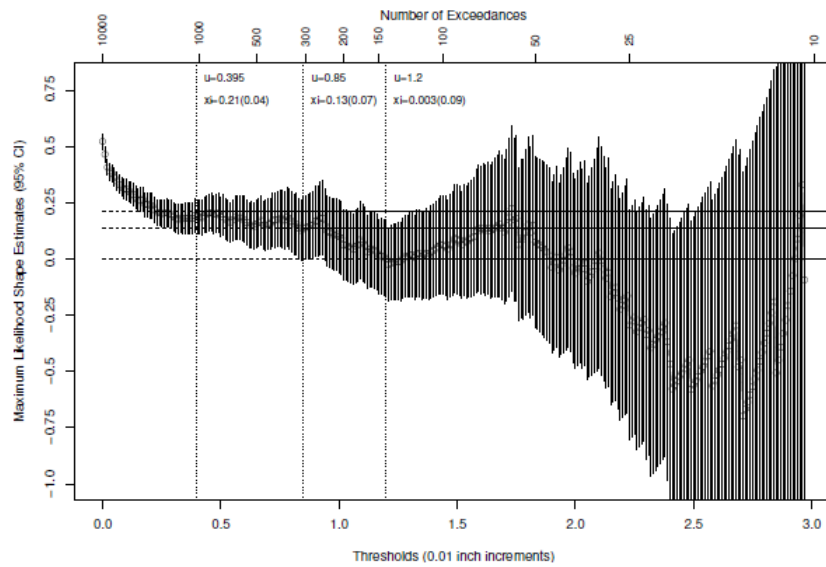


Figure 1.4: Threshold stability plot for the shape parameter of the Fort Collins daily precipitation data found in R package `extRemes`.

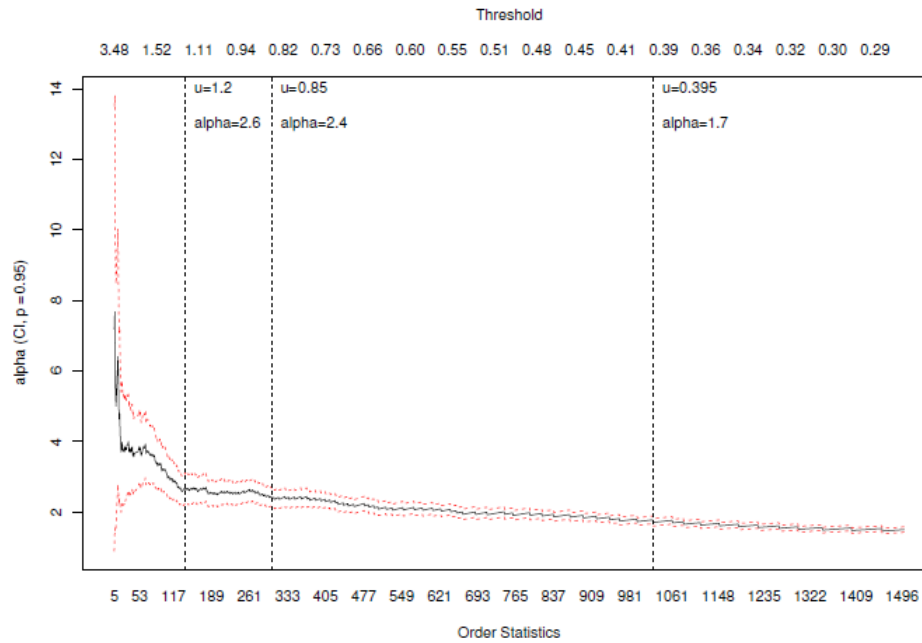


Figure 1.5: Hill plot of the Fort Collins daily precipitation data found in R package `extRemes`.

are continuous at the threshold point u_0 .

Goodness-of-fit testing can be used for threshold selection. A set of candidate thresholds $u_1 < \dots < u_l$ can be tested sequentially for goodness-of-fit to the GPD. The goal is to select a smaller threshold in order to reduce variance of the estimates, but not too low as to introduce bias. Various authors have developed methodology to perform such testing, but they do not consider the multiple testing issue, or it can be computational intensive to perform. For a more thorough and detailed review of the approaches discussed in this section, see Scarrott and MacDonald (2012) and section 3.1.

1.2.3 Estimation in Non-stationary RFA

Unless otherwise noted, going forward the assumption is that the marginal distribution used in fitting a regional frequency model is the GEV or block maxima method. It is well known that due to the non-regular shape of the likelihood function, the MLE may not exist when the shape parameter of the GEV distribution, $\xi < -0.5$ (Smith, 1985). This can cause estimation and/or optimization issues, especially in situations where the record length is short. Even so, maximum likelihood is widely popular and relatively straightforward to implement. As an alternative, in the stationary RFA case, one can use L-moments (Hosking, 1990) to estimate the parameters in RFA. L-moments has the advantage over MLE in that it only requires the existence of the mean, and has been shown to be more efficient in small samples (Hosking, Wallis, and Wood, 1985). However, for non-stationary RFA, it is not straightforward to incorporate covariates

using L-moments, and generally MLE is used – see (Katz, Parlange, and Naveau, 2002; López and Francés, 2013; Hanel, Buishand, and Ferro, 2009; Leclerc and Ouarda, 2007; Nadarajah, 2005) as examples.

One approach to estimate time trends is by applying the stationary L-moment approach over sliding time windows (Kharin and Zwiers, 2005; Kharin, Zwiers, Zhang, and Wehner, 2013); that is, estimate the stationary parameters in (mutually exclusive) periods and study the change in parameters. This is not a precise method, as it is hard to quantify whether change is significant or due to random variation. In the one sample case, there has been some progress to combine non-stationarity and L-moment estimation. Ribereau, Guillou, and Naveau (2008) provide a method to incorporate covariates in the location parameter, by estimating the covariates first via least squares, and then transforming the data to be stationary in order to estimate the remaining parameters via L-moments. Coles and Dixon (1999) briefly discuss an iterative procedure to estimate covariates through maximum likelihood and stationary parameters through L-moments. However, these approaches only consider non-stationarity in the location parameter and it may be of interest to perform linear modeling of the scale and shape parameters.

1.3 Outline of Thesis

The rest of this thesis is as follows. Chapter 2 builds on the discussion in Section 1.2.1, developing two goodness-of-fit tests for selection of r in the r largest order statistics

model. The first is a score test, which requires approximating the null distribution via a parametric or multiplier bootstrap approach. Second, named the entropy difference test, uses the expected difference between log-likelihood of the distributions of the r and $r - 1$ top order statistics to produce an asymptotic test based on normality. The tests are studied for their power and size, and newly developed error control methods for order, sequential testing is applied. The utility of the tests are shown via applications to extreme sea level and precipitation datasets.

Chapter 3 tackles the problem of threshold selection in the peaks over threshold model, discussed in Section 1.2.2. A goodness-of-fit testing approach is used, with an emphasis on automation and efficiency. Existing tests are studied and it is found that the Anderson–Darling has the most power in various scenarios testing a single, fixed threshold. The same error control method discussed in Section 2.6 can be adapted here to control for multiplicity in testing ordered, sequential thresholds for goodness-of-fit. Although the asymptotic null distribution of the Anderson–Darling testing statistic for the GPD has been derived (Choulakian and Stephens, 2001), it requires solving an integral equation. We develop a method to obtain approximate p-values in a computationally efficient manner. The test, combined with error control for the false discovery rate, is shown via a large scale simulation study to outperform familywise and no error controls. The methodology is applied to obtain a return level map of extreme precipitation of at hundreds of sites in the western United States.

When analyzing climate extremes at many sites, it may be desired to combine information across sites to increase efficiency of the estimates, for example, using a regional frequency model. In addition, one may want to incorporate non-stationarity. Currently, the only estimation methods available in this framework may have drawbacks in certain cases, as discussed in Section 1.2.3. In Chapter 4, we introduce two alternative methods of estimation in non-stationary RFA, that have advantageous theoretical properties when compared to current estimation methods such as MLE. It is shown via simulation of spatial extremes with extremal and non-extremal dependence that the two new estimation methods empirically outperform MLE. A non-stationary regional frequency flood-index model is fit to annual maximum daily winter precipitation events at 27 locations in California, with an interest in modeling the effect of the El Niño–Southern Oscillation Index on these events.

Chapter 5 provides a brief tutorial to the companion software package `eva`, which implements the majority of the methodology developed here. It provides new implementations of certain techniques, such as maximum product spacing estimation, and data generation and density estimation for the GEV_r distribution. Additionally, it improves on existing implementations of extreme value analysis, particularly numerical handling of the near-zero shape parameter, profile likelihood, and user-friendly model fitting for univariate extremes. Lastly, a discussion of this body of work, and possible future direction follows in Chapter 6.

Chapter 2

Automated Selection of r in the r Largest Order Statistics Model

2.1 Introduction

The largest order statistics approach is an extension of the block maxima approach that is often used in extreme value modeling. The focus of this chapter is (Smith, 1986, p.28–29): “Suppose we are given, not just the maximum value for each year, but the largest ten (say) values. How might we use this data to obtain better estimates than could be made just with annual maxima?” The r largest order statistics approach may use more information than just the block maxima in extreme value analysis, and is widely used in practice when such data are available for each block. The approach is based on the limiting distribution of the r largest order statistics which extends the generalized extreme value (GEV) distribution (e.g., Weissman, 1978). This distribution, given in (1.3) and denoted as GEV_r , has the same parameters as the GEV distribution, which makes it useful to estimate the GEV parameters when the r largest values are available for each

block. The approach was investigated by Smith (1986) for the limiting joint Gumbel distribution and extended to the more general limiting joint GEV_r distribution by Tawn (1988). Because of the potential gain in efficiency relative to the block maxima only, the method has found many applications such as corrosion engineering (e.g., Scarf and Laycock, 1996), hydrology (e.g., Dupuis, 1997), coastal engineering (e.g., Guedes Soares and Scotto, 2004), and wind engineering (e.g., An and Pandey, 2007).

In practice, the choice of r is a critical issue in extreme value analysis with the r largest order statistics approach. In general r needs to be small relative to the block size B (not the number of blocks n) because as r increases, the rate of convergence to the limiting joint distribution decreases sharply (Smith, 1986). There is a trade-off between the validity of the limiting result and the amount of information required for good estimation. If r is too large, bias can occur; if too small, the variance of the estimator can be high. Finding the optimal r should lead to more efficient estimates of the GEV parameters without introducing bias. Our focus here is the selection of r for situations where a number of largest values are available each of n blocks. In contrast, the methods for threshold or fraction selection reviewed in Scarrott and MacDonald (2012) deal with a single block ($n = 1$) of a large size B .

The selection of r has not been as actively researched as the threshold selection problem in the one sample case. Smith (1986) and Tawn (1988) used probability (also known as PP) plots for the marginal distribution of the r th order statistic to assess its goodness of fit. The probability plot provides a visual diagnosis, but different viewers

may reach different conclusions in the absence of a p-value. Further, the probability plot is only checking the marginal distribution for a specific r as opposed to the joint distribution. Tawn (1988) suggested an alternative test of fit using a spacings results in Weissman (1978). Let D_i be the spacing between the i th and $(i + 1)$ th largest value in a sample of size B from a distribution in the domain of attraction of the Gumbel distribution. Then $\{iD_i : i = 1, \dots, r - 1\}$ is approximately a set of independent and identically distributed exponential random variables as $B \rightarrow \infty$. The connections among the three limiting forms of the GEV distribution (e.g., Embrechts, Klüppelberg, and Mikosch, 1997, p.123) can be used to transform from the Fréchet and the Weibull distribution to the Gumbel distribution. Testing the exponentiality of the spacings on the Gumbel scale provides an approximate diagnosis of the joint distribution of the r largest order statistics when B is large. A limitation of this method, however, is that prior knowledge of the domain of attraction of the distribution is needed. Lastly, Dupuis (1997) proposed a robust estimation method, where the weights can be used to detect inconsistencies with the GEV_r distribution and assess the fit of the data to the joint Gumbel model. The method can be extended to general GEV_r distributions but the construction of the estimating equations is computing intensive with Monte Carlo integrations.

In this chapter, two specification tests are proposed to select r through a sequence of hypothesis testing. The first is the score test (e.g., Rao, 2005), but because of the nonstandard setting of the GEV_r distribution, the usual χ^2 asymptotic distribution

is invalid. A parametric bootstrap can be used to assess the significance of the observed statistic, but is computationally demanding. A fast, large sample alternative to parametric bootstrap based on the multiplier approach (Kojadinovic and Yan, 2012) is developed. The second test uses the difference in estimated entropy between the GEV_r and GEV_{r-1} models, applied to the r largest order statistics and the $r - 1$ largest order statistics, respectively. The asymptotic distribution is derived with the central limit theorem. Both tests are intuitive to understand, easy to implement, and have substantial power as shown in the simulation studies. Each of the two tests is carried out to test the adequacy of the GEV_r model for a sequence of r values. The very recently developed stopping rules for ordered hypotheses in G'Sell, Wager, Chouldechova, and Tibshirani (2016) are adapted to control the false discovery rate (FDR), the expected proportion of incorrectly rejected null hypotheses among all rejections, or familywise error rate (FWER), the probability of at least one type I error in the whole family of tests. All the methods are available in the R package `eva` (Bader and Yan, 2016) and some demonstration is seen in Chapter 5.

The rest of the chapter is organized as follows. The problem is set up in Section 2.2 with the GEV_r distribution, observed data, and the hypothesis to be tested. The score test is proposed in Section 2.3 with two implementations: parametric bootstrap and multiplier bootstrap. The entropy difference (ED) test is proposed and the asymptotic distribution of the testing statistic is derived in Section 2.4. A large scale simulation study on the empirical size and power of the tests are reported in Section 2.5. In

Section 2.6, the multiple, sequential testing problem is addressed by adapting recent developments on this application. The tests are applied to sea level and precipitation datasets in Section 2.7. A discussion concludes in Section 2.8. The Appendices A.1 and A.2 contain the details of random number generation from the GEV_r distribution and a sketch of the proof of the asymptotic distribution of the ED test statistic, respectively.

2.2 Model and Data Setup

The limit joint distribution (Weissman, 1978) of the r largest order statistics of a random sample of size B as $B \rightarrow \infty$ is the GEV_r distribution with probability density function given in (1.3).

The r largest order statistics approach is an extension of the block maxima approach in extreme value analysis when a number of largest order statistics are available for each one of a collection of independent blocks (Smith, 1986; Tawn, 1988). Specifically, let (y_{i1}, \dots, y_{ir}) be the observed r largest order statistics from block i for $i = 1, \dots, n$. Assuming independence across blocks, the GEV_r distribution is used in place of the GEV distribution (1.2) in the block maxima approach to make likelihood-based inference about θ . Let $l_i^{(r)}(\theta) = l^{(r)}(y_{i1}, \dots, y_{ir}|\theta)$, where

$$l^{(r)}(y_1, \dots, y_r|\theta) = -r \log \sigma - (1 + \xi z_r)^{-\frac{1}{\xi}} - \left(\frac{1}{\xi} + 1 \right) \sum_{j=1}^r \log(1 + \xi z_j) \quad (2.1)$$

is the contribution to the log-likelihood from a single block (y_1, \dots, y_r) with location

parameter μ , scale parameter $\sigma > 0$ and shape parameter ξ , where $y_1 > \dots > y_r$, $z_j = (y_j - \mu)/\sigma$, and $1 + \xi z_j > 0$ for $j = 1, \dots, r$. The maximum likelihood estimator (MLE) of θ using the r largest order statistics is $\hat{\theta}_n^{(r)} = \arg \max \sum_{i=1}^n l_i^{(r)}(\theta)$.

Model checking is a necessary part of statistical analysis. The rationale of choosing a larger value of r is to use as much information as possible, but not set r too high so that the GEV_r approximation becomes poor due to the decrease in convergence rate. Therefore, it is critical to test the goodness-of-fit of the GEV_r distribution with a sequence of null hypotheses

$H_0^{(r)}$: the GEV_r distribution fits the sample of the r largest order statistics well

for $r = 1, \dots, R$, where R is the maximum, predetermined number of top order statistics to test. Two test procedures for $H_0^{(r)}$ are developed for a fixed r first to help choose $r \geq 1$ such that the GEV_r model still adequately describes the data. The sequential testing process and the multiple testing issue are investigated in Section 2.6.

2.3 Score Test

A score statistic for testing goodness-of-fit hypothesis $H_0^{(r)}$ is constructed in the usual way with the score function and the Fisher information matrix (e.g., Rao, 2005). For ease of notation, the superscript (r) is dropped. Define the score function

$$S(\theta) = \sum_{i=1}^n S_i(\theta) = \sum_{i=1}^n \partial l_i(\theta) / \partial \theta$$

and Fisher information matrix $I(\theta)$, which have been derived in Tawn (1988). The behaviour of the maximum likelihood estimator is the same as that derived for the block maxima approach (Smith, 1985; Tawn, 1988), which requires $\xi > -0.5$. The score statistic is

$$V_n = \frac{1}{n} S^\top(\hat{\theta}_n) I^{-1}(\hat{\theta}_n) S(\hat{\theta}_n).$$

Under standard regularity conditions, V_n would asymptotically follow a χ^2 distribution with 3 degrees of freedom. The GEV_r distribution, however, violates the regularity conditions for the score test (e.g., Casella and Berger, 2002, pp. 516-517), as its support depends on the parameter values unless $\xi = 0$. For illustration, Figure 2.1 presents a visual comparison of the empirical distribution of V_n with $n = 5000$ from 5000 replicates, overlaid with the $\chi^2(3)$ distribution, for $\xi \in \{-0.25, 0.25\}$ and $r \in \{1, 2, 5\}$. The sampling distribution of V_n appears to be much heavier tailed than $\chi^2(3)$, and the mismatch increases as r increases as a result of the reduced convergence rate.

Although the regularity conditions do not hold, the score statistic still provides a measure of goodness-of-fit since it is a quadratic form of the score, which has expectation zero under the null hypothesis. Extremely large values of V_n relative to its sampling distribution would suggest lack of fit, and, hence, possible misspecification of $H_0^{(r)}$. So the key to applying the score test is to get an approximation of the sampling distribution of V_n . Two approaches for the approximation are proposed.

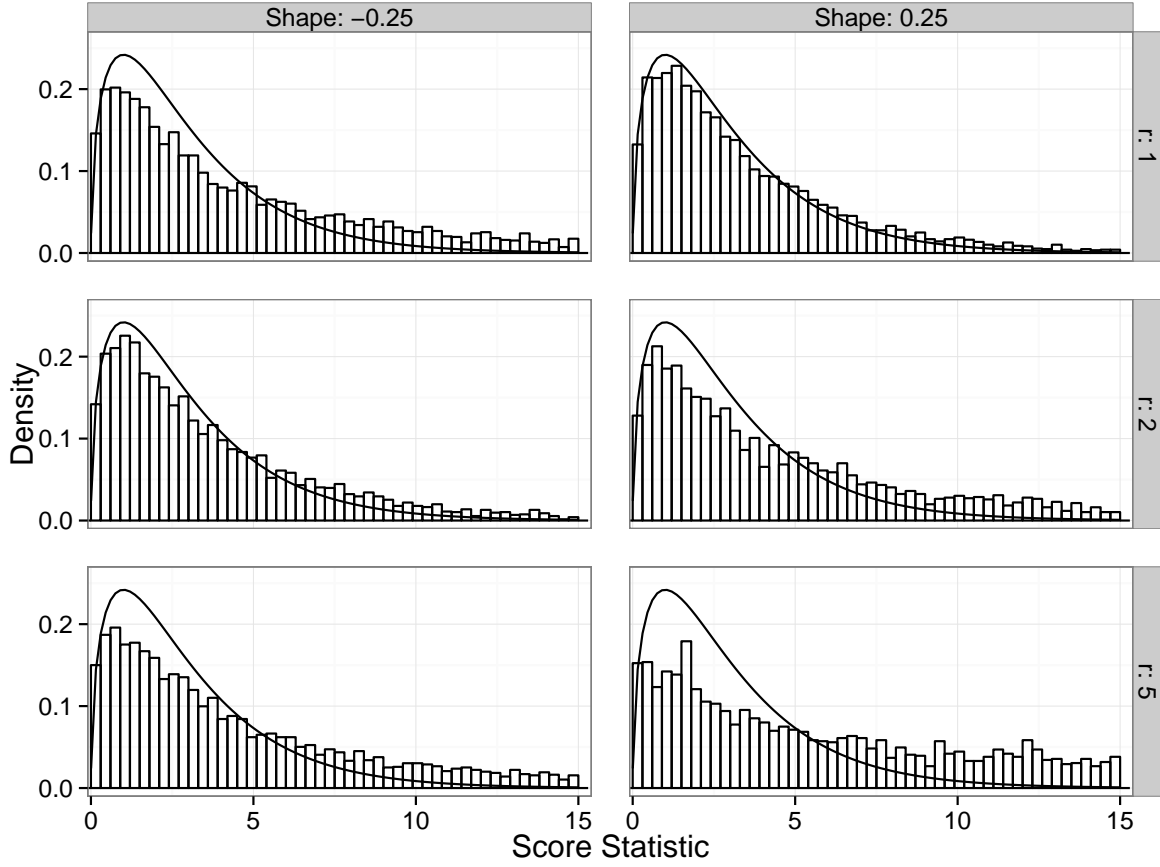


Figure 2.1: Comparisons of the empirical vs. $\chi^2(3)$ distribution (solid curve) based on 5000 replicates of the score test statistic under the null GEV_r distribution. The number of blocks used is $n = 5000$ with parameters $\mu = 0$, $\sigma = 1$, and $\xi \in (-0.25, 0.25)$.

2.3.1 Parametric Bootstrap

The first solution is parametric bootstrap. For hypothesis $H_0^{(r)}$, the test procedure goes as follows:

1. Compute $\hat{\theta}_n$ under H_0 with the observed data.
2. Compute the testing statistic V_n .
3. For every $k \in \{1, \dots, L\}$ with a large number L , repeat:

- (a) Generate a bootstrap sample of size n for the r largest statistics from GEV_r with parameter vector $\hat{\theta}_n$.
 - (b) Compute the $\hat{\theta}_n^{(k)}$ under H_0 with the bootstrap sample.
 - (c) Compute the score test statistic $V_n^{(k)}$.
4. Return an approximate p-value of V_n as $L^{-1} \sum_{k=1}^L 1(V_n^{(k)} > V_n)$.

Straightforward as it is, the parametric bootstrap approach involves sampling from the null distribution and computing the MLE for each bootstrap sample, which can be very computationally expensive. This is especially true as the sample size n and/or the number of order statistics r included in the model increases.

2.3.2 Multiplier Bootstrap

Multiplier bootstrap is a fast, large sample alternative to parametric bootstrap in goodness-of-fit testing (e.g., Kojadinovic and Yan, 2012). The idea is to approximate the asymptotic distribution of $n^{-1/2}I^{-1/2}(\theta)S(\theta)$ using its asymptotic representation

$$n^{-1/2}I^{-1/2}(\theta)S(\theta) = \frac{1}{\sqrt{n}} \sum_{i=1}^n \phi_i(\theta),$$

where $\phi_i(\theta) = I^{-1/2}(\theta)S_i(\theta)$. Its asymptotic distribution is the same as the asymptotic distribution of

$$W_n(\mathbf{Z}, \theta) = \frac{1}{\sqrt{n}} \sum_{i=1}^n (Z_i - \bar{Z})\phi_i(\theta),$$

conditioning on the observed data, where $\mathbf{Z} = (Z_1, \dots, Z_n)$ is a set of independent and identically distributed multipliers (independent of the data), with expectation 0 and variance 1, and $\bar{Z} = \frac{1}{n} \sum_{i=1}^n Z_i$. The multipliers must satisfy $\int_0^\infty \{\Pr(|Z_1| > x)\}^{\frac{1}{2}} dx < \infty$. An example of a possible multiplier distribution is $N(0, 1)$.

The multiplier bootstrap test procedure is summarized as follows:

1. Compute $\hat{\theta}_n$ under H_0 with the observed data.
2. Compute the testing statistic V_n .
3. For every $k \in \{1, \dots, L\}$ with a large number L , repeat:
 - (a) Generate $\mathbf{Z}^{(k)} = (Z_1^{(k)}, \dots, Z_n^{(k)})$ from $N(0, 1)$.
 - (b) Compute a realization from the approximate distribution of $W_n(\mathbf{Z}, \theta)$ with $W_n(\mathbf{Z}^{(k)}, \hat{\theta}_n)$.
 - (c) Compute $V_n^{(k)}(\hat{\theta}_n) = W_n^\top(\mathbf{Z}^{(k)}, \hat{\theta}_n) W_n(\mathbf{Z}^{(k)}, \hat{\theta}_n)$.
4. Return an approximate p-value of V_n as $L^{-1} \sum_{k=1}^L 1(V_n^{(k)} > V_n)$.

This multiplier bootstrap procedure is much faster than parametric bootstrap procedure because, for each sample, it only needs to generate \mathbf{Z} and compute $W_n(\mathbf{Z}, \hat{\theta}_n)$.

The MLE only needs to be obtained once from the observed data.

2.4 Entropy Difference Test

Another specification test for the GEV_r model is derived based on the difference in entropy for the GEV_r and GEV_{r-1} models. The entropy for a continuous random variable with density f is (e.g., Singh, 2013)

$$E[-\ln f(y)] = - \int_{-\infty}^{\infty} f(y) \log f(y) dy.$$

It is essentially the expectation of negative log-likelihood. The expectation can be approximated with the sample average of the contribution to the log-likelihood from the observed data, or simply the log-likelihood scaled by the sample size n . Assuming that the $r - 1$ top order statistics fit the GEV_{r-1} distribution, the difference in the log-likelihood between GEV_{r-1} and GEV_r provides a measure of deviation from $H_0^{(r)}$. Its asymptotic distribution can be derived. Large deviation from the expected difference under $H_0^{(r)}$ suggests a possible misspecification of $H_0^{(r)}$.

From the log-likelihood contribution in (2.1), the difference in log-likelihood for the i th block, $D_{ir}(\theta) = l_i^{(r)} - l_i^{(r-1)}$, is

$$D_{ir}(\theta) = -\log \sigma - (1 + \xi z_{ir})^{-\frac{1}{\xi}} + (1 + \xi z_{ir-1})^{-\frac{1}{\xi}} - \left(\frac{1}{\xi} + 1\right) \log(1 + \xi z_{ir}). \quad (2.2)$$

Let $\bar{D}_r = \frac{1}{n} \sum_{i=1}^n D_{ir}$ and $S_{Dr}^2 = \sum_{i=1}^n (D_{ir} - \bar{D}_r)^2 / (n - 1)$ be the sample mean and

sample variance, respectively. Consider a standardized version of \bar{D}_r as

$$T_n^{(r)}(\theta) = \sqrt{n}(\bar{D}_r - \eta_r)/S_{D_r}, \quad (2.3)$$

where $\eta_r = -\log \sigma - 1 + (1 + \xi)\psi(r)$, and $\psi(x) = d \log \Gamma(x)/dx$ is the digamma function. The asymptotic distribution of $T_n^{(r)}$ is summarized by Theorem 1 whose proof is relegated to Appendix A.2. This is essentially looking at the difference between the Kullback–Leibler divergence and its sample estimate. It is also worth pointing out that $T_n^{(r)}$ is only a function of the r and $r - 1$ top order statistics (i.e., only the conditional distribution $f(y_r|y_{r-1})$ is required for its computation). Alternative estimators of η_r can be used in place of \bar{D}_r as long as the regularity conditions hold; see Hall and Morton (1993) for further details.

Theorem 1. *Let $T_n^{(r)}(\theta)$ be the quantity computed based on a random sample of size n from the GEV_r distribution with parameters θ and assume that $H_0^{(r-1)}$ is true. Then $T_n^{(r)}$ converges in distribution to $N(0, 1)$ as $n \rightarrow \infty$.*

Note that in Theorem 1, $T_n^{(r)}$ is computed from a random sample of size n from a GEV_r distribution. If the random sample were from a distribution in the domain of attraction of a GEV_r distribution, the quality of the approximation of the GEV_r distribution to the r largest order statistics depends on the size of each block $B \rightarrow \infty$ with $r \ll B$. The block size B is not to be confused with the sample size n . Assuming $\xi > -0.5$, the proposed ED statistic for $H_0^{(r)}$ is $T_n^{(r)}(\hat{\theta}_n)$, where $\hat{\theta}_n$ is the MLE of θ with

the r largest order statistics for the GEV_r distribution. Since $\hat{\theta}_n$ is consistent for θ with $\xi > -0.5$, $T_n^{(r)}(\hat{\theta}_n)$ has the same limiting distribution as $T_n^{(r)}(\theta)$ under $H_0^{(r)}$.

To assess the convergence of $T_n^{(r)}(\hat{\theta}_n)$ to $N(0, 1)$, 1000 GEV_r replicates were simulated under configurations of $r \in \{2, 5, 10\}$, $\xi \in \{-0.25, 0, 0.25\}$, and $n \in \{50, 100\}$. Their quantiles are compared with those of $N(0, 1)$ via quantile-quantile plots (not presented). It appears that a larger sample size is needed for the normal approximation to be good for larger r and negative ξ . This is expected because larger r means higher dimension of the data, and because the MLE only exists for $\xi > -0.5$ (Smith, 1985). For r less than 5 and $\xi \geq 0$, the normal approximation is quite good; it appears satisfactory for sample size as small as 50. For r up to 10, sample size 100 seems to be sufficient.

2.5 Simulation Results

2.5.1 Size

The empirical sizes of the tests are investigated first. For the score test, the parametric bootstrap version and the multiplier bootstrap version are equivalent asymptotically, but may behave differently for finite samples. It is of interest to know how large a sample size is needed for the two versions of the score test to hold their levels. Random samples of size n were generated from the GEV_r distribution with $r \in \{1, 2, 3, 4, 5, 10\}$, $\mu = 0$, $\sigma = 1$, and $\xi \in \{-0.25, 0, 0.25\}$. All three parameters (μ, σ, ξ) were estimated.

When the sample size is small, there can be numerical difficulty in obtaining the

MLE. For the multiplier bootstrap score and ED test, the MLE only needs to be obtained once, for the dataset being tested. However, in addition, the parametric bootstrap score test must obtain a new sample and obtain the MLE for each bootstrap replicate. To assess the severity of this issue, 10,000 datasets were simulated for $\xi \in \{-0.25, 0, 0.25\}$, $r \in \{1, 2, 3, 4, 5, 10\}$, $n \in \{25, 50\}$, and the MLE was attempted for each dataset. Failure never occurred for $\xi \geq 0$. With $\xi = -0.25$ and sample size 25, the highest failure rate of 0.69% occurred for $r = 10$. When the sample size is 50, failures only occurred when $r = 10$, at a rate of 0.04%.

For the parametric bootstrap score test with sample size $n \in \{25, 50, 100\}$, Table 2.1 summarizes the empirical size of the test at nominal levels 1%, 5%, and 10% obtained from 1000 replicates, each carried out with bootstrap sample size $L = 1000$. Included only are the cases that converged successfully. Otherwise, the results show that the agreement between the empirical levels and the nominal level is quite good for samples as small as 25, which may appear in practice when long record data is not available.

For the multiplier bootstrap score test, the results for $n \in \{25, 50, 100, 200\}$ are summarized in Table 2.2. When the sample size is less than 100, it appears that there is a large discrepancy between the empirical and nominal level. For $\xi \in \{0, 0.25\}$, there is reasonable agreement between the empirical level and the nominal levels for sample size at least 100. For $\xi = -0.25$ and sample size at least 100, the agreement is good except for $r = 1$, in which case, the empirical level is noticeably larger than the nominal level. This may be due to different rates of convergence for various ξ values as ξ moves away

Table 2.1: Empirical size (in %) for the parametric bootstrap score test under the null distribution GEV_r , with $\mu = 0$ and $\sigma = 1$ based on 1000 samples, each with bootstrap sample size $L = 1000$.

| Sample Size | r | 25 | | | 50 | | | 100 | | |
|---------------|-----|-----|-----|------|-----|-----|------|-----|-----|------|
| Nominal Size | | 1.0 | 5.0 | 10.0 | 1.0 | 5.0 | 10.0 | 1.0 | 5.0 | 10.0 |
| $\xi = -0.25$ | 1 | 0.4 | 2.8 | 6.0 | 1.1 | 4.8 | 9.3 | 0.6 | 4.1 | 8.0 |
| | 2 | 0.1 | 2.6 | 6.0 | 0.8 | 3.4 | 6.5 | 0.6 | 3.6 | 8.1 |
| | 3 | 0.3 | 2.5 | 5.0 | 0.8 | 4.3 | 7.7 | 1.1 | 4.8 | 8.1 |
| | 4 | 0.3 | 1.8 | 5.4 | 0.6 | 3.1 | 6.9 | 1.1 | 5.1 | 8.8 |
| | 5 | 0.4 | 2.4 | 6.7 | 0.4 | 3.3 | 8.3 | 0.6 | 3.1 | 6.5 |
| | 10 | 2.7 | 5.3 | 8.7 | 0.5 | 3.9 | 8.4 | 0.7 | 4.2 | 7.6 |
| $\xi = 0$ | 1 | 1.3 | 5.2 | 8.9 | 1.6 | 5.3 | 9.0 | 0.8 | 4.7 | 9.3 |
| | 2 | 1.4 | 5.1 | 9.4 | 2.0 | 4.9 | 10.0 | 1.0 | 4.3 | 9.9 |
| | 3 | 1.7 | 6.2 | 10.9 | 2.1 | 6.0 | 10.2 | 0.8 | 4.9 | 9.8 |
| | 4 | 1.5 | 4.5 | 8.5 | 1.3 | 6.0 | 10.2 | 1.0 | 4.4 | 9.8 |
| | 5 | 1.6 | 5.8 | 10.4 | 2.4 | 6.2 | 9.9 | 1.2 | 5.0 | 9.7 |
| | 10 | 1.5 | 4.0 | 7.3 | 1.5 | 4.3 | 8.9 | 0.7 | 4.6 | 8.2 |
| $\xi = 0.25$ | 1 | 1.7 | 4.5 | 9.7 | 2.6 | 7.1 | 11.5 | 1.1 | 4.6 | 9.1 |
| | 2 | 1.8 | 5.1 | 8.7 | 1.8 | 4.4 | 8.5 | 0.5 | 2.9 | 7.5 |
| | 3 | 1.5 | 4.4 | 9.4 | 1.5 | 3.7 | 8.1 | 1.0 | 4.2 | 9.4 |
| | 4 | 1.2 | 3.3 | 8.1 | 1.1 | 4.6 | 9.7 | 1.1 | 4.3 | 9.6 |
| | 5 | 1.7 | 4.4 | 9.4 | 1.1 | 4.2 | 8.6 | 0.6 | 4.8 | 9.6 |
| | 10 | 1.1 | 4.6 | 8.3 | 1.5 | 6.1 | 10.7 | 1.0 | 3.9 | 8.5 |

from -0.5 . It is also interesting to note that, everything else being held, the agreement becomes better as r increases. This may be explained by the more information provided by larger r for the same sample size n , as can be seen directly in the Fisher information matrix (Tawn, 1988, pp. 247–249). For the most difficult case with $\xi = -0.25$ and $r = 1$, the agreement gets better as sample size increases and becomes acceptable when sample size was 1000 (not reported).

Table 2.2: Empirical size (in %) for multiplier bootstrap score test under the null distribution GEV_r , with $\mu = 0$ and $\sigma = 1$. 1000 samples, each with bootstrap sample size $L = 1000$ were used. Although not shown, the empirical size for $r = 1$ and $\xi = -0.25$ becomes acceptable when sample size is 1000.

| Sample Size | r | 25 | | | 50 | | | 100 | | | 200 | | |
|---------------|-----|-----|------|------|-----|------|------|-----|------|------|-----|------|------|
| Nominal Size | | 1.0 | 5.0 | 10.0 | 1.0 | 5.0 | 10.0 | 1.0 | 5.0 | 10.0 | 1.0 | 5.0 | 10.0 |
| $\xi = -0.25$ | 1 | 7.0 | 13.4 | 18.9 | 6.3 | 13.8 | 19.6 | 5.4 | 11.4 | 16.3 | 5.4 | 10.5 | 15.2 |
| | 2 | 2.0 | 6.9 | 13.4 | 1.3 | 6.4 | 12.4 | 1.6 | 6.9 | 13.6 | 1.4 | 6.7 | 12.8 |
| | 3 | 2.1 | 5.8 | 11.7 | 1.1 | 5.9 | 11.1 | 1.1 | 5.0 | 10.8 | 1.5 | 5.9 | 11.8 |
| | 4 | 3.3 | 7.2 | 12.3 | 1.1 | 4.9 | 10.8 | 1.0 | 5.2 | 11.9 | 1.1 | 5.6 | 10.6 |
| | 5 | 3.6 | 9.0 | 14.0 | 2.3 | 6.8 | 11.2 | 1.1 | 6.2 | 10.6 | 1.1 | 4.5 | 9.3 |
| | 10 | 2.0 | 7.0 | 10.3 | 2.6 | 7.4 | 12.8 | 2.1 | 6.4 | 10.1 | 1.4 | 6.4 | 11.6 |
| $\xi = 0$ | 1 | 3.3 | 8.4 | 15.3 | 2.2 | 7.0 | 12.5 | 1.1 | 4.6 | 9.2 | 1.3 | 6.1 | 11.2 |
| | 2 | 2.8 | 8.7 | 14.4 | 1.8 | 7.5 | 13.0 | 0.9 | 5.7 | 10.3 | 0.5 | 5.0 | 10.6 |
| | 3 | 6.1 | 12.1 | 16.5 | 3.0 | 7.2 | 12.2 | 1.5 | 6.0 | 10.4 | 1.4 | 4.5 | 9.8 |
| | 4 | 5.1 | 10.4 | 14.5 | 3.6 | 10.1 | 14.9 | 1.0 | 5.6 | 10.3 | 1.1 | 5.4 | 10.6 |
| | 5 | 4.2 | 9.0 | 14.5 | 2.2 | 8.2 | 12.5 | 1.7 | 6.5 | 12.0 | 1.8 | 6.2 | 12.5 |
| | 10 | 3.1 | 9.2 | 14.4 | 2.4 | 6.4 | 9.8 | 0.6 | 4.6 | 9.0 | 1.1 | 3.8 | 9.3 |
| $\xi = 0.25$ | 1 | 1.8 | 6.7 | 13.7 | 1.3 | 4.7 | 10.4 | 0.8 | 4.4 | 11.5 | 0.9 | 4.9 | 11.4 |
| | 2 | 5.7 | 12.7 | 17.1 | 4.7 | 9.9 | 14.9 | 3.5 | 7.4 | 11.6 | 3.2 | 7.9 | 11.7 |
| | 3 | 7.1 | 12.2 | 16.5 | 5.3 | 9.4 | 14.8 | 4.2 | 8.4 | 12.5 | 1.8 | 6.1 | 10.7 |
| | 4 | 5.4 | 9.8 | 16.8 | 3.7 | 9.0 | 13.4 | 2.6 | 6.0 | 11.4 | 1.2 | 4.9 | 11.2 |
| | 5 | 4.4 | 10.1 | 15.8 | 3.5 | 8.2 | 13.6 | 2.4 | 7.4 | 11.4 | 1.6 | 5.9 | 10.0 |
| | 10 | 3.3 | 8.9 | 15.3 | 2.4 | 6.6 | 12.3 | 1.6 | 5.8 | 10.9 | 1.7 | 6.6 | 12.4 |

To assess the convergence of $T_n^{(r)}(\hat{\theta}_n)$ to $N(0, 1)$, 10,000 replicates of the GEV_r distribution were simulated with $\mu = 0$ and $\sigma = 1$ for each configuration of $r \in \{2, 5, 10\}$, $\xi \in \{-0.25, 0, 0.25\}$, and $n \in \{50, 100\}$. A rejection for nominal level α , is denoted if $|T_n^{(r)}(\hat{\theta}_n)| > |Z_{\frac{\alpha}{2}}|$, where $Z_{\frac{\alpha}{2}}$ is the $\alpha/2$ percentile of the $N(0, 1)$ distribution. Using this result, the empirical size of the ED test can be summarized, and the results are presented in Table 2.3.

For sample size 50, the empirical size is above the nominal level for all configurations of r and ξ . As the sample size increases from 50 to 100, the empirical size stays the same or decreases in every setting. For sample size 100, the agreement between nominal and

Table 2.3: Empirical size (in %) for the entropy difference (ED) test under the null distribution GEV_r , with $\mu = 0$ and $\sigma = 1$ based on 10,000 samples.

| Sample Size | r | 50 | | | 100 | | |
|---------------|-----|-----|-----|------|-----|-----|------|
| Nominal Size | | 1.0 | 5.0 | 10.0 | 1.0 | 5.0 | 10.0 |
| $\xi = -0.25$ | 2 | 1.5 | 5.7 | 10.8 | 1.3 | 5.5 | 10.1 |
| | 5 | 2.4 | 6.8 | 11.9 | 1.6 | 5.9 | 10.6 |
| | 10 | 2.3 | 6.8 | 11.7 | 1.9 | 6.0 | 11.1 |
| $\xi = 0$ | 2 | 1.3 | 5.6 | 11.0 | 1.2 | 5.3 | 10.4 |
| | 5 | 1.6 | 5.9 | 11.2 | 1.5 | 5.7 | 10.6 |
| | 10 | 2.3 | 6.5 | 11.8 | 1.6 | 5.9 | 10.7 |
| $\xi = 0.25$ | 2 | 1.3 | 5.7 | 10.7 | 1.3 | 5.4 | 10.5 |
| | 5 | 1.6 | 5.8 | 11.5 | 1.3 | 5.6 | 10.2 |
| | 10 | 2.0 | 6.6 | 11.9 | 1.4 | 5.5 | 10.4 |

observed size appears to be satisfactory for all configurations of r and ξ . For sample size 50, the empirical size is slightly higher than the nominal size, but may be acceptable to some practitioners. For example, the empirical size for nominal size 10% is never above 12%, and for nominal size 5%, empirical size is never above 7%.

In summary, the multiplier bootstrap procedure of the score test can be used as a fast, reliable alternative to the parametric bootstrap procedure for sample size 100 or more when $\xi \geq 0$. When only small samples are available (less than 50 observations), the parametric bootstrap procedure is most appropriate since the multiplier version does not hold its size and the ED test relies upon samples of size 50 or more for the central limit theorem to take effect.

2.5.2 Power

The powers of the score tests and the ED test are studied with two data generating schemes under the alternative hypothesis. In the first scheme, 4 largest order statistics were generated from the GEV_4 distribution with $\mu = 0$, $\sigma = 1$, and $\xi \in \{-0.25, 0, 0.25\}$, and the 5th one was generated from a KumGEV distribution right truncated by the 4th largest order statistic. The KumGEV distribution is a generalization of the GEV distribution (Eljabri, 2013) with two additional parameters a and b which alter skewness and kurtosis. Defining $G_r(\mathbf{y})$ to be the distribution function of the $\text{GEV}_r(\mu, \sigma, \xi)$ distribution, the distribution function of the $\text{KumGEV}_r(\mu, \sigma, \xi, a, b)$ is given by $F_r(\mathbf{y}) = 1 - \{1 - [G_r(\mathbf{y})]^a\}^b$ for $a > 0$, $b > 0$. The score test and the ED test were applied to the top 5 order statistics with sample size $n \in \{100, 200\}$. When $a = b = 1$, the null hypothesis of GEV_5 is true. Larger difference from 1 of parameters a and b means larger deviation from the null hypothesis of GEV_5 .

Table 2.4 summarizes the empirical rejection percentages obtained with nominal size 5%, for a sequence value of $a = b$ from 0.4 to 2.0, with increment 0.2. Both tests hold their sizes when $a = b = 1$ and have substantial power in rejecting the null hypothesis for other values of $a = b$. Between the two tests, the ED test demonstrated much higher power than the score test in the more difficult cases where the deviation from the null hypothesis is small; for example, the ED test's power almost doubled the score test's power for $a = b \in \{0.8, 1.2\}$. As expected, the powers of both tests increase as $a = b$ moves away from 1 or as the sample sizes increases.

Table 2.4: Empirical rejection rate (in %) of the multiplier score test and the ED test in the first data generating scheme in Section 2.5.2 from 1000 replicates.

| Sample Size | ξ | Test | Value of $a=b$ | | | | | | | | |
|-------------|-------|-------|----------------|-------|------|-----|------|------|-------|-------|-------|
| | | | 0.4 | 0.6 | 0.8 | 1.0 | 1.2 | 1.4 | 1.6 | 1.8 | 2.0 |
| 100 | -0.25 | Score | 99.9 | 84.8 | 20.4 | 5.4 | 21.0 | 41.2 | 62.3 | 79.0 | 83.0 |
| | | ED | 100.0 | 99.0 | 46.5 | 4.6 | 48.7 | 89.5 | 99.2 | 100.0 | 99.8 |
| | 0 | Score | 100.0 | 87.0 | 21.6 | 7.4 | 24.2 | 48.9 | 67.8 | 79.6 | 89.4 |
| | | ED | 100.0 | 98.8 | 40.0 | 5.2 | 40.6 | 87.2 | 98.5 | 100.0 | 99.7 |
| | 0.25 | Score | 100.0 | 87.7 | 20.3 | 6.2 | 25.8 | 54.2 | 74.2 | 82.9 | 89.5 |
| | | ED | 100.0 | 97.5 | 37.7 | 4.8 | 34.8 | 78.1 | 96.1 | 99.5 | 99.7 |
| 200 | -0.25 | Score | 100.0 | 98.6 | 40.7 | 5.2 | 29.8 | 64.7 | 86.4 | 95.9 | 97.5 |
| | | ED | 100.0 | 100.0 | 78.4 | 6.2 | 70.0 | 99.2 | 100.0 | 100.0 | 100.0 |
| | 0 | Score | 100.0 | 99.4 | 44.6 | 6.1 | 34.9 | 75.0 | 92.4 | 97.3 | 98.6 |
| | | ED | 100.0 | 99.9 | 75.0 | 5.5 | 64.6 | 98.1 | 99.8 | 100.0 | 100.0 |
| | 0.25 | Score | 100.0 | 99.3 | 44.5 | 6.3 | 37.0 | 73.4 | 91.8 | 97.0 | 98.9 |
| | | ED | 100.0 | 100.0 | 71.0 | 5.2 | 57.2 | 95.9 | 100.0 | 100.0 | 100.0 |

In the second scheme, top 6 order statistics were generated from the GEV_6 distribution with $\mu = 0$, $\sigma = 1$, and $\xi \in \{-0.25, 0, 0.25\}$, and then the 5th order statistic was replaced from a mixture of the 5th and 6th order statistics. The tests were applied to the sample of first 5 order statistics with sample sizes $n \in \{100, 200\}$. The mixing rate p of the 5th order statistic took values in $\{0.00, 0.10, 0.25, 0.50, 0.75, 0.90, 1.00\}$. When $p = 1$ the null hypothesis of GEV_5 is true. Smaller values of p indicate larger deviations from the null. Again, both tests hold their sizes when $p = 1$ and have substantial power for other values of p , which increases as p decreases or as the sample sizes increases. The ED test again outperforms the score test with almost doubled power in the most difficult cases with $p \in \{0.75, 0.90\}$. For sample size 100 with $p = 0.50$, for instance, the ED test has power above 93% while the score test only has power above 69%. The full results are seen in Table 2.5.

Table 2.5: Empirical rejection rate (in %) of the multiplier score test and the ED test in the second data generating scheme in Section 2.5.2 from 1000 replicates.

| Sample Size | ξ | Test | Mixing Rate p | | | | | | |
|-------------|-------|-------|-----------------|-------|-------|-------|------|------|------|
| | | | 0.00 | 0.10 | 0.25 | 0.50 | 0.75 | 0.90 | 1.00 |
| 100 | -0.25 | Score | 99.7 | 99.5 | 95.5 | 69.4 | 24.1 | 7.8 | 5.8 |
| | | ED | 100.0 | 100.0 | 100.0 | 97.7 | 51.8 | 10.9 | 6.2 |
| | 0 | Score | 100.0 | 99.7 | 97.8 | 72.4 | 22.7 | 6.2 | 6.8 |
| | | ED | 100.0 | 100.0 | 100.0 | 96.0 | 47.6 | 10.3 | 5.6 |
| | 0.25 | Score | 99.9 | 99.7 | 96.6 | 70.8 | 24.7 | 5.8 | 5.3 |
| | | ED | 100.0 | 100.0 | 99.9 | 93.6 | 43.4 | 9.8 | 5.2 |
| 200 | -0.25 | Score | 99.9 | 100.0 | 99.7 | 95.6 | 43.4 | 11.4 | 5.1 |
| | | ED | 100.0 | 100.0 | 100.0 | 100.0 | 83.6 | 20.0 | 5.8 |
| | 0 | Score | 100.0 | 100.0 | 100.0 | 96.5 | 44.4 | 11.2 | 5.4 |
| | | ED | 100.0 | 100.0 | 100.0 | 100.0 | 79.5 | 20.0 | 5.5 |
| | 0.25 | Score | 100.0 | 100.0 | 100.0 | 97.2 | 46.9 | 9.2 | 5.5 |
| | | ED | 100.0 | 100.0 | 100.0 | 99.7 | 72.5 | 17.9 | 4.2 |

2.6 Automated Sequential Testing Procedure

As there are R hypotheses $H_0^{(r)}$, $r = 1, \dots, R$, to be tested in a sequence in the methods proposed, the sequential, multiple testing issue needs to be addressed. Most methods for error control assume that all the tests can be run first and then a subset of tests are chosen to be rejected (e.g., Benjamini, 2010a,b). The errors to be controlled are either the FWER (Shaffer, 1995), or the FDR (Benjamini and Hochberg, 1995; Benjamini and Yekutieli, 2001). In contrast to the usual multiple testing procedures, however, a unique feature in this setting is that the hypotheses must be rejected in an ordered fashion: if $H_0^{(r)}$ is rejected, $r < R$, then $H_0^{(k)}$ will be rejected for all $r < k \leq R$. Despite the extensive literature on multiple testing and the more recent developments on FDR control and

its variants, no definitive procedure has been available for error control in ordered tests until the recent work of G'Sell et al. (2016).

Consider a sequence of null hypotheses H_1, \dots, H_m . An ordered test procedure must reject H_1, \dots, H_k for some $k \in \{0, 1, \dots, m\}$, which rules out the classical methods for FDR control (Benjamini and Hochberg, 1995). Let $p_1, \dots, p_m \in [0, 1]$ be the corresponding p-values of the m hypotheses such that p_j is uniformly distributed over $[0, 1]$ when H_j is true. The methods of G'Sell et al. (2016) transform the sequence of p-values to a monotone sequence and then apply the original Benjamini–Hochberg procedure on the monotone sequence. They proposed two rejections rules, each returning a cutoff \hat{k} such that $H_1, \dots, H_{\hat{k}}$ are rejected. The first is called ForwardStop,

$$\hat{k}_F = \max \left\{ k \in \{1, \dots, m\} : -\frac{1}{k} \sum_{i=1}^k \log(1 - p_i) \leq \alpha \right\}, \quad (2.4)$$

and the second is called StrongStop,

$$\hat{k}_S = \max \left\{ k \in \{1, \dots, m\} : \exp \left(\sum_{j=k}^m \frac{\log p_j}{j} \right) \leq \frac{\alpha k}{m} \right\}, \quad (2.5)$$

where α is a pre-specified level. Both rules were shown to control the FDR at level α under the assumption of independent p-values. ForwardStop sets the rejection threshold at the largest k at which the average of first k transformed p-values is small enough. As it does not depend on those p-values with later indices, this rule is robust to potential

misspecification at later indices. StrongStop offers a stronger guarantee than ForwardStop. If the non-null p-values indeed precede the null p-values, it controls the FWER at level α in addition to the FDR. Thus, for ForwardStop, this α refers to the FDR and for StrongStop, α refers to the FWER. As the decision to stop at k depends on all the p-values after k , its power may be harmed if, for example, the very last p-values are slightly higher than expected under the null hypotheses.

To apply the two rules to our setting, note that our objective is to give a threshold \hat{r} such that the first \hat{r} of $m = R$ hypotheses are accepted instead of rejected. Therefore, we put the p-values in reverse order: let the ordered set of p-values $\{p_1, \dots, p_R\}$ correspond to hypotheses $\{H_0^{(R)}, \dots, H_0^{(1)}\}$. The two rules give a cutoff $\hat{k} \in \{1, \dots, R\}$ such that the hypotheses $H_0^{(R)}, \dots, H_0^{(R-\hat{k}+1)}$ are rejected. If no $\hat{k} \in \{1, \dots, R\}$ exists, then no rejection is made.

A caveat is that, unlike the setting of G'Sell et al. (2016), the p-values of the sequential tests are dependent. Nonetheless, the ForwardStop and StrongStop procedures may still provide some error control. For example, in the non-sequential multiple testing scenario Benjamini and Yekutieli (2001) show that their procedure controls the FDR under certain positive dependency conditions, while Blanchard and Roquain (2009) implement adaptive versions of step-up procedures that provably control the FDR under unspecified dependence among p-values.

The empirical properties of the two rules for the tests in this paper are investigated in simulation studies. To check the empirical FWER of the StrongStop rule,

only data under the null hypotheses are needed. With $R = 10$, $\xi \in \{-0.25, 0.25\}$, $n \in \{30, 50, 100, 200\}$, $\mu = 0$, and $\sigma = 1$, 1000 GEV_{10} samples were generated. For the ED, multiplier bootstrap score, and parametric bootstrap score test, the observed FWER is compared to the expected rates at various nominal α control levels. The StrongStop procedure is used, as well as no error control (i.e. a rejection occurs any time the raw p-value is below the nominal level). The results of this simulation are presented in Figure 2.2.

It is clear that the StrongStop reasonably controls the FWER for the ED test and the agreement between the observed and expected rate increases as the sample size increases. For both the parametric and multiplier bootstrap versions of the score test however, the observed FWER is above the expected rate, at times 10% higher. Regardless, it is apparent that using no error control results in an inflated FWER, and this inflation can only increase as the number of tests increase.

To check the empirical FDR of the ForwardStop rule, data need to be generated from a non-null model. To achieve this, consider the sequence of specification tests of GEV_r distribution with $r \in \{1, \dots, 6\}$, where the 5th and 6th order statistics are misspecified. Specifically, data from the GEV_7 distribution with $\mu = 0$ and $\sigma = 1$ were generated for n blocks; then the 5th order statistic is replaced with a 50/50 mixture of the 5th and 6th order statistics, and the 6th order statistic is replaced with a 50/50 mixture of the 6th and 7th order statistics. This is replicated 1000 times for each value of $\xi \in \{-0.25, 0.25\}$ and $n \in \{30, 50, 100, 200\}$. For nominal level α , the observed FDR

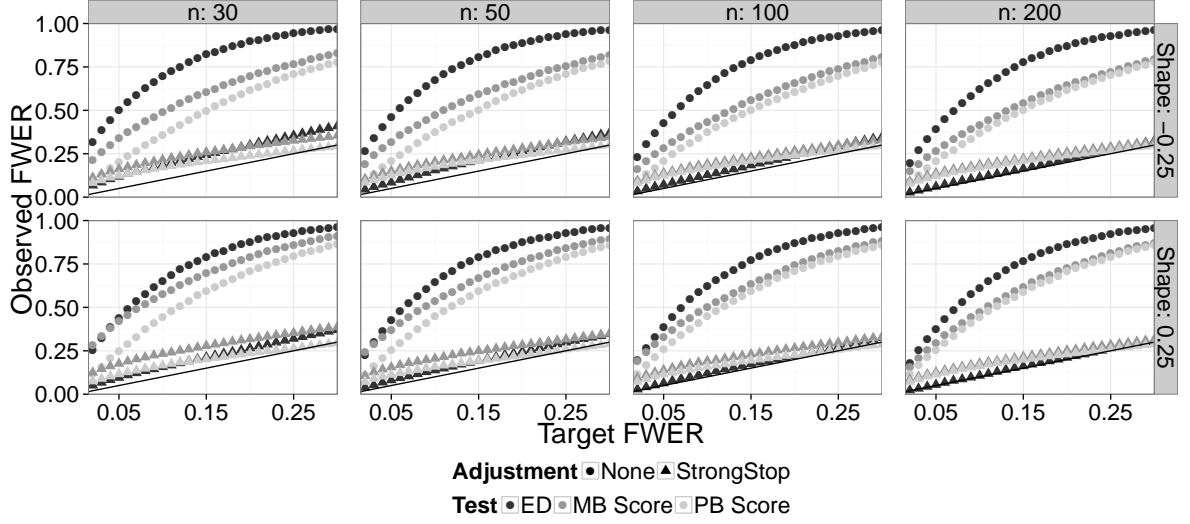


Figure 2.2: Observed FWER for the ED, parametric bootstrap (PB) score, and multiplier bootstrap (MB) score tests (using No Adjustment and StrongStop) versus expected FWER at various nominal levels. The 45 degree line indicates agreement between the observed and expected rates under H_0 .

is defined as the number of false rejections (i.e. any rejection of $r \leq 4$) divided by the number of total rejections.

The results are presented in Figure 2.3. The plots show that the ForwardStop procedure controls the FDR for the ED test, while for both versions of the score test, the observed FDR is slightly higher than the expected at most nominal rates. Here, sample size does not appear to effect the observed rates.

Similarly, the observed FWER rate in this particular simulation setting can be found by taking the number of simulations with at least one false rejection (here, any rejection of $r \leq 4$) and dividing that number by the total number of simulations. This calculation is performed for a variety of nominal levels α , using the StrongStop procedure. The results are presented in Figure 2.3. In this particular simulation setting, the StrongStop

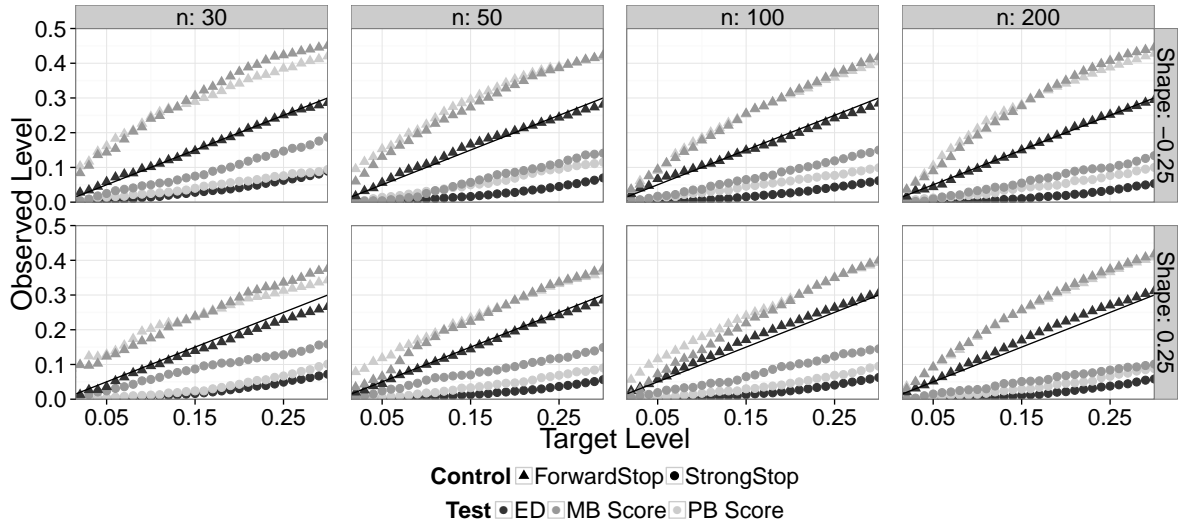


Figure 2.3: Observed FDR (from ForwardStop) and observed FWER (from StrongStop) versus expected FDR and FWER, respectively, at various nominal levels. This is for the simulation setting described in Section 2.6, using the ED, parametric bootstrap (PB) score, and multiplier bootstrap (MB) score tests. The 45 degree line indicates agreement between the observed and expected rates.

procedure controls the FWER for the ED test and both versions of the score test at all sample sizes investigated.

It is of interest to investigate the performance of the ForwardStop and StrongStop in selecting r for the r largest order statistics method. In the simulation setting described in the last paragraph, the correct choice of r should be 4, and a good testing procedure should provide a selection \hat{r} close to 4. The choice $\hat{r} \in \{0, \dots, 6\}$ is recorded using the ED test and bootstrap score tests with both ForwardStop and StrongStop. Due to space constraints, we choose to present one setting, where $\xi = 0.25$ and $n = 100$. The non-adjusted sequential procedure is also included, testing in an ascending manner from $r = 1$ and \hat{r} is chosen by the first rejection found (if any). The results are summarized

in Table 2.6.

In general, larger choices of α lead to a higher percentage of $\hat{r} = 4$ being correctly chosen with ForwardStop or StrongStop. Intuitively, this is not surprising since a smaller α makes it more difficult to reject the ‘bad’ hypotheses of $r \in \{5, 6\}$. A larger choice of α also leads to a higher probability of rejecting too many tests; i.e. choosing r too small. From the perspective of model specification, this is more desirable than accepting true negatives. A choice of 6, 5, or 0 is problematic, but choosing 1, 2, or 3 is acceptable, although some information is lost. When no adjustment is used and an ascending sequential procedure is used, both tests have reasonable classification rates. When $\alpha = 0.05$, the ED test achieves the correct choice of r 79.9% of the time, with the parametric bootstrap and multiplier bootstrap score tests achieving 68.1% and 59.6% respectively. Of course, as the number of tests (i.e., R) increase, with no adjustment the correct classification rates will go down and the ForwardStop/StrongStop procedures will achieve better rates. This may not be too big an issue here as R is typically small. In the case where rich data are available and R is big, the ForwardStop and StrongStop becomes more useful as they are designed to handle a large number of ordered hypothesis.

2.7 Illustrations

2.7.1 Lowestoft Sea Levels

Sea level readings in 60 and 15 minute intervals from a gauge at Lowestoft off the east coast of Britain during the years 1964–2014 are available from the UK Tide Gauge Network website. The readings are hourly from 1964–1992 and in fifteen minute intervals from 1993 to present. Accurate estimates of extreme sea levels are of great interest. The current data are of better quality and with longer record than those used in Tawn (1988) — annual maxima during 1953–1983 and hourly data during 1970–78 and 1980–82.

Justification of the statistical model was considered in detail by Tawn (1988). The three main assumptions needed to justify use of the GEV_r model are: (1) The block size B is large compared to the choice of r ; (2) Observations within each block and across blocks are approximately independent; and (3) The distribution of the block maxima follows GEV_1 . The first assumption is satisfied, by letting $R = 125$, and noting that the block size for each year is $B = 365 \times 24 = 8760$ from 1964–1992 and $B = 365 \times 96 = 35040$ from 1993–2014. This ensures that $r \ll B$. The third assumption is implicitly addressed in the testing procedure; if the goodness-of-fit test for the block maxima rejects, all subsequent tests for $r > 1$ are rejected as well.

The second assumption can be addressed in this setting by the concept of independent storms (Tawn, 1988). The idea is to consider each storm as a separate event, with each storm having some storm length, say τ . Thus, when selecting the r largest values from

each block, only a single contribution can be obtained from each storm, which can be considered the r largest independent annual events. By choosing τ large enough, this ensures both approximate independence of observations within each block and across blocks. The procedure to extract the independent r largest annual events is as follows:

1. Pick out the largest remaining value from the year (block) of interest.
2. Remove observations within a lag of $\tau/2$ from both sides of the value chosen in step 1.
3. Repeat (within each year) until the r largest are extracted.

A full analysis is performed on the Lowestoft sea level data using $\tau = 60$ as the estimated storm length (Tawn, 1988). Using $R = 125$, both the parametric bootstrap score (with bootstrap sample size $L = 10,000$) and ED test are applied sequentially on the data. The p-values of the sequential tests (adjusted and unadjusted) can be seen in Figure 2.4. Due to the large number of tests, the adjustment for multiplicity is desired and thus, ForwardStop is used to choose r . For this dataset, the score test is more powerful than the ED test. With ForwardStop and the score test, Figure 2.4 suggests that $r = 33$. The remainder of this analysis proceeds with the choice of $r = 33$. The estimated parameters and corresponding 95% profile confidence intervals for $r = 1$ through $r = 40$ are shown in Figure 2.5.

When $r = 33$, the parameters are estimated as $\hat{\mu} = 3.462$ (0.023), $\hat{\sigma} = 0.210$ (0.013), and $\hat{\xi} = -0.017$ (0.023), with standard errors in parenthesis. An important risk measure

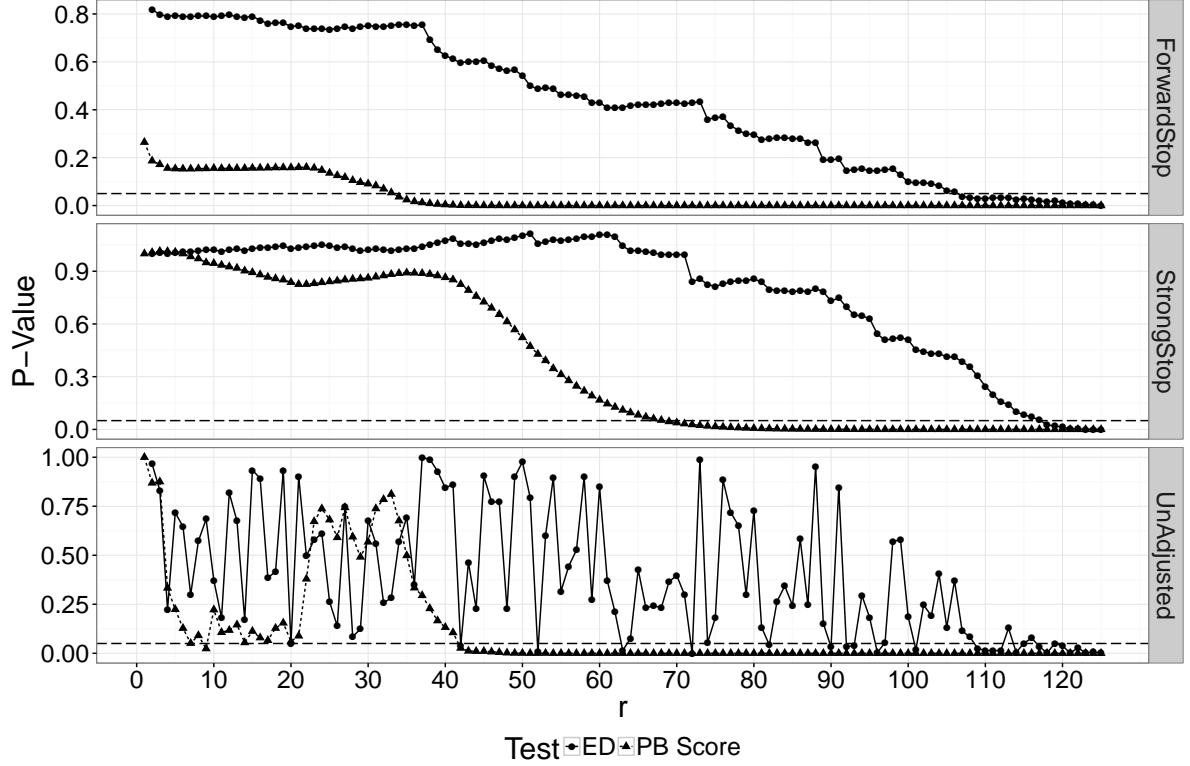


Figure 2.4: Adjusted p-values using ForwardStop, StrongStop, and raw (unadjusted) p-values for the ED and PB Score tests applied to the Lowestoft sea level data. The horizontal dashed line represents the 0.05 possible cutoff value.

is the t -year return level z_t (e.g., Hosking, 1990; Ribereau et al., 2008; Singo, Kundu, Odiyo, Mathivha, and Nkuna, 2012). It can be thought of here as the sea level that is exceeded once every t years on average. Specifically, the t -year return level is the $1 - 1/t$ quantile of the GEV distribution (which can be substituted with corresponding quantities from the GEV_r distribution), given by

$$z_t = \begin{cases} \mu - \frac{\sigma}{\xi} \{1 - [-\log(1 - \frac{1}{t})]^{-\xi}\}, & \xi \neq 0, \\ \mu - \sigma \log[-\log(1 - \frac{1}{t})], & \xi = 0. \end{cases} \quad (2.6)$$

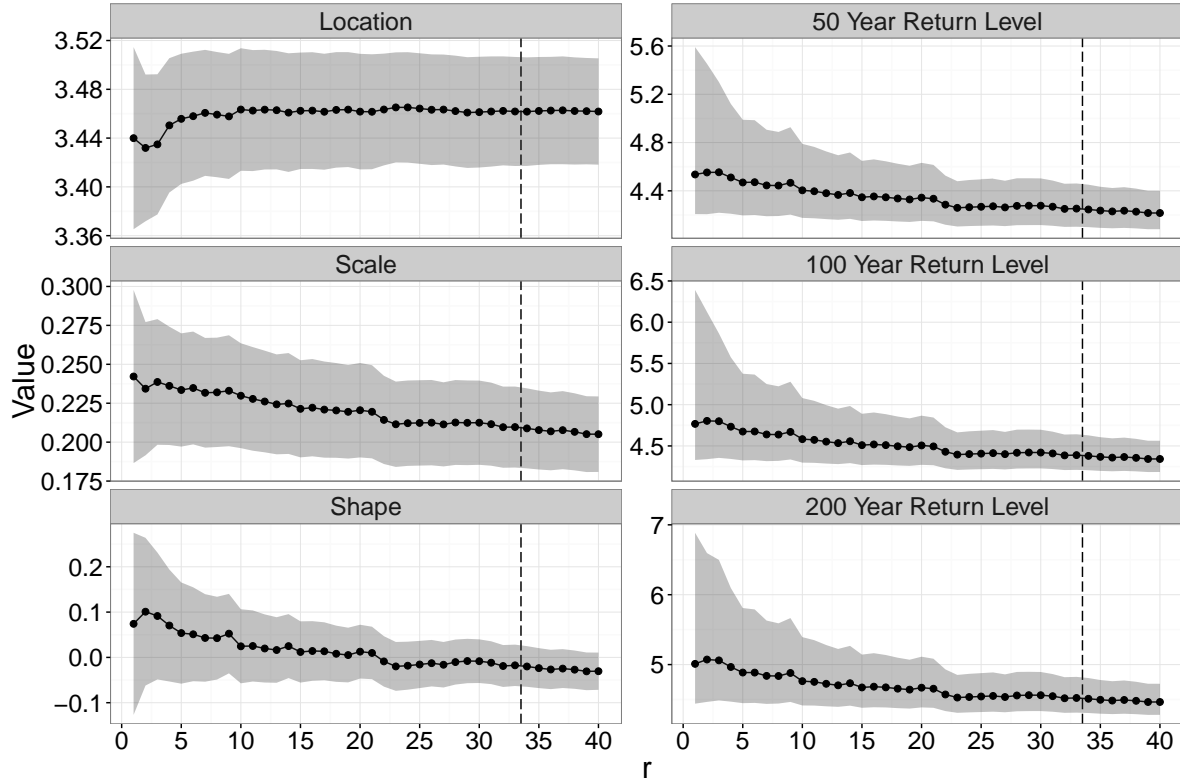


Figure 2.5: Location, scale, and shape parameter estimates, with 95% delta confidence intervals for $r = 1, \dots, 40$ for the Lowestoft sea level data. Also included are the estimates and 95% profile likelihood confidence intervals for the 50, 100, and 200 year return levels. The vertical dashed line represents the recommended cutoff value of r from the analysis in Section 2.7.1.

The return levels can be estimated with parameter values replaced with their estimates, and confidence intervals can be constructed using profile likelihood (e.g., Coles, 2001, p.57).

The 95% profile likelihood confidence intervals for the 50, 100, and 200 year return levels (i.e. z_{50}, z_{100}, z_{200}) are given by $(4.102, 4.461)$, $(4.210, 4.641)$ and $(4.312, 4.824)$, respectively. The benefit of using $r = 1$ versus $r = 33$ can be seen in the return level confidence intervals in Figure 2.5. For example, the point estimate of the 100 year

return level decreases slightly as r increases and the width of the 95% confidence interval decreases drastically from 2.061 ($r = 1$) to 0.432 ($r = 33$), as more information is used. The lower bound of the interval however remains quite stable, shifting from 4.330 to 4.210 — less than a 3% change. Similarly, the standard error of the shape parameter estimate decreases by over two-thirds when using $r = 33$ versus $r = 1$.

2.7.2 Annual Maximum Precipitation: Atlantic City, NJ

The top 10 annual precipitation events (in centimeters) were taken from the daily records of a rain gauge station in Atlantic City, NJ from 1874–2015. The year 1989 is missing, while the remaining records are greater than 98% complete. This provides a total record length of 141 years. The raw data is a part of the Global Historical Climatology Network (GHCN-Daily), with an overview given by Menne et al. (2012). The specific station identification in the dataset is USW00013724.

Unlike for the Lowestoft sea level data, a rather small value is set for R at $R = 10$ because of the much lower frequency of the daily data. Borrowing ideas from Section 2.7.1, a storm length of $\tau = 2$ is used to ensure approximate independence of observations. Both the parametric bootstrap score (with $L = 10,000$) and ED test are applied sequentially on the data. The p-values of the sequential tests (ForwardStop, StrongStop, and unadjusted) are shown in Figure 2.6. The score test does not pick up anything. The ED test obtains p-values 0.002 and 0.016, respectively, for $r = 9$ and $r = 10$, which translates into a rejection using ForwardStop. Thus, Figure 2.6 suggests that $r = 8$ be

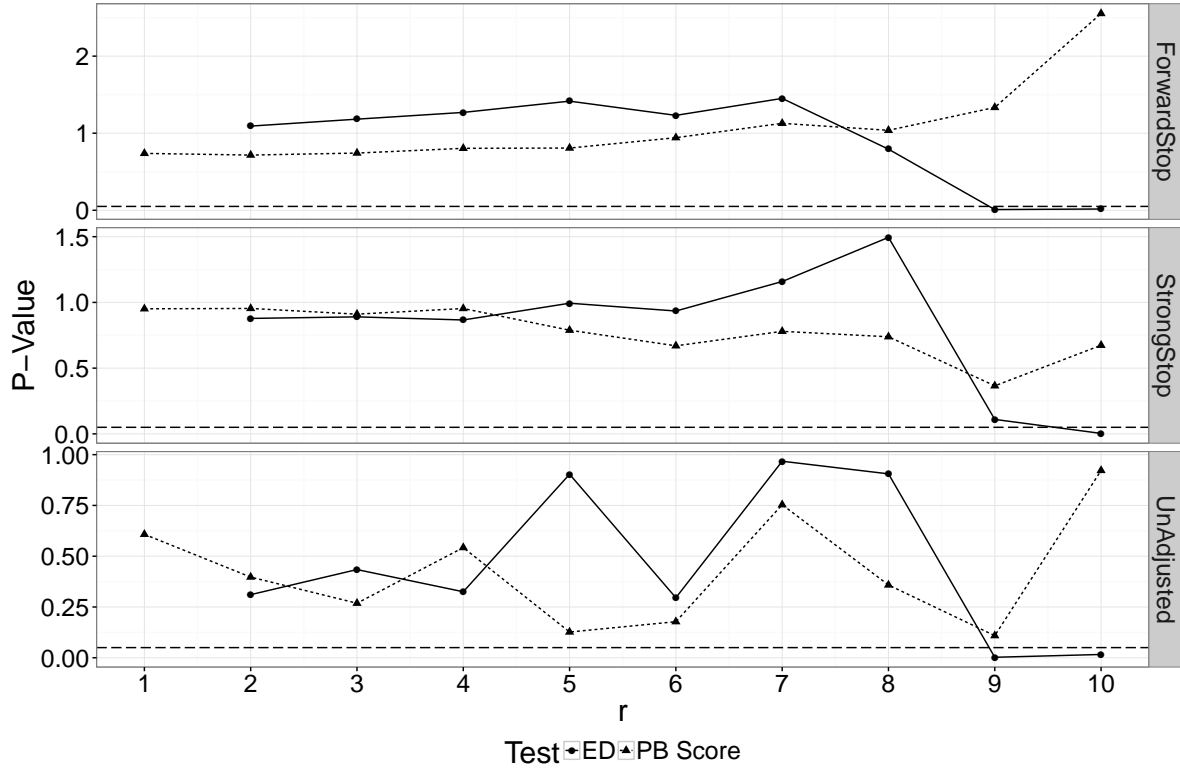


Figure 2.6: Adjusted p-values using ForwardStop, StrongStop, and raw (unadjusted) p-values for the ED and PB Score tests applied to the Atlantic City precipitation data. The horizontal dashed line represents the 0.05 possible cutoff value.

used for the analysis.

With $r = 8$, the estimated parameters are given as $\hat{\mu} = 6.118$ (0.139), $\hat{\sigma} = 2.031$ (0.118), and $\hat{\xi} = 0.219$ (0.032). This suggests a heavy upper tail for the estimated distribution (i.e. $\hat{\xi} > 0$). The progression of parameters and certain return level estimates can be seen in Figure 2.7. The 50, 100, and 200 year return level 95% confidence intervals for $r = 8$ are calculated using the profile likelihood method and are given by (16.019, 22.411), (18.606, 26.979), and (21.489, 31.136), respectively. The advantages of using $r = 8$ versus the block maxima for analysis are quite clear from Figure 2.7. The standard error of the

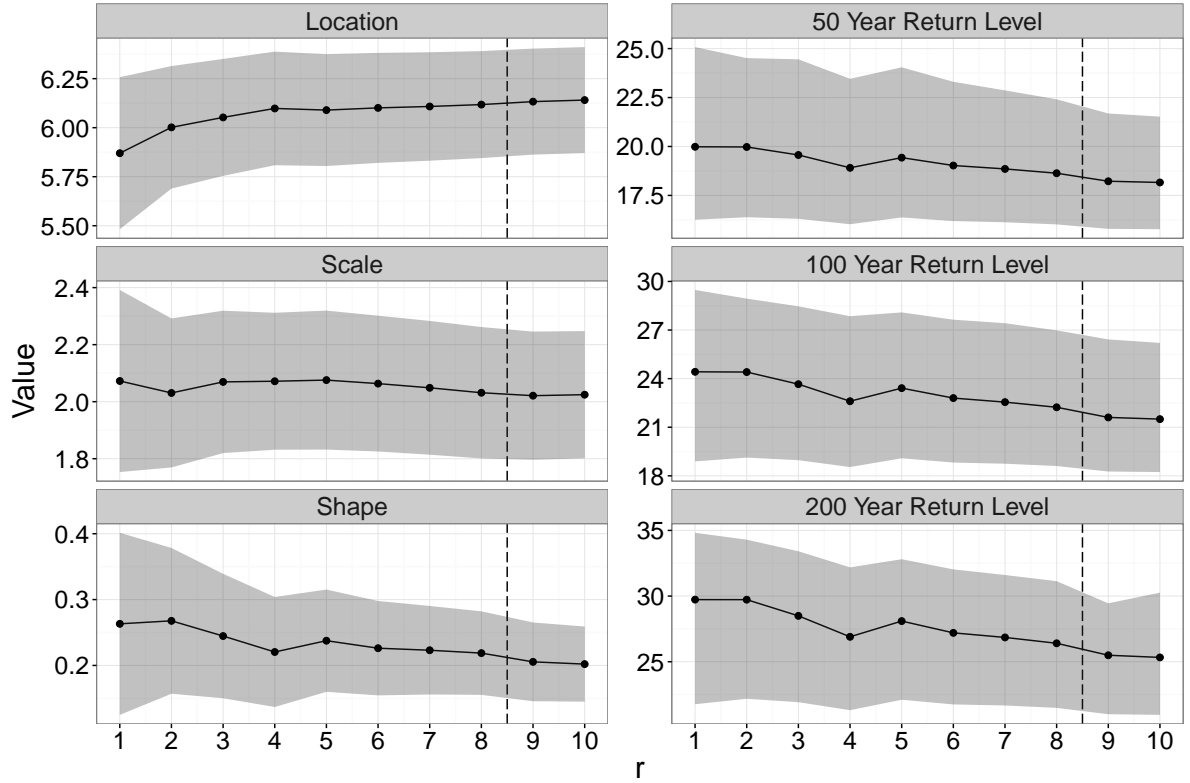


Figure 2.7: Location, scale, and shape parameter estimates, with 95% delta confidence intervals for $r = 1$ through $r = 10$ for the Atlantic City precipitation data. Also included are the estimates and 95% profile likelihood confidence intervals for the 50, 100, and 200 year return levels. The vertical dashed line represents the recommended cutoff value of r from the analysis in Section 2.7.2.

shape parameter decreases from 0.071 to 0.032, a decrease of over 50%. Similarly, the 50 year return level 95% confidence intervals decreases in width by over 25%.

2.8 Discussion

We propose two model specification tests for a fixed number of largest order statistics as the basis for selecting r for the r largest order statistics approach in extreme value

analysis. The score test has two versions of bootstrap procedure: the multiplier bootstrap method providing a fast, large sample alternative to the parametric bootstrap method, with a speedup of over 100 times. The ED test depends on an asymptotic normal approximation of the testing statistic, which becomes acceptable for sample size over 50. It assumes that the $r - 1$ top order statistics included already fits the GEV_{r-1} distribution. Therefore, the initial hypothesis at $r = 1$ needs to be tested with the score tests. Both tests hold their size better when the shape parameter is further away from the lower limit of -0.5 or sample size is larger. When only small samples are available (50 observations or less), the parametric bootstrap score test is recommended.

Alternative versions of the ED test have been explored. One may define the testing statistics as the difference in entropy between GEV_1 and GEV_r , instead of between GEV_{r-1} and GEV_r . Nonetheless, it appeared to require a larger sample to hold its size from our simulation studies (not reported). In the calculation of $T_n^{(r)}$, the block maxima MLE $\hat{\theta}_n^{(1)}$ can be used as an estimate for θ in place of $\hat{\theta}_n^{(r)}$. Again, in our simulation studies, this version of the ED test was too conservative, thus reducing the power, when the sample size was not large enough. This may be explained in that the resulting \hat{S}_{D_r} underestimates S_{D_r} .

If the initial block maxima distribution ($r = 1$) is rejected or a small r is selected, it may be worth noting that the choice of B , the block size must be sufficiently large relative to R , the number of largest order statistics to test. The rate of convergence for the r largest order statistics has been previously studied (Dziubdziela, 1978; Deheuvels, 1986,

1989; Falk, 1989). In particular, Falk (1989) showed that the best rate of convergence to the distribution in (1.3) is $O(r/B)$, uniformly in r and can be as slow as $O(r/\log(B))$ if the underlying distribution is normal. Hence, an initial rejection of $r = 1$ may indicate that a larger block size is needed.

Naively, the tests may be performed sequentially for each $r \in \{1, \dots, R\}$, for a prefixed, usually small $R \ll B$, at a certain significance level until $H_0^{(r)}$ is rejected. The issue of multiple, sequential testing is addressed in detail by adapting two very recent stopping rules to control the FDR and the FWER that are developed specifically for situations when hypotheses must be rejected in an ordered fashion (G'Sell et al., 2016). Based on the higher power of the ED test, a broad recommendation would be to use the score test for $r = 1$, then proceed using the ED test for testing $r = 2, \dots, R$. The choice of stopping rule to use in conjunction depends on the desired error control. ForwardStop controls the FDR and thus generally provides more rejections (i.e., smaller selected r), while StrongStop provides stricter control (FWER), thus possessing less power (i.e., larger selected r). Typically, correct specification of the GEV_r distribution is crucial in estimating large quantiles (e.g., return levels), so as a general guideline ForwardStop would be suggested.

Chapter 3

Automated Threshold Selection in the POT Approach

3.1 Introduction

Return levels, the levels of a measure of interest that is expected to be exceeded on average once every certain period of time (return period), are commonly a major goal of inference in extreme value analysis. As opposed to block-based methods, threshold methods involve modeling data exceeding a suitably chosen high threshold with the generalized Pareto distribution (GPD) (Balkema and De Haan, 1974; Pickands, 1975). Choice of the threshold is critical in obtaining accurate estimates of model parameters and return levels. The threshold should be chosen high enough for the excesses to be well approximated by the GPD to minimize bias, but not so high to substantially increase the variance of the estimator due to reduction in the sample size (the number of exceedances).

Although it is widely accepted in the statistics community that the threshold-based

approach, in particular peaks-over-threshold (POT), use data more efficiently than the block maxima method (e.g., Caires, 2009), it is much less used than the block maxima method in some fields such as climatology. The main issue is the need to conduct the analyses over many locations, sometimes over hundreds of thousands of locations (e.g., Kharin, Zwiers, Zhang, and Hegerl, 2007; Kharin et al., 2013), and there is a lack of efficient procedures that can automatically select the threshold in each analysis. For example, to make a return level map of annual maximum daily precipitation for three west coastal US states of California, Oregon, and Washington alone, one needs to repeat the estimation procedure including threshold selection, at each of the hundreds of stations. For the whole US, thousands of sites need to be processed. A graphical based diagnosis is clearly impractical. It is desirable to have an intuitive automated threshold selection procedure in order to use POT in analysis.

Many threshold selection methods are available in the literature; see Scarrott and MacDonald (2012) and Caeiro and Gomes (2016) for recent reviews. Among them, graphical diagnosis methods are arguably the most popular. The mean residual life (MRL) plot (Davison and Smith, 1990) uses the fact that, if X follows a GPD, then for $v > u$, the MRL $E[X - v | X > v]$, if existing, is linear in v . The threshold is chosen to be the smallest u such that the sample MRL is approximately linear above this point. Parameter stability plots check whether the estimates of GPD parameters, possibly transformed to be comparable across different thresholds, are stable above some level of threshold. Drees et al. (2000) suggested the Hill plot, which plots the Hill estimator of

the shape parameter based on the top k order statistics against k . Many variants of the Hill plot have been proposed (Scarrott and MacDonald, 2012, Section 4). The threshold is the k th smallest order statistic beyond which the parameter estimates are deemed to be stable. The usual fit diagnostics such as quantile plots, return level plots, and probability plots can be helpful too, as demonstrated in Coles (2001). Graphical diagnostics give close inspection of the data, but they are quite subjective and disagreement on a particular threshold can occur even among experts in the field; see, for example, a convincing demonstration of unclear choices using the Fort Collins precipitation data in Figures 1.3, 1.4, and 1.5 which are taken from Scarrott and MacDonald (2012).

Other selection methods can be grouped into various categories. One is based on the asymptotic results about estimators of properties of the tail distribution. The threshold is selected by minimizing the asymptotic mean squared error (MSE) of the estimator of, for example, tail index (Beirlant, Vynckier, and Teugels, 1996), tail probabilities (Hall and Weissman, 1997), or extreme quantiles (Ferreira, de Haan, and Peng, 2003). Theoretically sound as these methods are, their finite sample properties are not well understood. Some require second order assumptions, and computational (bootstrap) based estimators can require tuning parameters (Danielsson, de Haan, Peng, and de Vries, 2001) or may not be satisfactory for small samples (Ferreira et al., 2003). Irregardless, such resampling methods may be quite time-consuming in an analysis involving many locations.

A second category of methods are based on goodness-of-fit of the GPD, where the

threshold is selected as the lowest level above which the GPD provides adequate fit to the exceedances (e.g., Davison and Smith, 1990; Dupuis, 1999; Choulakian and Stephens, 2001; Northrop and Coleman, 2014). Goodness-of-fit tests are simple to understand and perform, but the multiple testing issue for a sequence of tests in an ordered fashion have not been addressed to the best of our knowledge. Methods in the third category are based on mixtures of a GPD for the tail and another distribution for the “bulk” joined at the threshold (e.g., MacDonald, Scarrott, Lee, Darlow, Reale, and Russell, 2011; Wadsworth and Tawn, 2012). Treating the threshold as a parameter to estimate, these methods can account for the uncertainty from threshold selection in inferences. However, there is little known about the asymptotic properties of this setup and how to ensure that the bulk and tail models are robust to one another in the case of misspecification.

Some automated procedures have been proposed. The simple naive method is *a priori* or fixed threshold selection based on expertise on the subject matter at hand. Various rules of thumb have been suggested; for example, select the top 10% of the data (e.g., DuMouchel, 1983), or the top square root of the sample size (e.g., Ferreira et al., 2003). Such one rule for all is not ideal in climate applications where high heterogeneity in data properties is the norm. The proportion of the number of rain days can be very different from wet tropical climates to dry subtropical climates; therefore the number of exceedances over the same time period can be very different across different climates. Additionally, the probability distribution of daily precipitation can also be different in different climates, affecting the speed the tails converge to the GPD (Raoult and Worms,

2003). Goodness-of-fit test based procedures can be automated to select the lowest one in a sequence of thresholds, at which the goodness-of-fit test is not rejected (e.g., Choulakian and Stephens, 2001). The error control, however, is challenging because of the ordered nature of the hypotheses, and the usual methods from multiple testing such as false discovery rate (e.g., Benjamini, 2010a,b) cannot be directly applied.

We propose an automated threshold selection procedure based on a sequence of goodness-of-fit tests with error control for ordered, multiple testing. The very recently developed stopping rules for ordered hypotheses in G'Sell et al. (2016) are adapted to control the familywise error rate (FWER), the probability of at least one type I error in the whole family of tests (Shaffer, 1995), or the false discovery rate (FDR), the expected proportion of incorrectly rejected null hypotheses among all rejections (Benjamini and Hochberg, 1995; Benjamini and Yekutieli, 2001). They are applied to four goodness-of-fit tests at each candidate threshold, including the Cramér–Von Mises test, Anderson–Darling test, Rao’s score test, and Moran’s test. For the first two tests, the asymptotic null distribution of the testing statistic is unwieldy (Choulakian and Stephens, 2001). Parametric bootstrap puts bounds on the approximate p-values which would reduce power of the stopping rules and lacks the ability to efficiently scale. We propose a fast approximation based on the results of Choulakian and Stephens (2001) to facilitate the application. The performance of the procedures are investigated in a large scale simulation study, and recommendations are made. The procedure is applied to annual maximum daily precipitation return level mapping for three west coastal states

of the US. Interesting findings are revealed from different stopping rules. The automated threshold selection procedure has applications in various fields, especially when batch processing of massive datasets is needed.

The outline of this chapter is as follows. Section 3.2 presents the generalized Pareto model, its theoretical justification, and how to apply the automated sequential threshold testing procedure. Section 3.3 introduces the tests proposed to be used in the automated testing procedure. A simulation study demonstrates the power of the tests for a fixed threshold under various misspecification settings and it is found that the Anderson–Darling test is most powerful in the vast majority of cases. A large scale simulation study in Section 3.4 demonstrates the error control and performance of the stopping rules for multiple ordered hypotheses, both under the null GPD and a plausible alternative distribution. In Section 3.5, we return to our motivating application and derive return levels for extreme precipitation at hundreds of west coastal US stations to demonstrate the usage of our method. A final discussion is given in Section 3.6.

3.2 Automated Sequential Testing Procedure

Threshold methods for extreme value analysis are based on that, under general regularity conditions, the only possible non-degenerate limiting distribution of properly rescaled exceedances of a threshold u is the GPD as $u \rightarrow \infty$ (e.g., Pickands, 1975). The GPD has cumulative distribution function given in (1.4) and also has the property that for

some threshold $v > u$, the excesses follow a GPD with the same shape parameter, but a modified scale $\sigma_v = \sigma_u + \xi(v - u)$.

Let X_1, \dots, X_n be a random sample of size n . If u is sufficiently high, the exceedances $Y_i = X_i - u$ for all i such that $X_i > u$ are approximately a random sample from a GPD. The question is to find the lowest threshold such that the GPD fits the sample of exceedances over this threshold adequately. Our solution is through a sequence of goodness-of-fit tests (e.g., Choulakian and Stephens, 2001) or model specification tests (e.g., Northrop and Coleman, 2014) for the GPD to the exceedances over each candidate threshold in an increasing order. The multiple testing issues in this special ordered setting are handled by the most recent stopping rules in G'Sell et al. (2016).

Consider a fixed set of candidate thresholds $u_1 < \dots < u_l$. For each threshold, there will be n_i excesses, $i = 1, \dots, l$. The sequence of null hypotheses can be stated as

$H_0^{(i)}$: The distribution of the n_i exceedances above u_i follows the GPD.

For a fixed u_i , many tests are available for this $H_0^{(i)}$. An automated procedure can begin with u_1 and continue until some threshold u_i provides an acceptance of $H_0^{(i)}$ (Choulakian and Stephens, 2001; Thompson, Cai, Reeve, and Stander, 2009). The problem, however, is that unless the test has high power, an acceptance may happen at a low threshold by chance and, thus, the data above the chosen threshold is contaminated. One could also begin at the threshold u_l and descend until a rejection occurs, but this would result in an increased type I error rate. The multiple testing problem obviously needs to be

addressed, but the issue here is especially challenging because these tests are ordered; if $H_0^{(i)}$ is rejected, then $H_0^{(k)}$ should be rejected for all $1 \leq k < i$. Despite the extensive literature on multiple testing and the more recent developments on FDR control and its variants (e.g., Benjamini and Hochberg, 1995; Benjamini and Yekutieli, 2001; Benjamini, 2010a,b), no definitive procedure has been available for error control in ordered tests until the recent work of G'Sell et al. (2016).

We adapt the stopping rules of G'Sell et al. (2016) to the sequential testing of (ordered) null hypotheses H_1, \dots, H_l . Let $p_1, \dots, p_l \in [0, 1]$ be the corresponding p-values of the l hypotheses. G'Sell et al. (2016) transform the sequence of p-values to a monotone sequence and then apply the original method of Benjamini and Hochberg (1995) on the monotone sequence. Two rejection rules are constructed, each of which returns a cutoff \hat{k} such that $H_1, \dots, H_{\hat{k}}$ are rejected. If no $\hat{k} \in \{1, \dots, l\}$ exists, then no rejection is made. The first is called ForwardStop (2.4) and the second StrongStop (2.5). In the notation of (2.4) and (2.5), m refers to the total number of tests to be performed, which is equivalent to the number of hypotheses, l .

Under the assumption of independence among the tests, both rules were shown to control the FDR at level α . In our setting, stopping at k implies that goodness-of-fit of the GPD to the exceedances at the first k thresholds $\{u_1, \dots, u_k\}$ is rejected. In other words, the first set of k null hypotheses $\{H_1, \dots, H_k\}$ are rejected. At each $H_0^{(i)}$, ForwardStop is a transformed average of the previous and current p-values, while StrongStop only accounts for the current and subsequent p-values. StrongStop provides

an even stronger guarantee of error control; that is that the FWER is controlled at level α . The tradeoff for stronger error control is reduced power to reject. Thus, the StrongStop rule tends to select a lower threshold than the ForwardStop rule. This is expected since higher thresholds are more likely to approximate the GPD well, and thus provide higher p-values. In this sense, ForwardStop could be thought of as more conservative (i.e., stopping at higher threshold by rejecting more thresholds).

The stopping rules, combined with the sequential hypothesis testing, provide an automated selection procedure — all that is needed are the levels of desired control for the ForwardStop and StrongStop procedures, and a set of thresholds. A caveat is that the p-values of the sequential tests here are dependent, unlike the setup of G'Sell et al. (2016). Nonetheless, the stopping rules may still provide some reasonable error control as their counter parts in the non-sequential multiple testing scenario (Benjamini and Yekutieli, 2001; Blanchard and Roquain, 2009). A simulation study is carried out in Section 3.4 to assess the empirical properties of the two rules.

3.3 The Tests

The automated procedure can be applied with any valid test for each hypothesis $H_0^{(i)}$ corresponding to threshold u_i . Four existing goodness-of-fit tests that can be used are presented. Because the stopping rules are based on transformed p-values, it is desirable to have testing statistics whose p-values can be accurately measured; bootstrap based

tests that put a lower bound on the p-values (1 divided by the bootstrap sample size) may lead to premature stopping. For the remainder of this section, the superscript i is dropped. We consider the goodness-of-fit of GPD to a sample of size n of exceedances $Y = X - u$ above a fixed threshold u .

3.3.1 Anderson–Darling and Cramér–von Mises Tests

The Anderson–Darling and the Cramér–von Mises tests for the GPD have been studied in detail (Choulakian and Stephens, 2001). Let $\hat{\theta}_n$ be the maximum likelihood estimator (MLE) of θ under H_0 from the the observed exceedances. Make the probability integral transformation based on $\hat{\theta}_n$ $z_{(i)} = F(y_{(i)}|\hat{\theta}_n)$, as in (1.4), for the order statistics of the exceedances $y_{(1)} < \dots < y_{(n)}$. The Anderson–Darling statistic is

$$A_n^2 = -n - \frac{1}{n} \sum_{i=1}^n (2i-1) \left[\log(z_{(i)}) + \log(1 - z_{(n+1-i)}) \right]. \quad (3.1)$$

The Cramér–von Mises statistic is

$$W_n^2 = \sum_{i=1}^n \left[z_{(i)} - \frac{2i-1}{2n} \right]^2 + \frac{1}{12n}. \quad (3.2)$$

The asymptotic distributions of A_n^2 and W_n^2 are unwieldy, both being sum of weighted chi-squared variables with one degree of freedom with weight found from the eigenvalues of an integral equation (Choulakian and Stephens, 2001, Section 6). The distributions

depend only on the estimate of ξ . The tests are often applied by referring to a table of a few upper tail percentiles of the asymptotic distributions (Choulakian and Stephens, 2001, Table 2), or through bootstrap. In either case, the p-values are truncated by a lower bound. Such truncation of a smaller p-value to a larger one can be proven to weaken the stopping rules given in (2.4) and (2.5). In order to apply these tests in the automated sequential setting, more accurate p-values for the tests are needed.

We provide two remedies to the table in Choulakian and Stephens (2001). First, for ξ values in the range of $(-0.5, 1)$, which is applicable for most applications, we enlarge the table to a much finer resolution through a pre-set Monte Carlo method. For each ξ value from -0.5 to 1 incremented by 0.1 , $2,000,000$ replicates of A_n^2 and W_n^2 are generated with sample size $n = 1,000$ to approximate their asymptotic distributions. A grid of upper percentiles from 0.999 to 0.001 for each ξ value is produced and saved in a table for future fast reference. Therefore, if $\hat{\xi}_n$ and the test statistic falls in the range of the table, the p-value is computed via log-linear interpolation.

The second remedy is for observed test statistics that are greater than that found in the table (implied p-value less than 0.001). As Choulakian pointed out (in a personal communication), the tails of the asymptotic distributions are exponential, which can be confirmed using the available tail values in the table. For a given $\hat{\xi}$, regressing $-\log(\text{p-value})$ on the upper tail percentiles in the table, for example, from 0.05 to 0.001 , gives a linear model that can be extrapolated to approximate the p-value of statistics outside of the range of the table. This approximation of extremely small p-values help

reduce loss of power in the stopping rules.

The two remedies make the two tests very fast and are applicable for most applications with $\xi \in (-0.5, 1)$. For ξ values outside of $(-0.5, 1)$, although slow, one can use parametric bootstrap to obtain the distribution of the test statistic, understanding that the p-value has a lower bound. The methods are implemented in R package `eva` (Bader and Yan, 2016).

3.3.2 Moran's Test

Moran's goodness-of-fit test is a byproduct of the maximum product spacing (MPS) estimation for estimating the GPD parameters. MPS is a general method that allows efficient parameter estimation in non-regular cases where the MLE fails or the information matrix does not exist (Cheng and Amin, 1983). It is based on the fact that if the exceedances are indeed from the hypothesized distribution, their probability integral transformation would behave like a random sample from the standard uniform distribution. Consider the ordered exceedances $y_{(1)} < \dots < y_{(n)}$. Define the spacings as

$$D_i(\theta) = F(y_{(i)}|\theta) - F(y_{(i-1)}|\theta)$$

for $i = 1, 2, \dots, n+1$ with $F(y_{(0)}|\theta) \equiv 0$ and $F(y_{(n+1)}|\theta) \equiv 1$. The MPS estimators are then found by minimizing

$$M(\theta) = - \sum_{i=1}^{n+1} \log D_i(\theta). \quad (3.3)$$

As demonstrated in Wong and Li (2006), the MPS method is especially useful for GPD estimation in the non-regular cases of Smith (1985). In cases where the MLE exists, the MPS estimator may have an advantage of being numerically more stable for small samples, and have the same properties as the MLE asymptotically.

The objective function evaluated at the MPS estimator $\check{\theta}$ is Moran's statistic (Moran, 1953). Cheng and Stephens (1989) showed that under the null hypothesis, Moran's statistic is normally distributed and when properly centered and scaled, has an asymptotic chi-square approximation. Define

$$\begin{aligned}\mu_M &= (n+1)(\log(n+1) + \gamma) - \frac{1}{2} - \frac{1}{12(n+1)}, \\ \sigma_M^2 &= (n+1) \left(\frac{\pi^2}{6} - 1 \right) - \frac{1}{2} - \frac{1}{6(n+1)},\end{aligned}$$

where γ is Euler's constant. Moran's goodness-of-fit test statistic is

$$T(\check{\theta}) = \frac{M(\check{\theta}) + 1 - C_1}{C_2}, \tag{3.4}$$

where $C_1 = \mu_M - (n/2)^{\frac{1}{2}}\sigma_M$ and $C_2 = (2n)^{-\frac{1}{2}}\sigma_M$. Under the null hypothesis, $T(\check{\theta})$ asymptotically follows a chi-square distribution with n degrees of freedom. Wong and Li (2006) show that for GPD data, the test empirically holds its size for samples as small as ten.

3.3.3 Rao's Score Test

Northrop and Coleman (2014) considered a piecewise constant specification of the shape parameter as the alternative hypothesis. For a fixed threshold u , a set of k higher thresholds are specified to generate intervals on the support space. That is, for the set of thresholds $u_0 = u < u_1 < \dots < u_k$, the shape parameter is given a piecewise representation

$$\xi(x) = \begin{cases} \xi_i & u_i < x \leq u_{i+1} \quad i = 0, \dots, k-1, \\ \xi_k & x > u_k. \end{cases} \quad (3.5)$$

The null hypothesis is tested as $H_0 : \xi_0 = \xi_1 = \dots = \xi_k$. Rao's score test has the advantage that only restricted MLE $\tilde{\theta}$ under H_0 is needed, in contrast to the asymptotically equivalent likelihood ratio test or Wald test. The testing statistic is

$$S(\tilde{\theta}) = U(\tilde{\theta})^T I^{-1}(\tilde{\theta}) U(\tilde{\theta}),$$

where U is the score function and I is the fisher information matrix, both evaluated at the restricted MLE $\tilde{\theta}$. Given that $\xi > -0.5$ (Smith, 1985), the asymptotic null distribution of S is χ_k^2 .

Northrop and Coleman (2014) tested suitable thresholds in an ascending manner, increasing the initial threshold u and continuing the testing of H_0 . They suggested two possibilities for automation. First, stop testing as soon as an acceptance occurs, but the p-values are not guaranteed to be non-decreasing for higher starting thresholds. Second,

stop as soon as all p-values for testing at subsequent higher thresholds are above a certain significance level. The error control under multiple, ordered testing were not addressed.

3.3.4 A Power Study

The power of the four goodness-of-fit tests are examined in an individual, non-sequential testing framework. The data generating schemes in Choulakian and Stephens (2001) are used, some of which are very difficult to distinguish from the GPD:

- Gamma with shape 2 and scale 1.
- Standard lognormal distribution (mean 0 and scale 1 on log scale).
- Weibull with scale 1 and shape 0.75.
- Weibull with scale 1 and shape 1.25.
- 50/50 mixture of $\text{GPD}(1, -0.4)$ and $\text{GPD}(1, 0.4)$.
- 50/50 mixture of $\text{GPD}(1, 0)$ and $\text{GPD}(1, 0.4)$.
- 50/50 mixture of $\text{GPD}(1, -0.25)$ and $\text{GPD}(1, 0.25)$.

Finally, the $\text{GPD}(1, 0.25)$ was also used to check the empirical size of each test. Four sample sizes were considered: 50, 100, 200, 400. For each scenario, 10,000 samples are generated. The four tests were applied to each sample, with a rejection recorded if the p-value is below 0.05. For the score test, a set of thresholds were set according to the deciles of the generated data.

Table 3.1: Empirical rejection rates of four goodness-of-fit tests for GPD under various data generation schemes described in Section 3.3.4 with nominal size 0.05. GPDMix(a, b) refers to a 50/50 mixture of GPD(1, a) and GPD(1, b).

| Sample Size | 50 | | | | 100 | | | |
|---------------------|-------|-------|------|------|-------|-------|------|------|
| Test | Score | Moran | AD | CVM | Score | Moran | AD | CVM |
| Gamma(2, 1) | 7.6 | 9.7 | 47.4 | 43.5 | 8.0 | 14.3 | 64.7 | 59.7 |
| LogNormal | 6.0 | 5.9 | 13.3 | 8.6 | 5.4 | 8.2 | 28.3 | 23.4 |
| Weibull(0.75) | 11.5 | 7.8 | 55.1 | 23.5 | 12.1 | 9.5 | 65.1 | 39.4 |
| Weibull(1.25) | 6.6 | 11.3 | 29.1 | 27.3 | 5.6 | 12.5 | 20.8 | 19.2 |
| GPDMix(−0.4, 0.4) | 11.4 | 7.5 | 19.2 | 9.9 | 16.0 | 8.6 | 24.3 | 20.4 |
| GPDMix(0, 0.4) | 7.8 | 6.0 | 6.5 | 5.9 | 7.4 | 5.9 | 9.6 | 5.6 |
| GPDMix(−0.25, 0.25) | 8.1 | 6.5 | 6.0 | 7.4 | 8.9 | 6.5 | 11.1 | 8.4 |
| GPD(1, 0.25) | 6.9 | 5.5 | 6.7 | 6.1 | 5.0 | 5.2 | 5.2 | 5.2 |

| Sample Size | 200 | | | | 400 | | | |
|---------------------|-------|-------|------|------|-------|-------|-------|-------|
| Test | Score | Moran | AD | CVM | Score | Moran | AD | CVM |
| Gamma(2, 1) | 15.4 | 23.3 | 95.3 | 93.1 | 36.5 | 42.2 | 100.0 | 100.0 |
| LogNormal | 5.7 | 11.9 | 69.3 | 59.7 | 7.9 | 19.1 | 97.8 | 95.0 |
| Weibull(0.75) | 16.5 | 10.7 | 84.8 | 66.4 | 32.1 | 14.6 | 98.2 | 93.0 |
| Weibull(1.25) | 8.0 | 14.7 | 40.9 | 36.7 | 15.5 | 19.2 | 79.8 | 74.6 |
| GPDMix(−0.4, 0.4) | 31.5 | 9.7 | 45.1 | 44.0 | 63.8 | 11.9 | 79.9 | 80.2 |
| GPDMix(0, 0.4) | 8.9 | 6.5 | 8.8 | 7.3 | 12.3 | 6.2 | 10.8 | 10.3 |
| GPDMix(−0.25, 0.25) | 13.9 | 6.7 | 16.6 | 14.8 | 26.2 | 7.9 | 33.0 | 32.4 |
| GPD(1, 0.25) | 5.3 | 5.8 | 7.2 | 5.2 | 4.7 | 5.3 | 5.8 | 4.7 |

The rejection rates are summarized in Table 3.1. Samples in which the MLE failed were removed, which accounts for roughly 10.8% of the Weibull samples with shape 1.25 and sample size 400, and around 10.7% for the Gamma distribution with sample size 400. Decreasing the sample size in these cases actually decreases the percentage of failed MLE samples. This may be due to the shape of these two distributions, which progressively become more distinct from the GPD as their shape parameters increase. In the other distribution cases, no setting resulted in more than a 0.3% failure rate. As expected,

all tests appear to hold their sizes, and their powers all increase with sample size. The mixture of two GPDs is the hardest to detect. For the GPD mixture of shape parameters 0 and 0.4, quantile matching between a single large sample of generated data and the fitted GP distribution shows a high degree of similarity. In the vast majority of cases, the Anderson–Darling test appears to have the highest power, followed by the Cramér–von Mises test. Between the two, the Anderson–Darling statistic is a modification of the Cramér–von Mises statistic giving more weight to observations in the tail of the distribution, which explains the edge of the former.

3.4 Simulation Study of the Automated Procedures

The empirical properties of the two stopping rules for the Anderson–Darling test are investigated in simulation studies. To check the empirical FWER of the StrongStop rule, data only need to be generated under the null hypothesis. For $n \in \{50, 100, 200, 400\}$, $\xi \in \{-0.25, 0.25\}$, $\mu = 0$, and $\sigma = 1$, 10,000 GPD samples were generated in each setting of these parameters. Ten thresholds are tested by locating ten percentiles, 5 to 50 by 5. Since the data is generated from the GPD, data above each threshold is also distributed as GP, with an adjusted scale parameter. Using the StrongStop procedure and with no adjustment, the observed FWER is compared to the expected rates for each setting at various nominal levels. At a given nominal level and setting of the parameters, the observed FWER is calculated as the number of samples with a rejection of H_0 at any

of the thresholds, divided by the total number of samples. The results of this study can be seen in Figure 3.1.

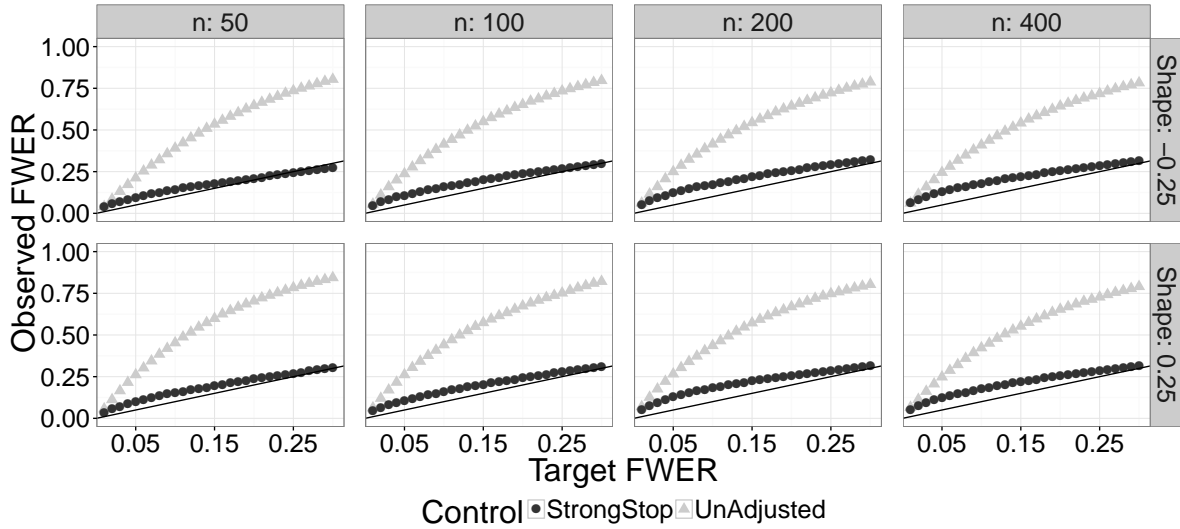


Figure 3.1: Observed FWER for the Anderson–Darling test (using StrongStop and no adjustment) versus expected FWER at various nominal levels under the null GPD at ten thresholds for 10,000 replicates in each setting as described in Section 3.4. The 45 degree line indicates agreement between the observed and expected rates under H_0 .

It can be seen that the observed FWER under H_0 using the StrongStop procedure is nearly in agreement with the expected rate at most nominal levels for the Anderson–Darling test (observed rate is always within 5% of the expected error rate). However, using the naive, unadjusted stopping rule (simply rejecting for any p-value less than the nominal level), the observed FWER is generally 2–3 times the expected rate for all sample sizes.

It is of interest to investigate the performance of the ForwardStop and StrongStop in selecting a threshold under misspecification. To check the ability of ForwardStop and StrongStop to control the false discover rate (FDR), data need to be generated under

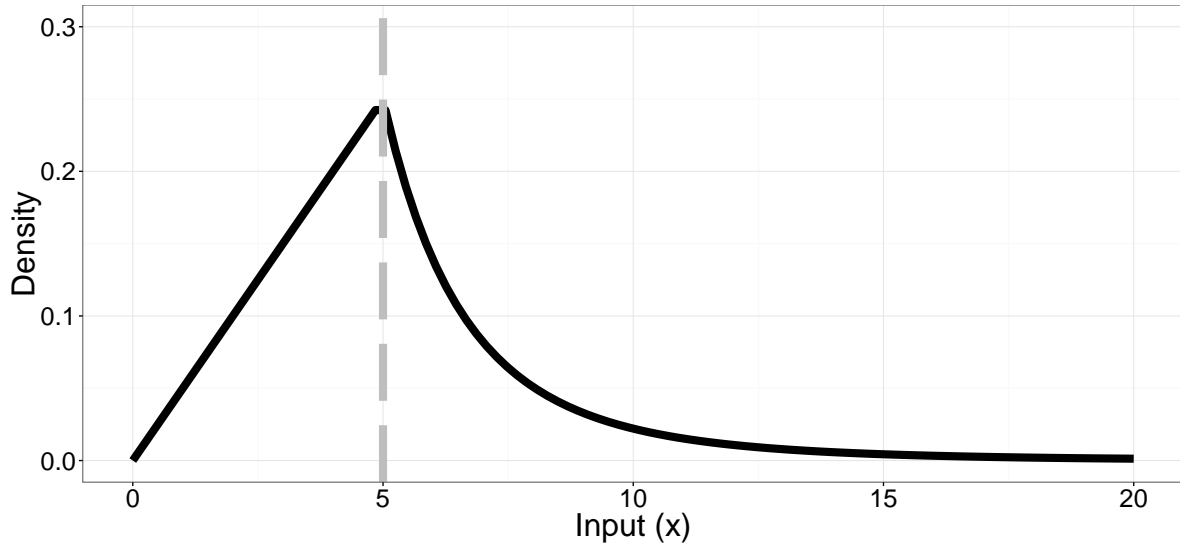


Figure 3.2: Plot of the (scaled) density of the mixture distribution used to generate misspecification of H_0 for the simulation in Section 3.4. The vertical line indicates the continuity point of the two underlying distributions.

misspecification. Consider the situation where data is generated from a 50/50 mixture of distributions. Data between zero and five are generated from a Beta distribution with $\alpha = 2$, $\beta = 1$ and scaled such that the support is on zero to five. Data above five is generated from the $\text{GPD}(\mu = 5, \sigma = 2, \xi = 0.25)$. Choosing misspecification in this way ensures that the mixture distribution is at least continuous at the meeting point. See Figure 3.2 for a visual assessment.

A total of $n = 1000$ observations are generated, with $n_1 = 500$ from the Beta distribution and $n_2 = 500$ from the GP distribution. 1000 datasets are simulated and 50 thresholds are tested, starting by using all $n = 1000$ observations and removing the 15 lowest observations each time until the last threshold uses just 250 observations. In this way, the correct threshold is given when the lowest n_1 observations are removed.

The results are presented here. The correct threshold is the 34th, since $n_1 = 500$ and $\lceil 500/15 \rceil = 34$. Rejection of less than 33 tests is problematic since it allows contaminated data to be accepted. Thus, a conservative selection criteria is desirable. Rejection of more than 33 tests is okay, although some non-contaminated data is being thrown away. By its nature, the StrongStop procedure has less power-to-reject than ForwardStop, since it has a stricter error control (FWER versus FDR).

Figure 3.3 displays the frequency distribution for threshold choice using the Anderson–Darling test at the 5% nominal level for the three stopping rules. There is a clear hierarchy in terms of power-to-reject between the ForwardStop, StrongStop, and no adjustment procedures. StrongStop, as expected, provides the least power-to-reject, with all 1000 simulations selecting a threshold below the correct one. ForwardStop is more powerful than the no adjustment procedure and on average selects a higher threshold. The median number of thresholds rejected is 33, 29, and 22 for ForwardStop, no adjustment, and StrongStop respectively.

The observed versus expected FDR using ForwardStop and the observed versus expected FWER using StrongStop using the Anderson–Darling test for the data generated under misspecification can be seen in Figure 3.4. There appears to be reasonable agreement between the expected and observed FDR rates using ForwardStop, while StrongStop has observed FWER rates well below the expected rates.

To further evaluate the performance of the combination of tests and stopping rules, it is of interest to know how well the data chosen above each threshold can estimate

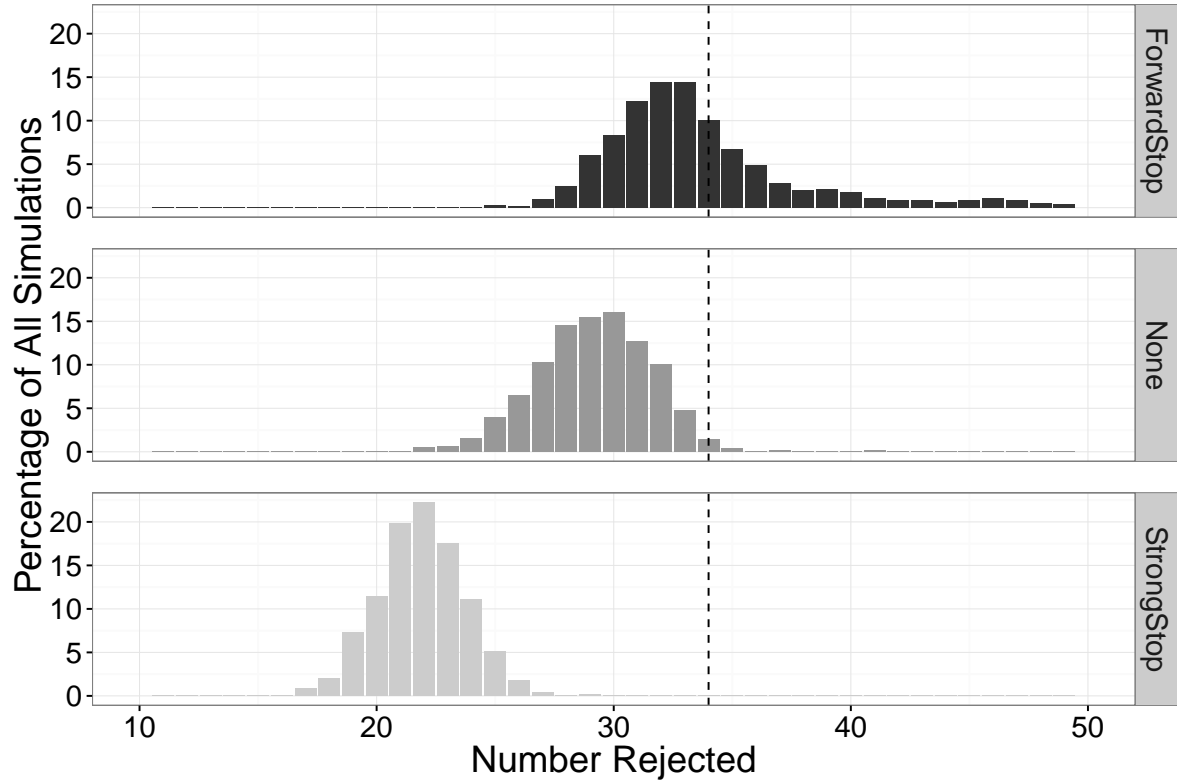


Figure 3.3: Frequency distribution (out of 1000 simulations) of the number of rejections for the Anderson–Darling test and various stopping rules (ForwardStop, StrongStop, and no adjustment), at the 5% nominal level, for the misspecified distribution sequential simulation setting described in Section 3.4. 50 thresholds are tested, with the 34th being the true threshold.

parameters of interest. Two such parameters are the shape and return level. The N year return level for the GPD (e.g., Coles, 2001, Section 4.3.3) is given by

$$z_N = \begin{cases} u + \frac{\sigma}{\xi} [(Nn_y\zeta_u)^\xi - 1], & \xi \neq 0, \\ u + \sigma \log(Nn_y\zeta_u), & \xi = 0, \end{cases} \quad (3.6)$$

for a given threshold u , where n_y is the number of observations per year, and ζ_u is the

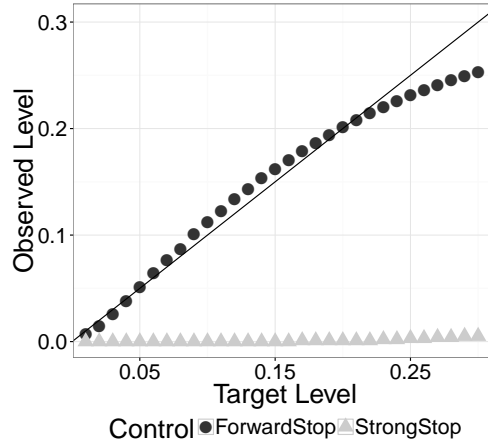


Figure 3.4: Observed FDR (using ForwardStop) and observed FWER (using StrongStop) versus expected FDR and FWER respectively using the Anderson–Darling test, at various nominal levels. This is for the sequential simulation setting under misspecification described in Section 3.4. The 45 degree line indicates agreement between the observed and expected rates.

rate, or proportion of the data exceeding u . The rate parameter has a natural estimator simply given by the number of exceeding observations divided by the total number of observations. A confidence interval for z_N can easily be found using the delta method, or preferably and used here, profile likelihood. The ‘true’ return levels are found by letting $u = 34$, $n_y = 365$, and treating the data as the tail of some larger dataset, which allows computation of the rate ζ_u for each threshold.

For ease of presentation, focus will be on the performance of the Anderson–Darling test in conjunction with the three stopping rules. In each of the 1000 simulated datasets (seen in Figure 3.2), the threshold selected for each of the three stopping rules is used to determine the bias, squared error, and confidence interval coverage (binary true/false) for the shape parameter and 50, 100, 250, and 500 year return levels. An average of the

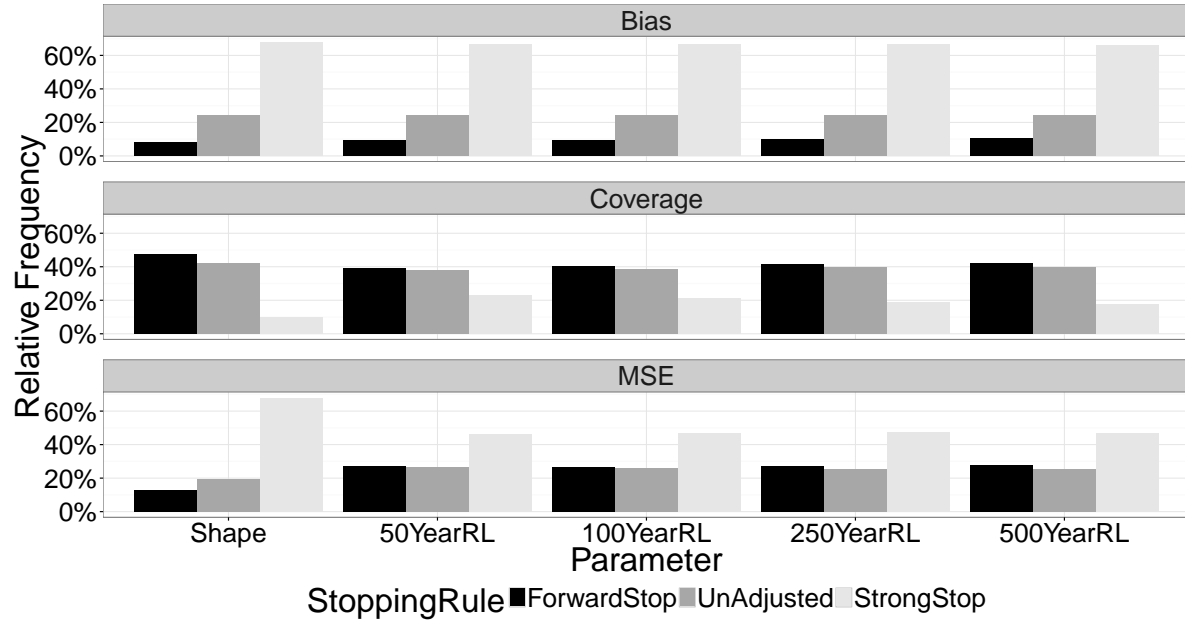


Figure 3.5: Average performance comparison of the three stopping rules in the simulation study under misspecification in Section 3.4, using the Anderson–Darling test for various parameters. Shown are the relative frequencies of the average value of each metric (bias, squared error, and coverage) for each stopping rule and parameter of interest. For each parameter of interest and metric, the sum of average values for the three stopping rules equates to 100%. RL refers to return level.

bias, squared error, and coverage across the 1000 simulations is taken, for each stopping rule and parameter value. For each parameter and statistic of interest (mean bias, mean squared error (MSE), and mean coverage), a relative percentage is calculated for the three stopping rules. A visual assessment of this analysis is provided in Figure 3.5.

It is clear from the result here that ForwardStop is the most preferable stopping rule in application. For all parameters, it has the smallest average bias (by a proportion of 2-1) and highest coverage rate. In addition, the MSE is comparable or smaller than the unadjusted procedure in all cases. Arguably, StrongStop has the worst performance,

obtaining the highest average bias and MSE, and the lowest coverage rates for all parameters. Replacing the Anderson–Darling test with the other tests provides similar results (not shown here).

3.5 Application to Return Level Mapping of Extreme Precipitation

One particularly useful application of the automated threshold selection method is generating an accurate return level map of extreme precipitation in the three western US coastal states of California, Oregon, and Washington. The automated procedure described in Section 3.2 provides a method to quickly obtain an accurate map without the need for visual diagnostics at each site. Return level maps are of great interest to hydrologists (Katz et al., 2002) and can be used for risk management and land planning (Blanchet and Lehning, 2010; Lateltin and Bonnard, 1999).

Daily precipitation data is available for tens of thousands of surface sites around the world via the Global Historical Climatology Network (GHCN). A description of the data network can be found in Menne et al. (2012). After an initial screening to remove sites with less than 50 years of available data, there are 720 remaining sites across the three chosen coastal states.

As the annual maximum daily amount of precipitation mainly occurs in winter, only the winter season (November - March) observations are used in modeling. A set of

thresholds for each site are chosen based on the data percentiles; for each site the set of thresholds is generated by taking the 75th to 97th percentiles in increments of 2, then in increments of 0.1 from the 97th to 99.5th percentile. This results in 37 thresholds to test at each site. If consecutive percentiles result in the same threshold due to ties in data, only one is used to guarantee uniqueness of thresholds and thus reducing the total number of thresholds tested at that site.

As discussed in the beginning of Section 3.2, modeling the exceedances above a threshold with the Generalized Pareto requires the exceedances to be independent. This is not always the case with daily precipitation data; a large and persistent synoptic system can bring large storms successively. The extremal index is a measure of the clustering of the underlying process at extreme levels. Roughly speaking, it is equal to $(\text{limiting mean cluster size})^{-1}$. It can take values from 0 to 1, with independent series exhibiting a value of exactly 1. To get a sense for the properties of series in this dataset, the extremal index is calculated for each site using the 75th percentile as the threshold via the R package `texmex` (Southworth and Heffernan, 2013). In summary, the median estimated extremal index for all 720 sites is 0.9905 and 97% of the sites have an extremal index above 0.9. Thus, we do not do any declustering on the data. A more thorough description of this process can be found in Ferro and Segers (2003) and Heffernan and Southworth (2012).

The Anderson–Darling test is used to test the set of thresholds at each of the 720 sites, following the procedure outlined in Section 3.3.1. This is arguably the most powerful test

out of the four examined in Section 3.3.4. Three stopping rules are used — ForwardStop, StrongStop, and with no adjustment, which proceeds in an ascending manner until an acceptance occurs. Figure 3.6 shows the distribution of chosen percentiles for the 720 sites using each of the three stopping rules.

As expected, ForwardStop is the most conservative, rejecting all thresholds at 348 sites, with the unadjusted procedure rejecting 63, and StrongStop only rejecting all thresholds at 3 sites. Figure 3.7 shows the geographic representation of sites in which all thresholds are rejected. Note that there is a pattern of rejections by ForwardStop, particularly in the eastern portion of Washington and Oregon, and the Great Valley of California. This may be attributed to the climate differences in these regions – rejected sites had a smaller number of average rain days than non-rejected sites (30 vs. 34), as well as a smaller magnitude of precipitation (an average of 0.62cm vs. 1.29cm). The highly selective feature of the ForwardStop procedure is desired as it suggests not to fit GPD at even the highest threshold at these sites, a guard that is not available from those unconditionally applied, one-for-all rules. Further investigation is needed for the sites in which all thresholds were rejected; one possibility is to consider a generalization of the GPD in these cases.

For the sites at which a threshold was selected for both the ForwardStop and StrongStop rules, the return level estimates based on the chosen threshold for each stopping rule can be compared. The result of this comparison can be seen in Figure 3.8. For a smaller return period (50 years), the agreement between estimates for the two stopping rules is

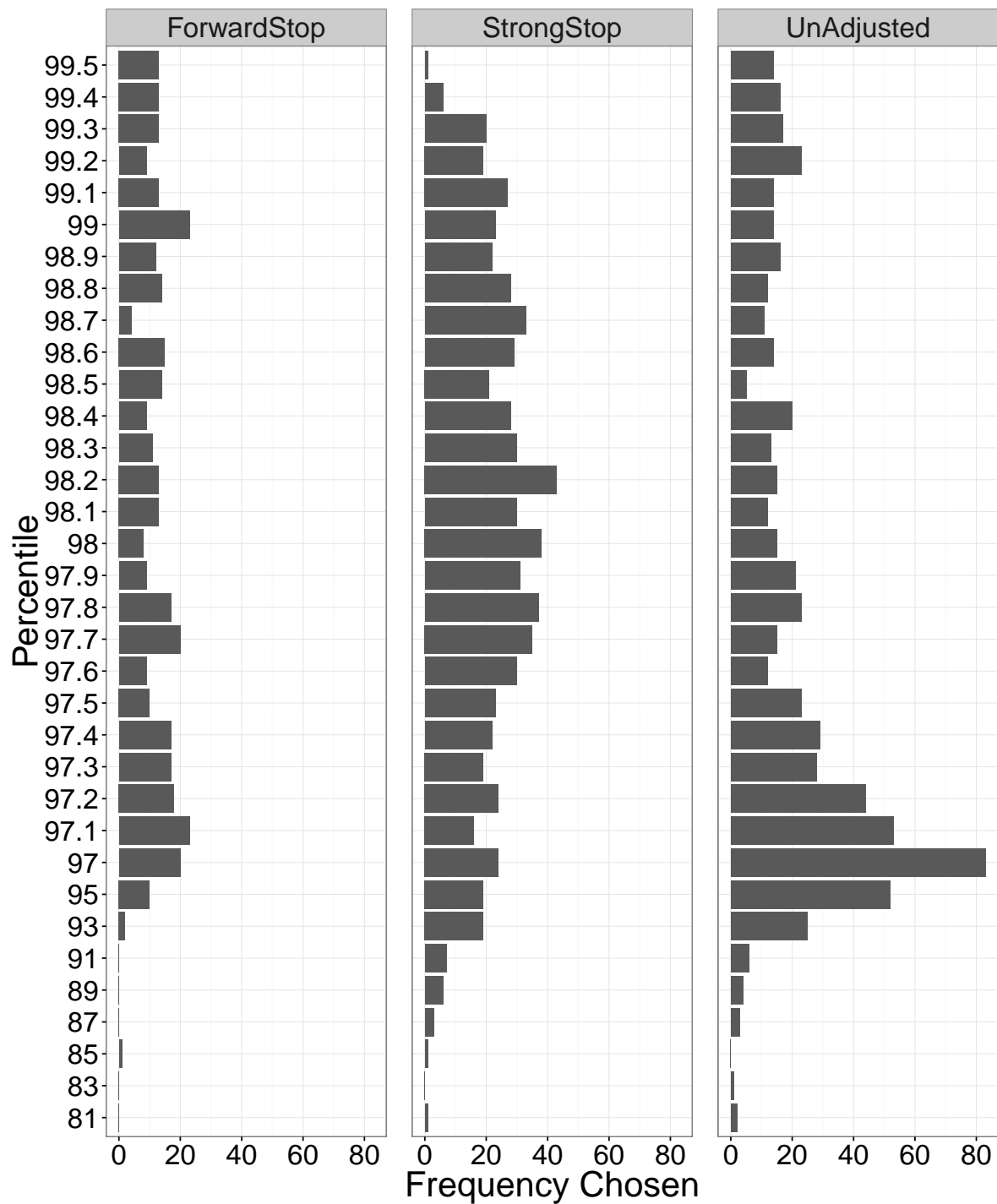


Figure 3.6: Distribution of chosen percentiles (thresholds) for the 720 western US coastal sites, as selected by each stopping rule. Note that this does not include sites where all thresholds were rejected by the stopping rule.

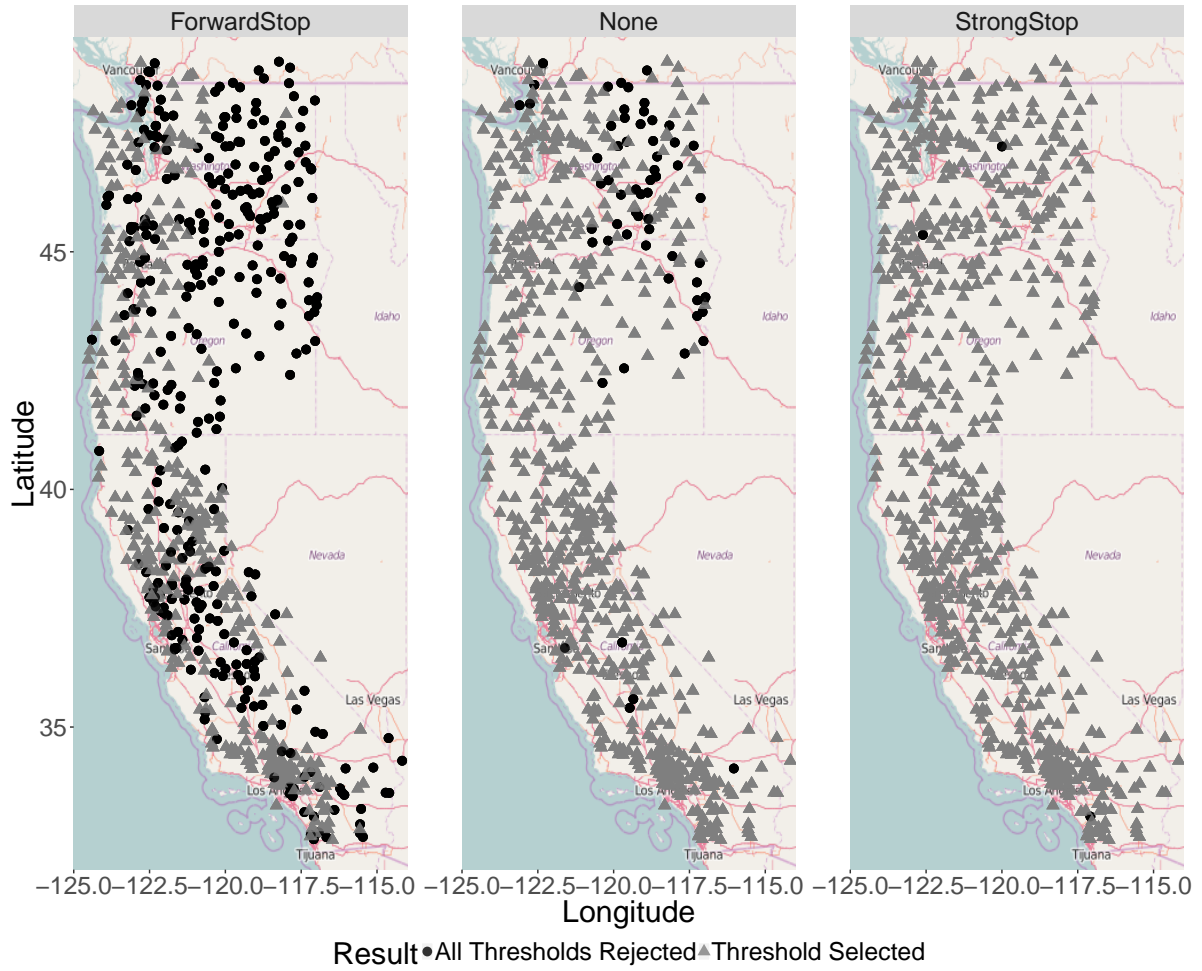


Figure 3.7: Map of US west coast sites for which all thresholds were rejected (black / circle) and for which a threshold was selected (grey / triangle), by stopping rule.

quite high. This is a nice confirmation to have confidence in the analysis, however it is slightly misleading in that it does not contain the sites rejected by ForwardStop.

The end result of this automated batch analysis provides a map of return level estimates. The 50, 100, and 250 year map of return level estimates from threshold selection using ForwardStop and the Anderson–Darling test can be seen in Figure 3.9. To provide an estimate at any particular location in this area, some form of interpolation

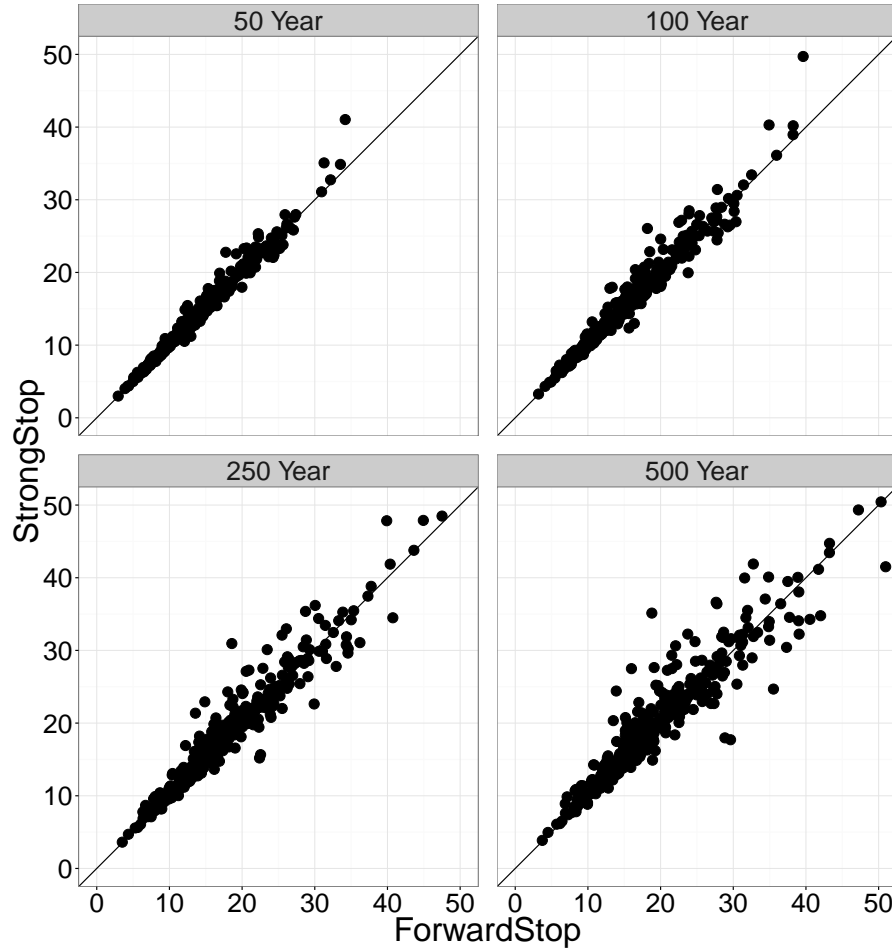


Figure 3.8: Comparison of return level estimates (50, 100, 250, 500 year) based on the chosen threshold for ForwardStop vs. StrongStop for the US west coast sites. The 45 degree line indicates agreement between the two estimates. This is only for the sites in which both stopping rules did not reject all thresholds.

can be applied.

3.6 Discussion

We propose an intuitive and comprehensive methodology for automated threshold selection in the peaks over threshold approach. In addition, it is not as computationally

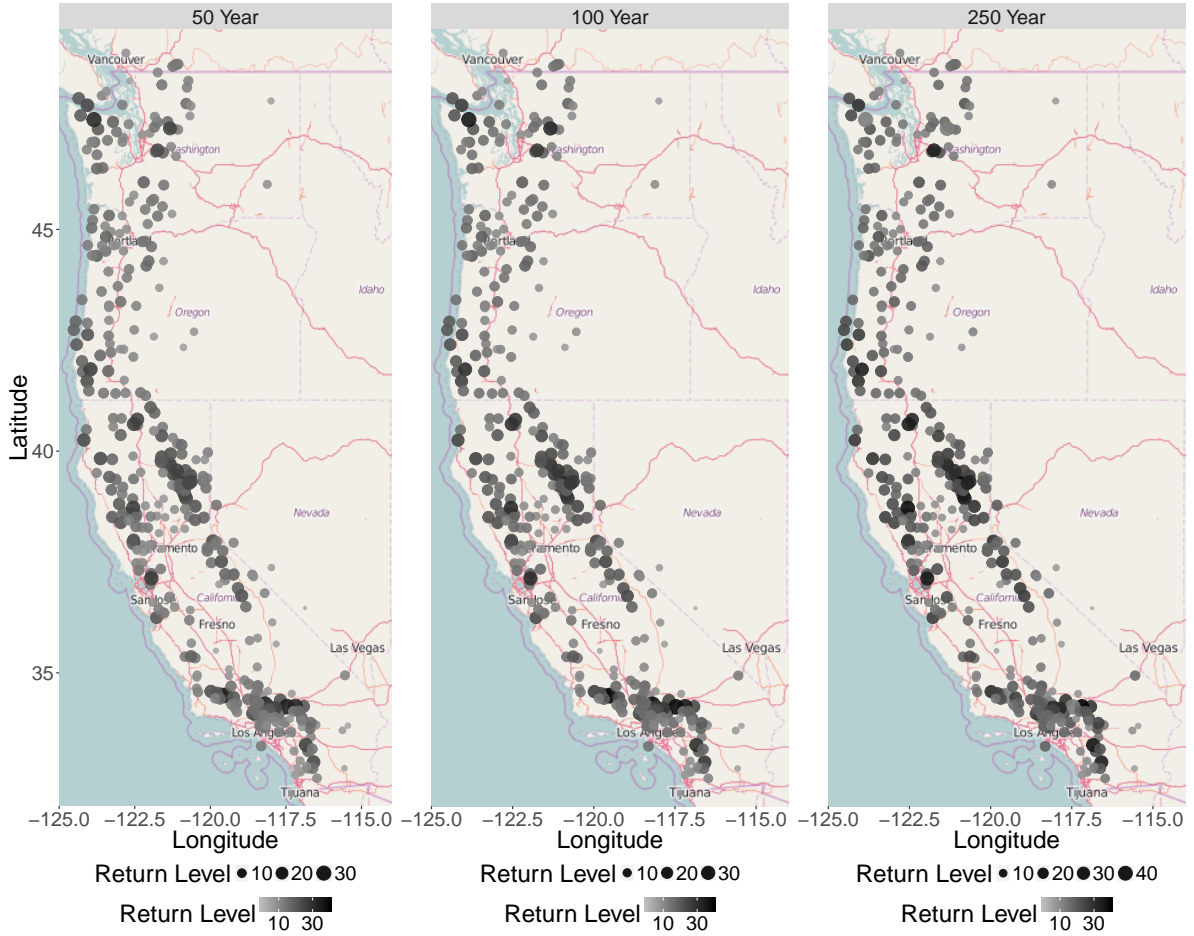


Figure 3.9: Map of US west coast sites with 50, 100, and 250 year return level estimates for the threshold chosen using ForwardStop and the Anderson–Darling test. This is only for the sites in which a threshold was selected.

intensive as some competing resampling or bootstrap procedures (Danielsson et al., 2001; Ferreira et al., 2003). Automation and efficiency is required when prediction using the peaks over threshold approach is desired at a large number of sites. This is achieved through sequentially testing a set of thresholds for goodness-of-fit to the generalized Pareto distribution (GPD). Previous instances of this sequential testing procedure did not account for the multiple testing issue. We apply two recently developed stopping

rules (G'Sell et al., 2016) ForwardStop and StrongStop, that control the false discovery rate and familywise error rate, respectively in the setting of (independent) ordered, sequential testing. It is a novel application of them to the threshold selection problem. There is a slight caveat in our setting, that the tests are not independent, but it is shown via simulation that these stopping rules still provide reasonable error control here.

Four tests are compared in terms of power to detect departures from the GPD at a single, fixed threshold and it is found that the Anderson–Darling test has the most power in various non-null settings. Choulakian and Stephens (2001) derived the asymptotic null distribution of the Anderson–Darling test statistic. However this requires solving an integral equation. Our contribution, with some advice from the author, provides an approximate, but accurate and computationally efficient version of this test. To investigate the performance of the stopping rules in conjunction with the Anderson–Darling test, a large scale simulation study was conducted. Data is generated from a plausible distribution – misspecified below a certain threshold and generated from the null GPD above. In each replicate, the bias, coverage, and squared error is recorded for the stopping threshold of each stopping rule for various parameters.

The results of this simulation suggest that the ForwardStop procedure has on average the best performance using the aforementioned metrics. Thus, a recommendation would be to use the Anderson–Darling test, in unison with the ForwardStop procedure for error control to test a fixed set of thresholds. The methodology is applied to daily precipitation data at hundreds of sites in three U.S. west coast states, with the goal of

creating a return level map.

Chapter 4

Robust and Efficient Estimation in Non-Stationary RFA

4.1 Introduction

Regional frequency analysis (RFA) is commonly used when historical records are short, but are available at multiple sites within a homogeneous region. Sites within a homogeneous region are assumed to possess similar characteristics (defined in Section 4.2). From this assumption, with some care, the data can essentially be pooled in order to estimate the shared parameters across sites. By doing so, efficiency in the shared parameter estimation is greatly improved when record length is short. Various models can be used within this context, depending on the application and outcome variable. One area of application is to model extremes, such as maximum precipitation or wind speeds. For this, the Generalized Extreme Value (GEV) distribution is a natural model choice and will be focused on in this paper.

There have been many applications of RFA with non-stationarity modeled through

external covariates; see Khaliq, Ouarda, Ondo, Gachon, and Bobée (2006) for a review in the one sample case. The most common estimation method is maximum likelihood estimation (MLE), typically with climate indices and temporal trends as covariates; see (Katz et al., 2002; López and Francés, 2013; Hanel et al., 2009; Leclerc and Ouarda, 2007; Nadarajah, 2005) as examples. The MLE has some nice properties, in that the model parameters and covariates can easily be adjusted, and standard errors are provided implicitly when maximizing the likelihood function. There are some drawbacks however; the MLE can provide absurd estimates of the shape parameter or fail entirely, typically in small samples.

Coles and Dixon (1999) develop a penalized maximum likelihood estimator that still has the flexibility of the traditional MLE, but has better performance in small samples. Martins and Stedinger (2000) propose a generalized maximum likelihood (GML) method which imposes a prior distribution on the shape parameter to restrict its estimates to plausible values within the GEV model. El Adlouni, Ouarda, Zhang, Roy, and Bobée (2007) applied the GML approach with non-stationarity, via temporal trends in the parameters. Note that both of these approaches are only explicitly developed here for the one sample case. At the time of writing, it appears that neither of these approaches have been applied to the RFA setting.

In the stationary RFA model, L-moments can be used as an alternative to MLE. The L-moment approach (Hosking et al., 1985) estimates the parameters by matching the sample moments with their population counterparts and then solving the system

of equations. It has the advantage over MLE in that it only requires the existence of the mean, and has been shown to be more efficient in small samples (Hosking et al., 1985). Hosking and Wallis (1988) show that any bias in the parameter estimates is unaffected by intersite dependence. To apply the L-moment method in the stationary RFA model, the site-specific scaling parameter is estimated, then the data is scaled and pooled across sites. Afterwards, the shared, across site parameters can be estimated from the pooled data. This method is widespread; see Smithers and Schulze (2001); Kumar and Chatterjee (2005); Kjeldsen, Smithers, and Schulze (2002) for examples.

It is not straightforward to extend this methodology to the non-stationary case; in particular when non-site specific covariates are used, moment matching may not be possible. One approach to estimate time trends is by applying the stationary L-moment approach over sliding time windows (Kharin and Zwiers, 2005; Kharin et al., 2013); that is, estimate the stationary parameters in t -year periods and look for changes between each. In the one sample case, there has been some progress to combine non-stationarity and L-moment estimation. Ribereau et al. (2008) provide a method to incorporate covariates in the location parameter, by estimating the covariates first via least squares, and then transforming the data to be stationary in order to estimate the remaining parameters via L-moments. Coles and Dixon (1999) briefly discuss an iterative procedure to estimate covariates through maximum likelihood and stationary parameters through L-moments.

Two new approaches are implemented here for estimation in the RFA setting with

non-stationarity. The first uses maximum product spacing (MPS) estimation (Cheng and Amin, 1983), which maximizes the geometric mean of spacings in the data. It is as efficient as maximum likelihood estimation and since it only relies on the cumulative density function, it can provide estimators when MLE fails. It can easily incorporate covariates in the objective function as well. The second approach builds on the ideas of Coles and Dixon (1999) and Ribereau et al. (2008), providing extensions to a hybrid estimation procedure (L-moment / MLE) in the RFA framework. Both of these methods are shown to outperform MLE in terms of root mean squared error (RMSE), through a large scale simulation of spatially dependent data. To illustrate the differences in the three estimation methods, a non-stationary regional frequency model is applied to extreme precipitation events at rain gauge sites in California. To account for spatial dependence, a semi-parametric bootstrap procedure is applied to obtain standard errors for all the estimators.

Section 4.2 discusses the model and existing methods of estimation within this framework. Section 4.3 introduces the two new estimation methods and implementation in the RFA setting. A large scale simulation study of homogeneous multi-site data generated under various extremal and non-extremal spatial dependence settings is carried out in Section 4.4 to establish the superiority of the new estimation methods over MLE. In Section 4.5 a real analysis of extreme precipitation at 27 sites in California is conducted to examine the effect of El Niño–Southern Oscillation on these events. Lastly, a discussion is provided in Section 4.6.

4.2 Non-Stationary Homogeneous Region Model

In regional frequency analysis, data from a number of sites within a homogeneous region can be pooled together in a particular way to improve the reliability and efficiency of parameter estimates within a model. Suppose there exist m sites in a homogeneous region, over n periods. Define Y_{st} to be the observation at site $s \in \{1, \dots, m\}$ in period $t \in \{1, \dots, n\}$. Observations from period to period are assumed to be independent, but observations from sites within the same period exhibit some form of spatial dependence. The type of spatial dependence will be defined explicitly later. The assumption is that each site has the full record of observations. Methodology to accommodate missing records is not straightforward – imputation would require additional assumptions and in the case of data missing completely at random (MCAR), care is still needed due to the semi-parametric bootstrap procedure necessary to obtain parameter confidence intervals. A further discussion is provided in Section 6.1.

The idea behind the flood index model is that the variables Y_{st} , after being scaled by a site specific scaling factor, are identically distributed. In other words, the T -period return level or quantile function of Y_{st} can be represented as

$$Q_t(T) = g(\mu_{st}, q_t(T))$$

where $q_t(T)$ is the non-site specific quantile function and the flood index is μ_{st} . Typically, this is chosen as the mean or median of Y_{st} . In this paper, the Generalized Extreme

Value (GEV) distribution (1.1) is used to model the extreme events at each site. It is essentially the limiting distribution of the maximum of a sequence of independent and identically distributed random variables, normalized by appropriate constants. Because of this mathematical formulation, it is a natural distribution choice to model extremes.

Formally, let $Y_{st} \sim \text{GEV}(\mu_{st}, \gamma_t \mu_{st}, \xi_t)$ where here the flood index is given by μ_{st} . It follows that $Y_{st} = \mu_{st} Z_t$ where $Z_t \sim \text{GEV}(1, \gamma_t, \xi_t)$. It is then clear that each site in the homogeneous region marginally follows a GEV distribution indexed only in terms of its location parameter, with a shared proportionality scale parameter and shape parameter.

To incorporate the non-stationarity, link functions between the covariates and parameters can be used as follows. Let

$$\begin{aligned}\mu_{st} &= f_\mu(\beta^\mu, x_{st}^\mu) \\ \gamma_t &= f_\gamma(\beta^\gamma, x_t^\gamma) \\ \xi_t &= f_\xi(\beta^\xi, x_t^\xi)\end{aligned}$$

where $f(\cdot)$ is the parameter specific link function. The set of parameters $\beta^\mu, \beta^\gamma, \beta^\xi$ and covariates $x_{st}^\mu, x_t^\gamma, x_t^\xi$ are vectors of length $(m + p_\mu), p_\gamma, p_\xi$, respectively, representing the number of covariates associated with each. The indexing in the vector of location parameters allows for each site to have its own marginal mean β_s^μ for $s = 1, \dots, m$. Covariates associated with γ and ξ must be shared across sites, while covariates associated with μ can be both shared and/or site-specific. $\mathbf{X}_{(m \cdot n) \times (m + p_\mu)}^\mu, \mathbf{X}_{n \times p_\gamma}^\gamma, \mathbf{X}_{n \times p_\xi}^\xi$ are design matrices

for the appropriate parameters, where each row represents the corresponding vector x .

To fix ideas, the following link functions and covariates will be used in the succeeding sections unless explicitly stated otherwise:

$$\begin{aligned}\mu_{st} &= x_{st}^{\mu \top} \beta^{\mu} \\ \gamma_t &= \exp \left(x_t^{\gamma \top} \beta^{\gamma} \right) \\ \xi_t &= x_t^{\xi \top} \beta^{\xi}\end{aligned}\tag{4.1}$$

which implies $\sigma_{st} = \gamma_t \mu_{st}$. Also, note that the stationary (intercept) parameters are given by $\beta_0^{\gamma}, \beta_0^{\xi}$, which are shared across all sites and β_s^{μ} , a stationary marginal mean for each site $s = 1, \dots, m$. This is similar to the model used in Hanel et al. (2009) and the exponential link in the proportionality parameter γ assures the scale parameter at each site is positive valued since μ_{st} is generally positive in application. An explicit restriction on the positiveness of the scale parameter can be enforced in the estimation procedure. In the stationary case, the subscript t is dropped, but the same model applies. This stationary model has been used previously by Buishand (1991) and Wang et al. (2014).

4.2.1 Existing Estimation Methods

Maximum Likelihood

The independence likelihood (e.g. Hanel et al., 2009; Kharin and Zwiers, 2005) seeks to maximize the log-likelihood function

$$\sum_{s=1}^m \sum_{t=1}^n \log f(y_{st} | \mu_{st}, \gamma_t \mu_{st}, \xi_t, x_{st}^\mu, x_t^\gamma, x_t^\xi)$$

where $f(\cdot)$ is the probability density function (1.2) of site s at time t . Note that estimation in this approach assumes independence between sites and only specifies the marginal density at each site. Other likelihood approaches such as a pairwise likelihood can be used, but then the dependence between sites must be specified. See Ribatet (2009) for details.

Pseudo Non-Stationary L-moments

To the best of the author's knowledge, currently there are no methods that directly incorporate L-moment estimation in the non-stationary RFA setting. Kharin et al. (2013) uses the stationary method in conjunction with moving time windows to get a sense of the trend in the parameters. That is, the data is subset into mutually exclusive time windows (say 20 years) and the stationary L-moment method is used to obtain GEV parameter estimates. This can provide some indication of non-stationarity, however it is difficult to interpret precisely.

Ribereau et al. (2008) provides methodology for mixture L-moment estimation in the one sample case with non-stationarity modeled through the location parameter. The idea is to fit a GEV regression model, where the error terms ϵ are assumed to be IID stationary $\text{GEV}(0, \sigma, \xi)$ random variables and the design matrix consists of covariates that describe the location parameter. From this regression setup, estimates for the location parameters can be found. Next, those estimates are used to transform the data to stationary “psuedo-residuals” from which estimates for σ and ξ can be obtained by a variant of L-moments.

It should be possible to extend this setup to the RFA setting by fitting a GEV regression model to data from all the sites. To handle this, the error structure can be given, for example, as

$$\begin{aligned}
Cov(\epsilon_{si}, \epsilon_{si}) &= \delta_s & i &\in \{1, \dots, n\} & s &\in \{1, \dots, m\} \\
Cov(\epsilon_{s_1 i}, \epsilon_{s_2 j}) &= 0 & i &\neq j \in \{1, \dots, n\} & s_1, s_2 &\in \{1, \dots, m\} \\
Cov(\epsilon_{s_1 i}, \epsilon_{s_2 i}) &= \rho_{s_1 s_2} & i &\in \{1, \dots, n\} & s_1 \neq s_2 &\in \{1, \dots, m\}
\end{aligned}$$

and then estimates for the non-stationary location parameters can be found using suitable methods (e.g. weighted least squares or generalized estimating equations). These ideas were not pursued here, but it may be of interest to look into in the future.

4.3 New Methods

4.3.1 Hybrid Likelihood / L-moment Approach

Our approach to handle non-stationarity in a regional frequency model using the L-moment method involves an iterative hybrid procedure. Coles and Dixon (1999) briefly discussed this approach in the one-sample case with non-stationarity in the location parameter. The procedure is as follows.

Initialize with some starting estimates for all the parameters $\beta^\mu, \beta^\gamma, \beta^\xi$.

1. Transform the variables Y_{st} (via a probability integral transformation) such that each site has a (site-specific) stationary mean and shared (across sites) stationary proportionality and shape parameters.¹ Call this transformed variable \tilde{Y}_{st} and note that $\tilde{Y}_{st} \sim \text{GEV}(\beta_s^\mu, \beta_s^\mu \exp(\beta_0^\gamma), \beta_0^\xi)$.
2. Estimate β_s^μ from the transformed data \tilde{Y}_{st} , $t = 1, \dots, n$ for each site s using the one sample stationary L-moment method. Let $\tilde{Y}'_{st} = \tilde{Y}_{st} / \hat{\beta}_s^\mu$ and note that $\tilde{Y}'_{st} \sim \text{GEV}(1, \exp(\beta_0^\gamma), \beta_0^\xi)$.
3. Pool the \tilde{Y}' data from all sites and estimate $(\beta_0^\gamma, \beta_0^\xi)$ by setting the first two sample L-moments (I_1, I_2) of the pooled data to match its population counterparts. This

¹This can be done in R using functions `gev2frech` and `frech2gev` in package `SpatialExtremes` (Ribatet, 2015).

yields the set of estimating equations:

$$I_1 = 1 - \frac{\exp(\beta_0^\gamma)[1 - \Gamma(1 - \beta_0^\xi)]}{\beta_0^\xi} \quad I_2 = -\frac{\exp(\beta_0^\gamma)(1 - 2^{\beta_0^\xi})\Gamma(1 - \beta_0^\xi)}{\beta_0^\xi}$$

where $\beta_0^\xi < 1$. The solution² to the set of equations yields the L-moment estimates for $(\beta_0^\gamma, \beta_0^\xi)$.

4. Maximize the log-likelihood

$$\sum_{s=1}^m \sum_{t=1}^n \log f(y_{st} | \beta^\mu, \beta^\gamma, \beta^\xi, x_{st}^\mu, x_t^\gamma, x_t^\xi)$$

with respect to only the non-stationary parameters to obtain their estimates.

5. Go back to step 1 using the estimates obtained in steps 2–4, unless convergence is reached (i.e. the change in maximized log-likelihood value is within tolerance between iterations).

While this procedure still requires a likelihood function, it generally provides better estimates of the non-stationary parameters than a regression approach (Coles and Dixon, 1999). Additionally, the regression approach is restricted to incorporating non-stationarity in the location parameter. The hybrid procedure only needs to maximize the likelihood with respect to the non-stationary parameters, thus reducing the complexity of the optimization routine.

²An additional, explicit restriction is imposed such that $\beta_0^\xi > -1$ to ensure the log-likelihood in step 4 does not become irregular.

4.3.2 Maximum Product Spacing

One Sample Case

Maximum product spacing (MPS) is an alternative estimation procedure to the MLE and L-moment methods. The MPS was established by Cheng and Amin (1983). It allows efficient estimation in non-regular cases where the MLE may not exist. This is especially relevant to the GEV distribution, in which the MLE does not exist when $\xi < -1$ (Smith, 1985). In the GEV distribution setting, the MPS also exhibits convergence at the same rate as MLE, and its estimators are asymptotically normal (Wong and Li, 2006). While the L-moment approach has been shown to be efficient in small samples, it inherently restricts $\xi < 1$ (Hosking et al., 1985), and asymptotic confidence intervals are not available for $\xi > 0.5$.

The general setup for MPS estimation in the one sample case is given in Section 3.3.2. The advantage of MPS over MLE can be seen (3.3) directly in the form of the objective function $M(\theta)$. By using only the GEV cumulative density function, $M(\theta)$ does not collapse for $\xi < -1$ as $y \downarrow \mu - \frac{\sigma}{\xi}$.

Wong and Li (2006, Section 4) perform extensive simulations comparing the MPS, MLE, and L-moment estimators in the one sample case. They find that the MPS is generally more stable and comparable to the MLE, and does not suffer from bias as does the L-moment in certain cases. In addition, they find that MLE failure rates are generally higher than those of MPS.

RFA Setting

Let Y_{st} be the observation in year $t \in \{1, \dots, n\}$ from site $s \in \{1, \dots, m\}$. It has been assumed that $Y_{st} \sim \text{GEV}(\mu_{st}, \gamma_t \mu_{st}, \xi_t)$. Via the transformation, discussed in detail in Coles (2001),

$$Z_{st} = \left[1 + \xi_t \left(\frac{Y_{st} - \mu_{st}}{\gamma_t \mu_{st}} \right) \right]^{1/\xi_t}$$

it follows that Z_{st} is distributed according to the standard unit Fréchet distribution.

Let $F(z)$ be the cdf of Z , and the MPS estimation proceeds as follows. Order the observations within each site s as $z_{s(1)} < \dots < z_{s(n)}$ and define the spacings as before:

$$D_{si}(\theta) = F(z_{s(i)}) - F(z_{s(i-1)})$$

for $i = 1, 2, \dots, n+1$ where $F(z_{s(0)}) \equiv 0$ and $F(z_{s(n+1)}) \equiv 1$. The MPS estimators are then found by minimizing

$$M(\theta) = - \sum_{s=1}^m \sum_{i=1}^{n+1} \log D_{si}(\theta). \quad (4.2)$$

Denote the MPS estimates as $\{\check{\beta}^\mu, \check{\beta}^\gamma, \check{\beta}^\xi\}$. MPS estimation assumes the set of observations are independent and identically distributed. Here, observations can be assumed to be identically distributed, although the transformed observations z may still exhibit spatial dependence. However, point estimation can still be carried out with semi-parametric bootstrap procedures ensuring adequate adjustment to the variance of the estimators.

4.4 Simulation Study

A large-scale simulation study is conducted to assess the performance of the estimation procedures for data generated under various types of spatial dependence. Data from the GEV distribution were generated for m sites over n years in a study region $[l_1, l_2] = [0, 10]^2$. Max-stable processes are used in order to obtain a spatial dependence structure via R package **SpatialExtremes** (Ribatet, 2015). Roughly speaking, a max-stable process is the limit process of the component-wise sample maxima of a stochastic process, normalized by appropriate constants (e.g., De Haan and Ferreira, 2007). Its marginal distributions are GEV and its copula has to be an extreme-value (or equivalently, max-stable) copula (Gudendorf and Segers, 2010). Two characterizations of max-stable processes are used - the Smith (SM) model (Smith, 1990) and the Schlather (SC) model (Schlather, 2002). In addition, a non-extremal dependence structure is examined. One such choice is the Gaussian copula (Renard and Lang, 2007), also known as the meta-Gaussian model and will be denoted here as GC. See Davison et al. (2012) for a thorough review of these processes.

There are four factors that dictate each setting of the simulation: the number of sites m , the number of observations within each site n , the spatial dependence model (SM, SC, or GC), and the dependence level. Each setting generates 1,000 data sets, with $m \in \{10, 20\}$, $n \in \{10, 25\}$, and three levels of spatial dependence – weak, medium, strong abbreviated as W, M, S respectively. The dependence levels are chosen as in

Wang et al. (2014). For the Smith model, the correlation structure is given as $\Sigma = \tau I_2$ where I_2 is the identity matrix of dimension 2 and τ is 4, 16, 64 corresponding to W, M, and S. For the Schlather model, the correlation function is chosen as a special case of the powered exponential $\rho(h) = \exp[-(|h|/\phi)^\nu]$ with shape parameter fixed at $\nu = 2$ and range parameter ϕ equal to 2.942, 5.910 and 12.153 corresponding to W, M, and S dependence levels. These were chosen such that the extremal coefficient function from the SC model matches as close as possible to that from the SM model. For the GC model, the exponential correlation function $\rho(h) = \exp[-(|h|/\phi)]$ is used, with range parameter ϕ as 6, 12, and 20 corresponding to weak, medium, and strong dependence respectively. This leads to 36 possible scenarios to consider.

Fréchet scale data are generated using R package **SpatialExtremes** with the parameters across all replicates and settings assigned the following values,

$$\beta_0^\gamma = -1.041 \quad \beta_0^\xi = -0.0186 \quad \beta_0^\mu = 0.003 \quad \beta_1^\gamma = \beta_1^\xi = 0$$

with the marginal location mean values generated once for the m sites from a normal distribution with mean 5.344 and standard deviation of 1.865. Data are then transformed from the original Fréchet scale to GEV following the link functions in (4.1). The parameter values chosen here are from the estimated parameters fitting the flood index model to a subset of northern California sites from the GHCN dataset described in the next section. The covariates corresponding to the non-stationary location parameter β_0^μ are

the latest available winter-averaged Southern Oscillation Index (SOI) values described in Section 4.5.

The estimation methods proposed should produce asymptotically unbiased estimates under various forms of spatial dependence; as noted by Stedinger (1983), as well as Hosking and Wallis (1988), intersite dependence does not introduce significant bias, but can have a dramatic effect on the variance of these estimators. Another advantage of our proposed methods of estimation is the ability to obtain adjusted variance estimates, without needing to specify the form of the dependence.

Since bias has been previously shown to be negligible in the RFA setting, root mean squared error (RMSE) is used to assess the performance of each of the three estimators (MLE, MPS, and L-moment / likelihood hybrid). RMSE is defined as, for some parameter ω ,

$$\sqrt{\frac{1}{J} \sum_{j=1}^J (\omega_j - \hat{\omega}_j)^2} \quad (4.3)$$

where ω_j is the true and $\hat{\omega}_j$ is the estimated parameter value in replicate j .

Optimization failure rates for the three estimation methods can be seen in Table 4.1. For the L-moment hybrid method, starting parameters are initialized by setting each marginal mean β_s^μ to the stationary one-sample L-moment estimate for data from site s , non-stationary parameters equal to zero, and $\beta_0^\gamma, \beta_0^\xi$ equal to the stationary L-moment estimators from pooling data across all sites. For the MLE and MPS methods, optimization is attempted first with these starting parameters and if the routine fails, then

Table 4.1: Failure rate (%) in optimization for the three estimation methods in the combined 12 settings of number of sites, observations, and dependence levels within each spatial dependence structure (SC, SM, and GC) out of 10,000 replicates. The setup is described in detail in Section 4.4.

| Setting | | Weak | | | Medium | | | Strong | | |
|---------|------------------|------|------|--------|--------|------|--------|--------|------|--------|
| | | MPS | MLE | Hybrid | MPS | MLE | Hybrid | MPS | MLE | Hybrid |
| SC | $m = 10, n = 10$ | 0.01 | 0.10 | 0.01 | 0.00 | 0.30 | 0.01 | 0.01 | 1.05 | 0.12 |
| | $m = 10, n = 25$ | 0.01 | 0.25 | 0.00 | 0.00 | 0.29 | 0.01 | 0.01 | 0.35 | 0.02 |
| | $m = 20, n = 10$ | 0.02 | 0.61 | 0.01 | 0.02 | 0.52 | 0.04 | 0.07 | 0.77 | 0.17 |
| | $m = 20, n = 25$ | 0.05 | 0.79 | 0.01 | 0.08 | 0.68 | 0.01 | 0.03 | 0.56 | 0.04 |
| SM | $m = 10, n = 10$ | 0.02 | 0.12 | 0.00 | 0.00 | 0.34 | 0.07 | 0.00 | 0.95 | 0.20 |
| | $m = 10, n = 25$ | 0.00 | 0.26 | 0.00 | 0.00 | 0.26 | 0.00 | 0.01 | 0.23 | 0.00 |
| | $m = 20, n = 10$ | 0.03 | 0.50 | 0.01 | 0.07 | 0.54 | 0.02 | 0.04 | 0.66 | 0.15 |
| | $m = 20, n = 25$ | 0.08 | 0.75 | 0.02 | 0.05 | 0.62 | 0.02 | 0.05 | 0.61 | 0.02 |
| GC | $m = 10, n = 10$ | 0.01 | 0.21 | 0.00 | 0.00 | 0.22 | 0.02 | 0.00 | 0.27 | 0.03 |
| | $m = 10, n = 25$ | 0.01 | 0.37 | 0.00 | 0.00 | 0.30 | 0.00 | 0.02 | 0.26 | 0.00 |
| | $m = 20, n = 10$ | 0.01 | 0.48 | 0.01 | 0.04 | 0.38 | 0.00 | 0.02 | 0.65 | 0.04 |
| | $m = 20, n = 25$ | 0.03 | 0.66 | 0.01 | 0.06 | 0.71 | 0.00 | 0.08 | 0.59 | 0.00 |

uses the estimates from the L-moment hybrid method to initialize. In all settings, the MLE has the highest levels of optimization failures, and in some settings, the rate was 10-fold versus the MPS and L-moment hybrid. Between the MPS and L-moment hybrid methods, the rates are similar, with neither method dominating in all settings. However, even when the procedures did not strictly fail in optimization, there are cases where they provide absurd estimates. For example, in the setting of $m = 10, n = 10$, strong SC dependence, the maximum squared error seen for the shape parameter using MLE was over 24. Thus, a trimmed mean of squared errors are used in the RMSE calculations, discarding the top 2% of values.

Figures 4.1, 4.2, and 4.3 show the RMSE for each of the simulation settings for the Schlather, Smith, and Gaussian Copula dependence structures, respectively. In every

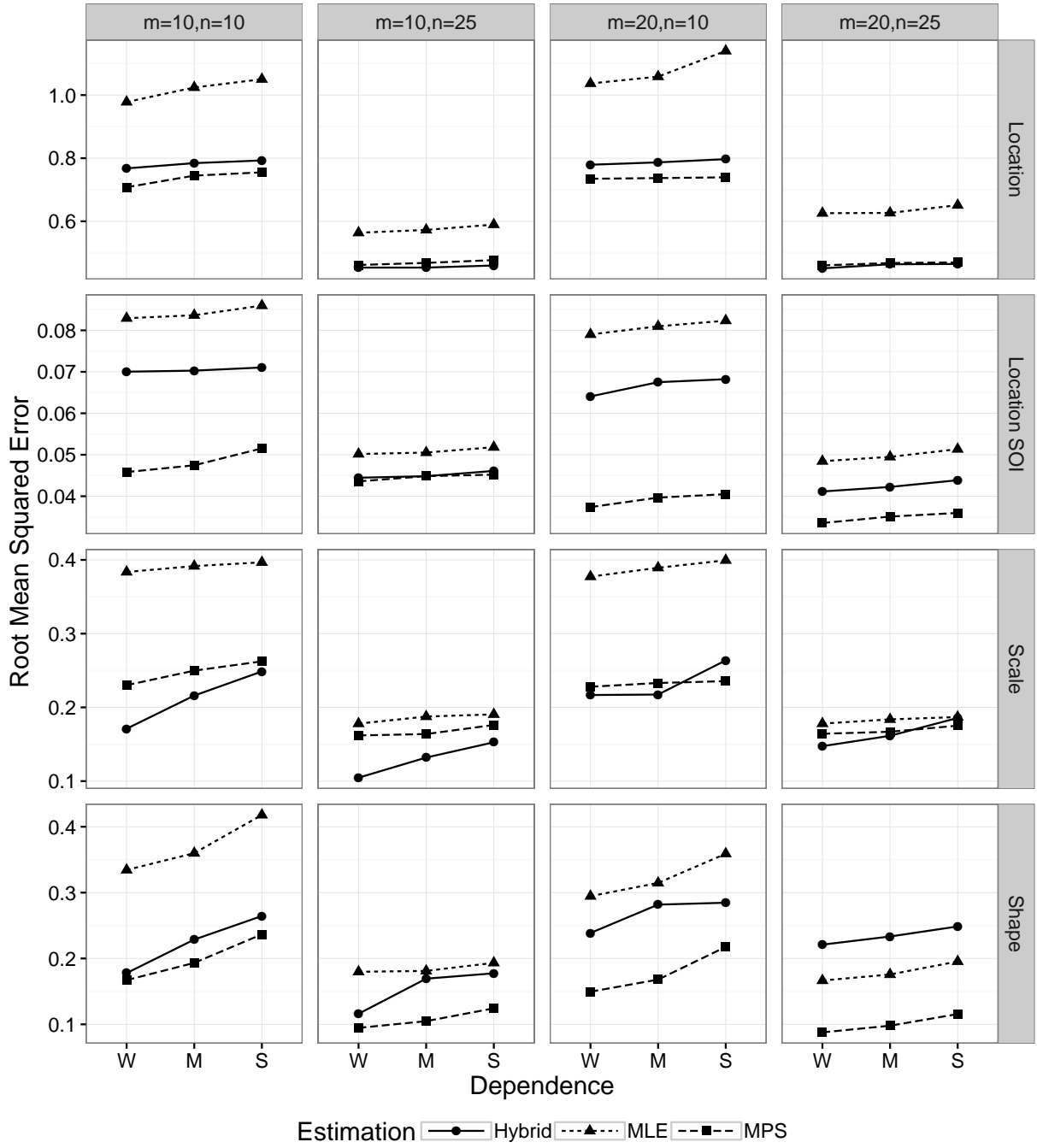


Figure 4.1: Schlather model root mean squared error of the parameters for each estimation method, from 1000 replicates of each setting discussed in Section 4.4. W, M, S refers to weak, medium, and strong dependence, with m being the number of sites and n , the number of observations within each site.

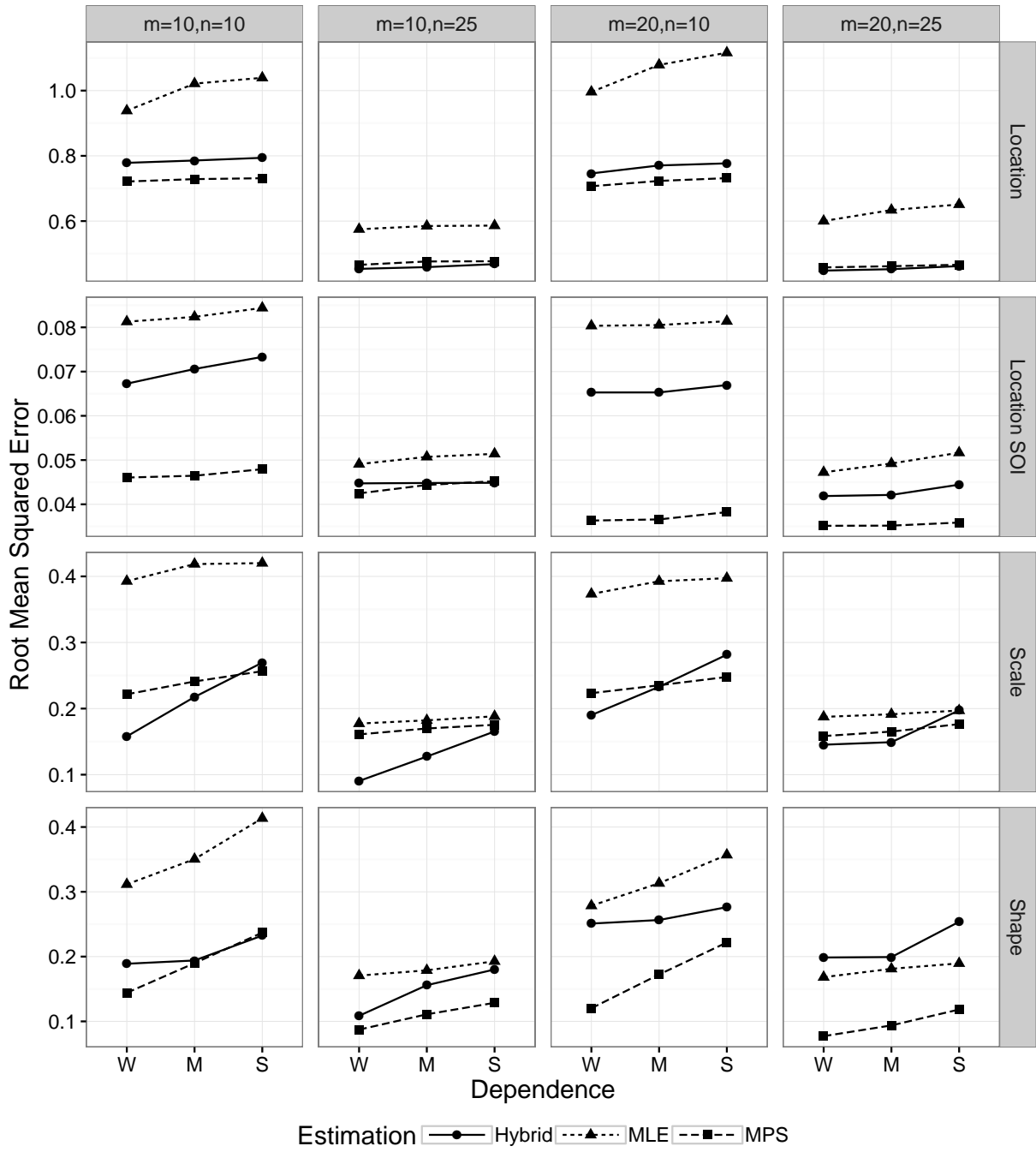


Figure 4.2: Smith model root mean squared error of the parameters for each estimation method, from 1000 replicates of each setting discussed in Section 4.4. W, M, S refers to weak, medium, and strong dependence, with m being the number of sites and n , the number of observations within each site.

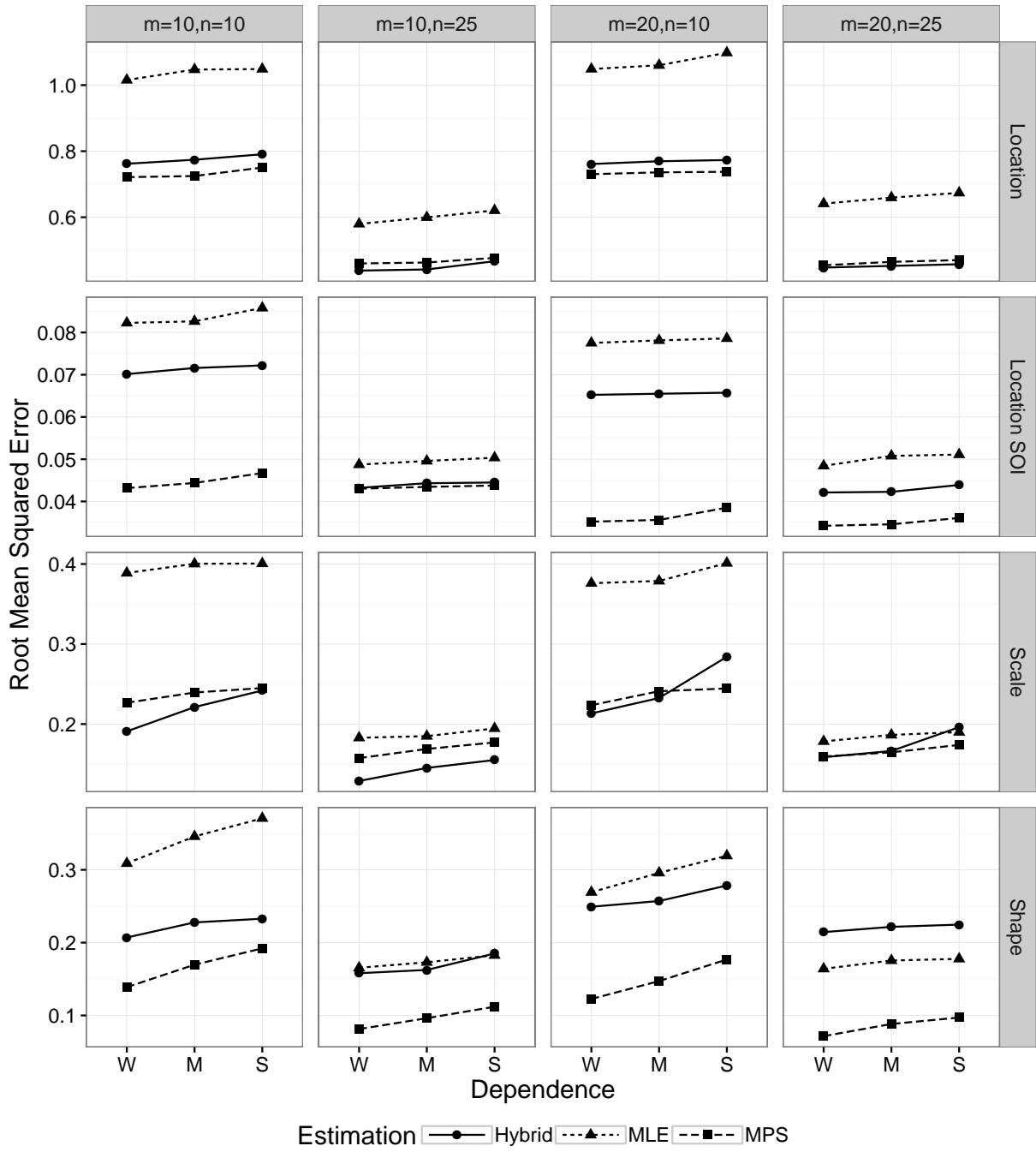


Figure 4.3: Gaussian copula model root mean squared error of the parameters for each estimation method, from 1000 replicates of each setting discussed in Section 4.4. W, M, S refers to weak, medium, and strong dependence, with m being the number of sites and n , the number of observations within each site.

case, the RMSE of the MPS estimation procedure is smaller than that of MLE. The hybrid MLE / L-moment outperforms the MLE in the smallest sample case ($n = 10$), but has a larger RMSE for the shape parameter when $m = 20$ and $n = 25$. As expected, an increase in sample size corresponds to a reduction in RMSE for all methods. However, the MLE and MLE / L-moment hybrid tend to see a more significant reduction than MPS, suggesting the stability of MPS estimates in small sample sizes.

4.5 California Annual Daily Maximum Winter Precipitation

Daily precipitation data (in cm) is available for tens of thousands of surface sites around the world via the Global Historical Climatology Network (GHCN). An overview of the dataset can be found in Menne et al. (2012). Although some California sites have records dating before the year 1900, it is quite sparse. To ensure a large enough and non-biased collection of sites, only the most recent 53 years (1963 – 2015) are considered. In this period, there are 27 sites with complete records available in the state of California. Their locations can be seen in Figure 4.4.

For each year, the block maxima is observed as the daily maximum winter precipitation event for the period of December 1 through March 31. If more than 10% of the observations in this period were missing, the block maxima from that year is considered as missing. A process suspected to be related to extreme precipitation events (e.g.,

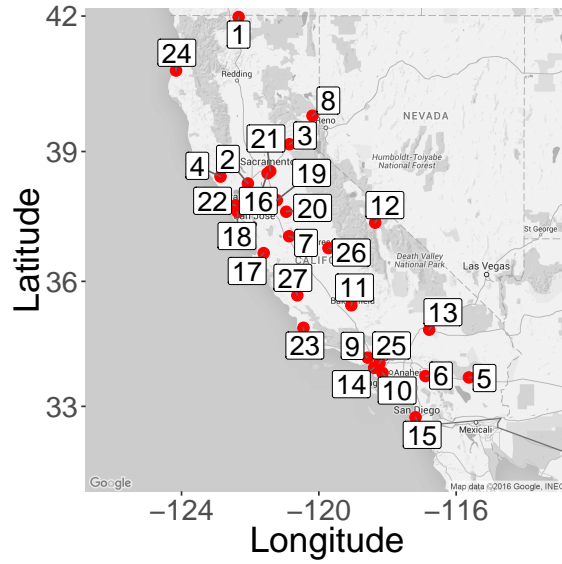


Figure 4.4: Locations of the 27 California sites used in the non-stationary regional frequency analysis of annual daily maximum winter precipitation events.

Schubert, Chang, Suarez, and Pegion, 2008) is El Niño–Southern Oscillation (ENSO). ENSO can be represented using the Southern Oscillation Index (SOI), a measure of observed sea level pressure differences and typically has one measurement per calendar month. For purposes here, the mean SOI value over current winter months (December through March) is treated as a covariate in the non-stationary regional frequency analysis model. The raw SOI data is taken from the Australia Bureau of Meteorology’s website, <http://www.bom.gov.au/climate/current/soihtml1.shtml>.

To get a sense of the dependence among sites, Figure 4.5 displays a scatterplot of the pairwise spearman correlations by euclidean distance for the 27 sites. There appears to be a decreasing trend as the distance between two sites increases. Over 25% of the

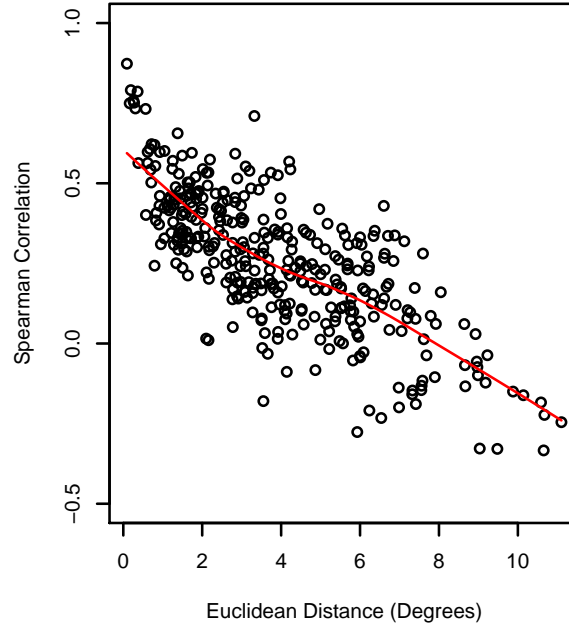


Figure 4.5: Scatterplot of Spearman correlations by euclidean distance between each pair of the 27 California sites used in the non-stationary regional frequency analysis of annual daily maximum winter precipitation events.

correlation coefficients are above 0.41, so there is a need to account for this spatial dependence in the variance of the estimators.

The flood index model is fit with the links given in (4.1), treating the intercept shape and proportionality terms as shared across sites, denoted as ξ_0 and γ_0 respectively. Site-specific marginal mean parameters are assigned. An exploratory visual analysis of SOI and the winter precipitation maximums show an increase in magnitude of events for negative SOI years, with a less clear trend for positive SOI values. Thus, piecewise linear terms for positive and negative SOI values are incorporated into the location parameter. The two distinct SOI piecewise linear terms can be defined as $\text{SOI} \cdot \mathbb{1}(\text{SOI} >$

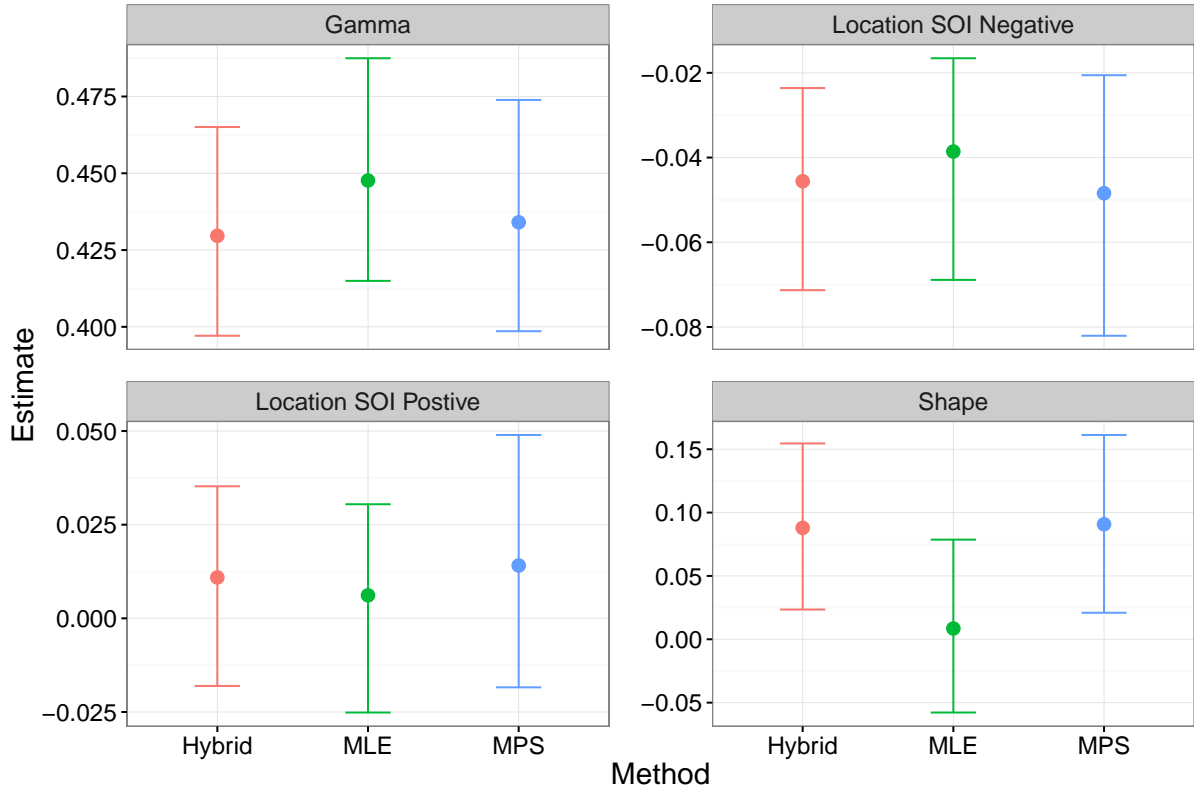


Figure 4.6: Estimates and 95% semi-parametric bootstrap confidence intervals of the location parameter covariates (postive and negative SOI piecewise terms), proportionality, and shape parameters for the three methods of estimation in the non-stationary RFA of the 27 California site annual winter maximum precipitation events.

0) and $\text{SOI} \cdot \mathbb{1}(\text{SOI} \leq 0)$. The model parameters are estimated with the three methods discussed previously. Standard errors of the estimates need to be adjusted due to spatial dependence and can be obtained via semi-parametric bootstrap. The resampling method of Heffernan and Tawn (2004) is implemented as described in Appendix A.3. Though computationally expensive, this bootstrap procedure can be directly extended to run in parallel.

The results of the analysis are seen in Figures 4.6 and 4.7. The semi-parametric

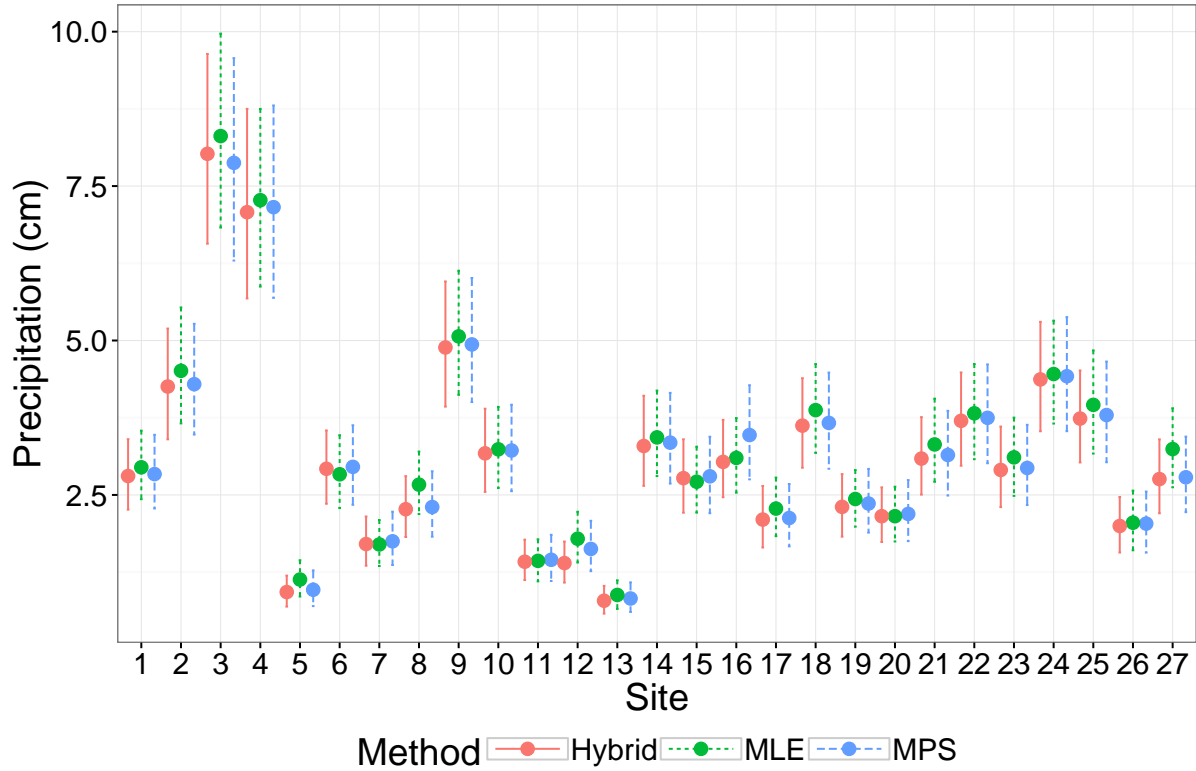


Figure 4.7: Estimates and 95% semi-parametric bootstrap confidence intervals of the marginal site-specific location means for the three estimation methods in the non-stationary RFA of the 27 California site annual winter maximum precipitation events.

bootstrap confidence intervals show that all three methods of estimation provide negative estimates of the negative linear SOI term at the 5% significance level. For the positive linear SOI term, all three methods do not detect a significant difference from zero. Interestingly, only maximum likelihood estimation fails to detect a significant difference from zero in the shape parameter; both MPS and the hybrid L-moment method indicate a heavy-tailed ($\xi > 0$) distribution.

To further demonstrate the differences between the three methods, a subset of years from the original 53 year sample was taken, keeping just one out of every three years,

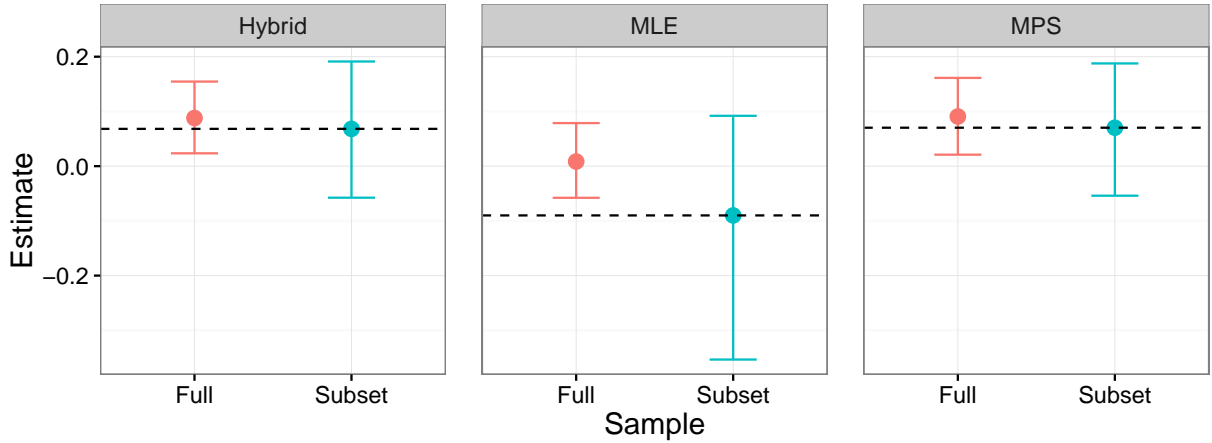


Figure 4.8: Estimates and 95% semi-parametric bootstrap confidence intervals of the shape parameter by the three estimation methods, for the full 53 year and 18 year subset sample of California annual winter precipitation extremes. The horizontal dashed line corresponds to the shape parameter estimate of each method for the subset sample.

making this subset sample of record length 18. The same analysis was performed on this subset of data and estimates of the parameters are compared to the full sample. For all three methods, the two SOI parameters fail to detect departures from zero at the 5% level. Stark differences can be seen in Figure 4.8 for the shape parameter estimates between the three methods. The MPS and hybrid L-moment estimates for the shape parameter are quite stable between the two samples, both decreasing approximately the same, from 0.09 to 0.07. The MLE shape estimate for the subset sample is completely outside the 95% interval range based on the full sample, switching from a positive to negative estimate. For simplicity, the remainder of the analysis (on the full sample) will use the MPS estimators.

A quantity of great interest to researchers are the t -year return levels, which can be thought of as the maximum event that will occur on average every t years. The marginal

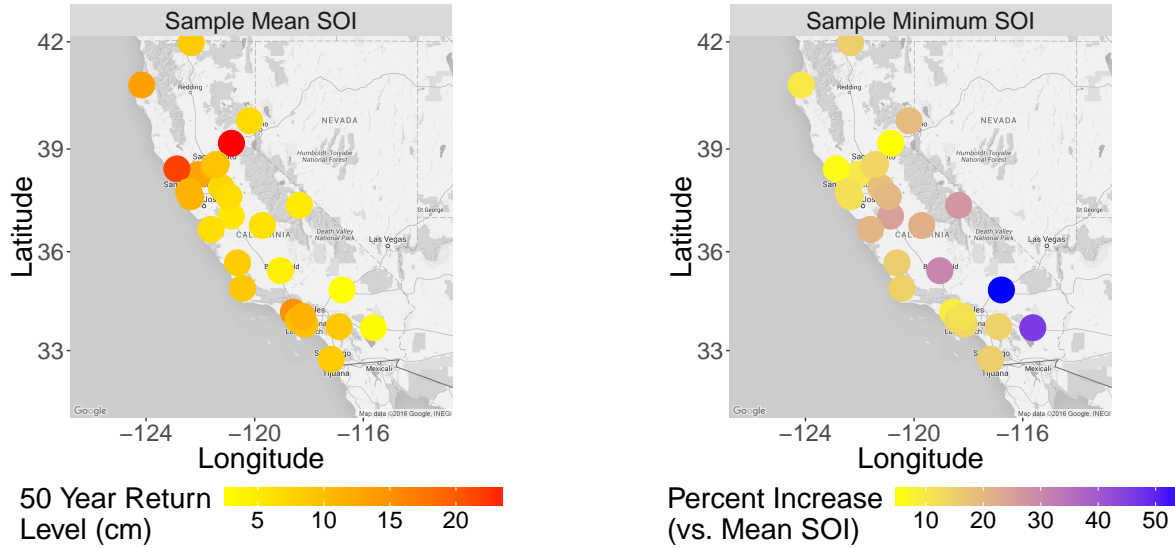


Figure 4.9: Left: 50 year return level estimates (using MPS) at the 27 sites, conditioned on the mean sample SOI value (-0.40). Right: Estimated percent increase in magnitude of the 50 year event at the sample minimum SOI (-28.30) versus the mean SOI value.

return levels at each site are determined jointly from the regional frequency model, dependent on estimates of the shared parameters and site-specific marginal means. Calculation of the quantity can be found in (2.6), replacing the stationary parameters with the appropriate non-stationary values. The left half of Figure 4.9 shows the 50 year return level estimates of precipitation (in centimeters) using the MPS estimation, conditioned on the mean value of SOI in the sample, -0.40 . In other words, these are the estimated maximum 50 year daily winter precipitation events for an average ENSO year.

To determine the effect of ENSO on return levels, we compare the 50 year return levels conditioned on the sample minimum (-28.30) SOI values to the mean SOI. The right half of Figure 4.9 shows the percent change of the estimated 50 year return levels conditioned on the sample minimum SOI, versus the mean value of SOI. The findings

suggest that strong El Niño (negative SOI) years increase the estimated effects of a 50 year precipitation event significantly (in some cases over 50% larger estimates), while strong La Niña (positive SOI) events do not see a significant change from the average ENSO year.

4.6 Discussion

We propose two alternative estimation methods to maximum likelihood (ML) for fitting non-stationary regional frequency models. The first, maximum product spacing (MPS) estimation seeks to maximize the geometric mean of spacing in the data and the second is a hybrid of ML and L-moment estimation. These are studied in the context of a flood index model with extreme value marginal distributions, but the methodology can be generalized to any regional frequency model.

In the context of distributions in the extremal domain, ML estimation has some known drawbacks; in small samples the L-moment estimation method is more efficient and the ML estimate may not exist for certain values of the shape parameter. Additionally, it has been shown Wong and Li (2006) empirically that MLE can provide absurd estimates in small samples even if optimization does not fail entirely. In stationary RFA, an efficient alternative procedure can estimate the parameters using only L-moments (e.g., Wang et al., 2014). However, extending this method to the non-stationary case is not straightforward. Existing attempts have serious limitations and

are reviewed in Section 4.2.1.

MPS estimation is well-studied in the one-sample case and this contribution is an extension to the RFA setting. As with MLE, it is intuitive to incorporate covariates in all parameters, is as efficient asymptotically, and exists for all values of the shape parameter. The hybrid MLE / L-moment procedure is an iterative estimation procedure that estimates stationary parameters using L-moments and non-stationary parameters via likelihood. While the procedure itself is not as straightforward as MPS or strictly MLE, it is more computationally efficient as it only has to perform optimization over the non-stationary parameters.

The performance of the three estimation procedures are evaluated in the flood index non-stationary RFA model via a large scale study of data simulated under extremal and Gaussian dependence with parameters chosen from real data. It is shown that the root mean squared error (RMSE) of the MPS estimator is smaller than that of MLE in all cases. In most cases, the hybrid L-moment / MLE outperformed the pure MLE method as well. Additionally, the MPS method is stable for sample sizes as small as 10, which is desirable in environmental applications with extremal data as historical record is often short.

The three estimation methods are applied to a flood-index model for maximum annual precipitation events in California with an emphasis on using the Southern Oscillation Index (SOI) as a predictor. To avoid explicitly specifying the spatial dependence structure, a semi-parametric bootstrap procedure based on the ideas of Heffernan and

Tawn (2004) is used to obtain adjusted standard errors of estimates. The three methods find a statistically significant negative association between negative values of SOI (El Niño) and maximum precipitation magnitudes, but not for positive SOI values (La Niña). The MPS and hybrid L-moment methods indicate a positive shape parameter value, while the MLE does not find this to be significant. Using MPS, the effect of SOI on return levels is studied and it is found that El Niño has an increasing effect on the magnitude of these events. Strong El Niño years are estimated to increase the magnitude of 50 year return level events on average 23.6% and up to 60% at some sites. The findings agree with previous studies (e.g., El Adlouni et al., 2007; Schubert et al., 2008; Shang, Yan, and Zhang, 2011; Zhang, Wang, Zwiers, and Groisman, 2010).

Based on the simulation performance, stability in the subset versus full sample estimates for the California precipitation RFA, and ease to incorporate covariates, the recommendation to practitioners would be to use the MPS method. On a more general note, a current limitation of this analysis is the requirement of complete and balanced data. As missingness is common in historical climate records, there is a need to develop methodology to handle missing data in the semi-parametric resampling schemes in Appendix A.3. A further discussion on this subject is provided in Section 6.1.

Chapter 5

An R Package for Extreme Value

Analysis: `eva`

5.1 Introduction

It is quite apparent that statistics cannot be separated from computing and there are some particular challenges in extreme value analysis that need to be addressed. A thorough review of existing packages can be found in Gilleland (2016) and Gilleland, Ribatet, and Stephenson (2013).

The `eva` package, short for ‘Extreme Value Analysis with Goodness-of-Fit Testing’, provides functionality that allows data analysis of extremes from beginning to end, with model fitting and a set of newly available tests for diagnostics. In particular, some highlights are:

- Efficient handling of the near-zero shape parameter.
- Implementation of the r largest order statistics (GEV_r) model - data generation, non-stationary fitting, and return levels.

- Maximum product spacing (MPS) estimation for parameters in the block maxima (GEV_1) and Generalized Pareto distribution (GPD).
- Sequential tests for the choice of r in the GEV_r model, as well as tests for the selection of threshold in the peaks-over-threshold (POT) approach. For the bootstrap based tests, the option to run in parallel is provided.
- P-value adjustments to control for the false discovery rate (FDR) and family-wise error rate (FWER) in the sequential testing setting.
- Profile likelihood for return levels and shape parameters of the GEV_r and GPD.

While some of these issues / features may have been implemented in some existing packages, it is not predominant and there are some new features in the `eva` package that to the best of our knowledge have not been implemented elsewhere. In particular, completely new implementations are MPS estimation, p-value adjustments for error control in sequential ordered hypothesis testing, data generation and density calculations for the GEV_r distribution. Additionally, the goodness-of-fit tests for the selection of r in the stationary GEV_r distribution are the only non-visual diagnostics currently available – see Chapter 2 for more details. Similarly related, the only model fitting whatsoever for the GEV_r distribution (stationary or non-stationary) can be found in R package `ismev` (Heffernan and Stephenson, 2016), which requires specification of the exact design matrix and does not explicitly handle the numerical issue for small values of the shape parameter. The `eva` package introduces model formulations similar to base function

`lm` and `glm`, provides improved optimization, and inherits usual class functionality for modeling data such as `AIC`, `BIC`, `logLik`, etc. A similar implementation is provided for fitting the non-stationary GPD. The last major improvement worth noting is profile likelihood estimation. Other R packages such as `extRemes` (Gilleland and Katz, 2011b) and `ismev` require specification of the boundaries of the interval, making automation less straightforward. The package `fExtremes` (Wuertz, 2013) does not require this; however it does not provide functionality for the GEV_r distribution. The `eva` package includes semi-automated profile likelihood confidence interval estimation of the shape and return levels for the GPD and GEV_r (implicitly block maxima) stationary models.

5.2 Efficient handling of near-zero shape parameter

One of the interesting and theoretical aspects of the GEV / GEV_r and GP distributions is the limiting form of each as the shape parameter ξ approaches zero. In practice, numerical instabilities can occur, particularly when working with the form $(1 + x\xi)^{(-1/\xi)}$ as $\xi \rightarrow 0$. Figure 5.1 shows both a naive and the efficient implementation in `eva` of the GEV cumulative distribution function (1.1) at $x = 1$, $\mu = 0$ and $\sigma = 1$, with ξ varying from -0.0001 to 0.0001 on the cubic scale. Note that the true value of the CDF function at $\xi = 0$ is approximately 0.692. A similar demonstration can be carried out for the probability density function and for the GPD.

Handling of this issue is critical, particularly in optimization when the shape parameter may change its sign as the parameter space is navigated. The **eva** package handles these cases by rewriting certain functions to utilize high precision operations such as `log1p`, `expm1` and some of the use cases in R discussed in Mächler (2012).

```
# A naive implementation of the GEV cumulative distribution function
pgev_naive <- function(q, loc = 0, scale = 1, shape = 0) {
  q <- (q - loc) / scale
  ifelse(shape == 0, exp(-exp(-q)),
         exp(-(1 + shape * q)^(-1/shape)))
}
```

5.3 The GEV_r distribution

The GEV_r distribution has the density function given in (1.3). When $r = 1$, this distribution is exactly the GEV distribution or block maxima. The **eva** package includes data generation (`rgev`), density function (`dgev`), non-stationary fitting (`gevFit`), and return levels (`gevRl`) for this distribution. To the best of the author's knowledge, there is no current implementation whatsoever for the density function and data generation of the GEV_r distribution. Appendix A.1 gives the psuedo code and a simplified version of the data generation algorithm.

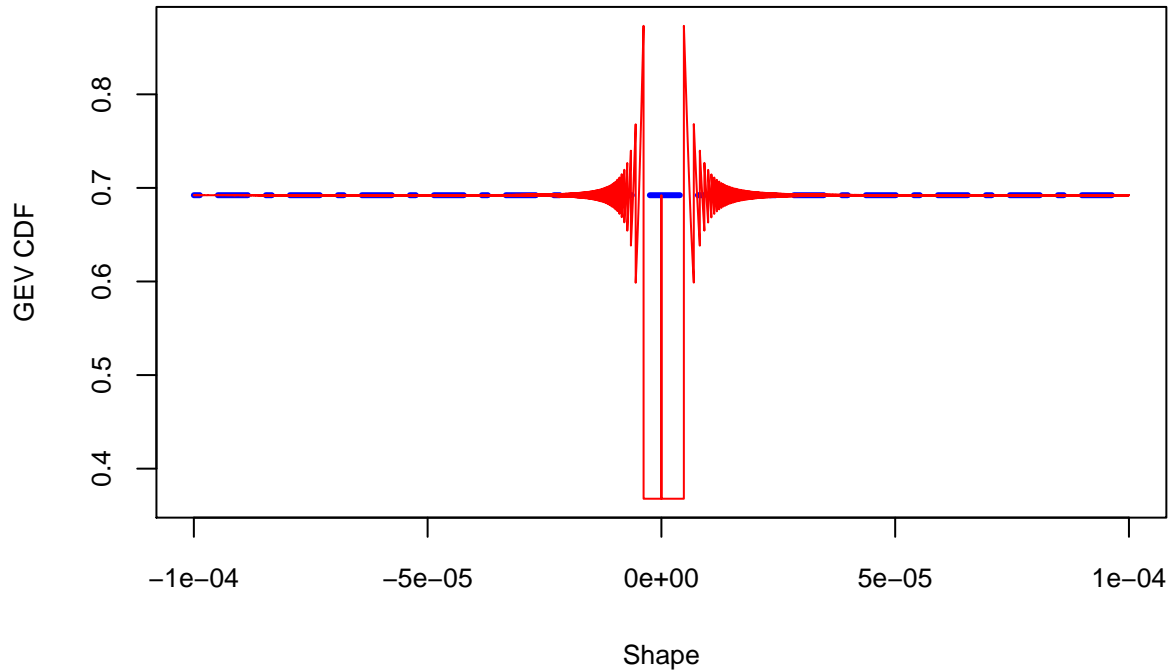


Figure 5.1: Plot of GEV cumulative distribution function with $x = 1$, $\mu = 0$ and $\sigma = 1$, with ξ ranging from -0.0001 to 0.0001 on the cubic scale. The naive implementation is represented by the solid red line, with the implementation in R package **eva** as the dashed blue line.

5.3.1 Goodness-of-fit testing

When modeling the r largest order statistics, if one wants to choose $r > 1$, goodness-of-fit must be tested. This can be done using function `gevrSeqTests`, which can be used for the selection of r , via the entropy difference test and score tests discussed in Sections 2.4 and 2.3 respectively. Take, for example, the Lowestoft dataset in Section 2.7.1 which includes the top hourly sea level readings for the period of 1964 – 2014.

```
data(lowestoft)
gevrSeqTests(lowestoft, method = "ed")
```

```
##  r  p.values ForwardStop StrongStop  statistic  est.loc est.scale est.shape
##  2 0.9774687    1.455825  0.9974711  0.02824258 3.431792 0.2346591 0.10049739
##  3 0.7747741    1.163697  1.0869254 -0.28613586 3.434097 0.2397408 0.09172687
##  4 0.5830318    1.116989  1.1500564  0.54896156 3.447928 0.2404563 0.06802070
##  5 0.6445475    1.157363  1.2470248  0.46135009 3.452449 0.2376723 0.05451138
##  6 0.4361569    1.181963  1.2676077 -0.77869930 3.455478 0.2396332 0.04709329
##  7 0.6329943    1.334209  1.4133341  0.47751655 3.454680 0.2372572 0.04555449
##  8 0.4835074    1.444819  1.4790559 -0.70067260 3.455901 0.2376215 0.03838020
##  9 0.8390270    1.836882  2.0321878 -0.20313820 3.458135 0.2356543 0.02536685
## 10 0.8423291    1.847245  3.4235418  0.19891516 3.459470 0.2342272 0.01964612
```

The entropy difference test fails to reject for any value of r from 1 to 10. In the previous output, the adjusted ForwardStop (2.4) and StrongStop (2.5) p-values are also included.

5.3.2 Profile likelihood

A common quantity of interest in extreme value analysis are the t -year return levels, which can be thought of as the average maximum value that will be exceeded over a period of t years. For the LoweStoft data, the 250 year sea level return levels, with 95% confidence intervals are plotted for r from 1 to 10. The advantage of using more top order statistics can be seen in the plots below. The width of the intervals decrease by

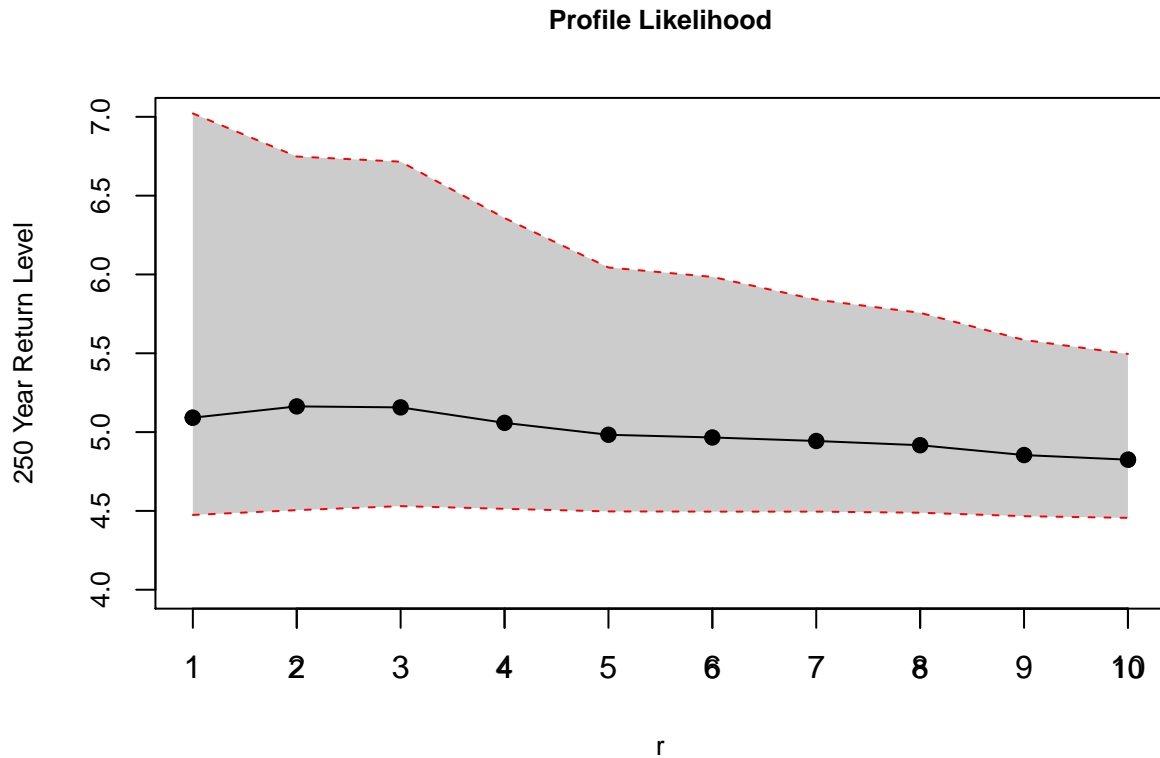


Figure 5.2: Estimates and 95% profile likelihood confidence intervals for the 250 year return level of the LoweStoft sea level dataset, for $r = 1$ through $r = 10$.

over two-thirds from $r = 1$ to $r = 10$. Similarly decreases can be seen in the parameter intervals.

In addition, the profile likelihood confidence intervals (Figure 5.2) are compared with the delta method intervals (Figure 5.3). The advantage of using profile likelihood over the delta method is the allowance for asymmetric intervals. This is especially useful at high quantiles, or large return level periods. At the moment, no other software package provides a straightforward way to obtain profile likelihood confidence intervals for the GEV_r distribution. In Figure 5.2, the asymmetry can be seen in the stable lower

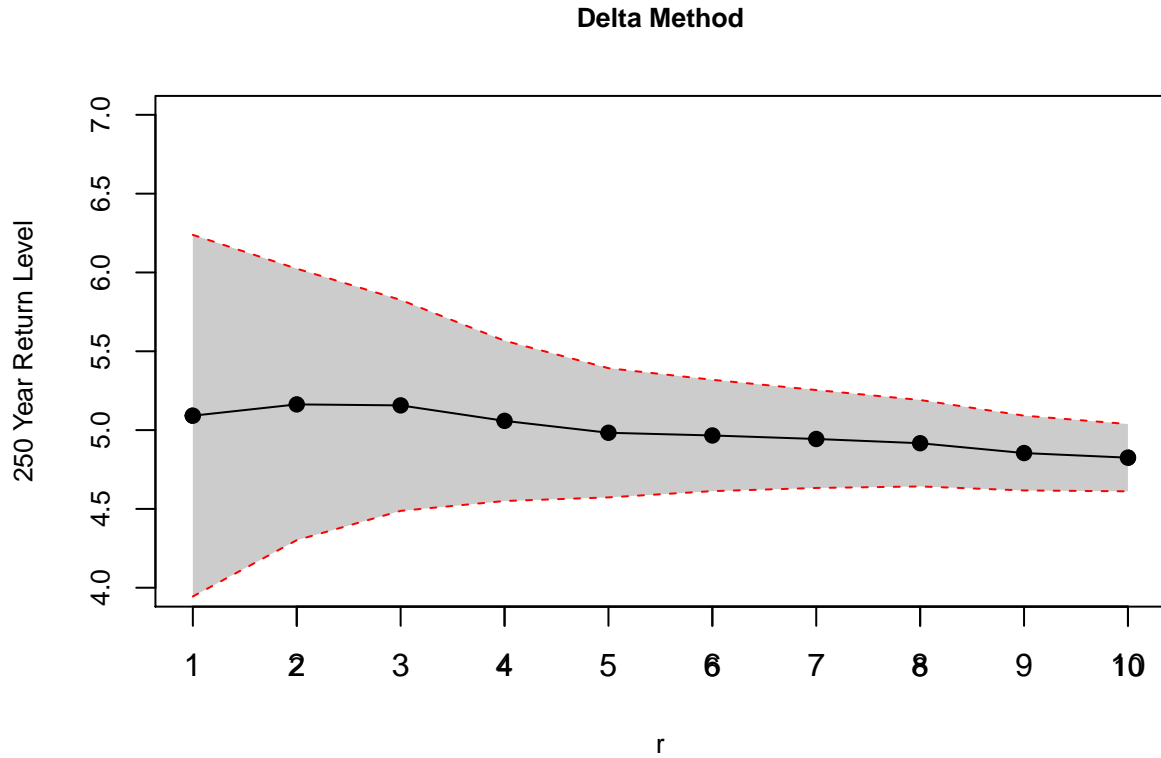


Figure 5.3: Estimates and 95% delta method confidence intervals for the 250 year return level of the LoweStoft sea level dataset, for $r = 1$ through $r = 10$.

bound across values of r , while the upper bound decreases. Profile likelihood is also implemented for estimating the shape parameter and in the same settings for the GPD.

5.3.3 Fitting the GEV_r distribution

The `eva` package allows generalized linear modeling in each parameter (location, scale, and shape), as well as specifying specific link functions. As opposed to some other packages, one can use formulas when specifying the models, so it is quite user friendly.

Additionally, to benefit optimization, there is efficient handling of the near-zero shape parameter in the likelihood and covariates are automatically centered and scaled when appropriate (they are transformed back to the original scale in the output). The `gevrFit` function includes certain class definitions such as `logLik`, `AIC`, and `BIC` to ease the steps in data analysis and model selection. As with profile likelihood, the equivalent functionality is implemented for fitting the non-stationary GPD.

In the following chunk of code, we look at non-stationary fitting in the GEV_r distribution. First, data of sample size 100 are generated from the GEV_{10} distribution with stationary shape parameter $\xi = 0$. The location and scale have an intercept of 100 and 1, with positive trends of 0.02 and 0.01, respectively. A plot of the largest order statistic (block maxima) can be seen in Figure 5.4.

```
set.seed(7)

n <- 100

r <- 10

x <- rgevr(n, r, loc = 100 + 1:n / 50, scale = 1 + 1:n / 100, shape = 0)
```

```
## Creating covariates (linear trend first)

covs <- as.data.frame(seq(1, n, 1))

names(covs) <- c("Trend1")

## Create some unrelated covariates

covs$Trend2 <- rnorm(n)

covs$Trend3 <- 30 * runif(n)
```

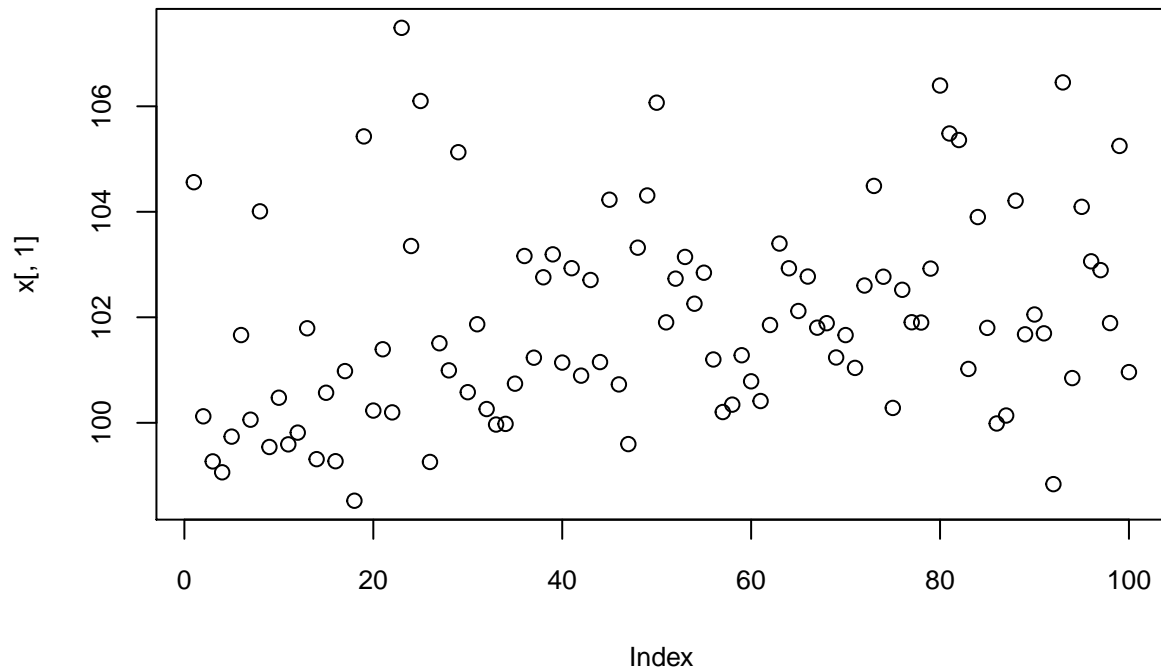


Figure 5.4: Plot of the largest order statistic (block maxima) from a GEV_{10} distribution with shape parameter $\xi = 0$. The location and scale have an intercept of 100 and 1, with positive trends of 0.02 and 0.01, respectively. The indices (1 to 100) are used as the corresponding trend coefficients.

```
## Use full data

fit_full <- gevrFit(data = x, method = "mle",
                    locvars = covs, locform = ~ Trend1 + Trend2*Trend3,
                    scalevars = covs, scaleform = ~ Trend1)

## Only use r = 1

fit_top_only <- gevrFit(data = x[, 1], method = "mle",
```

```
locvars = covs, locform = ~ Trend1 + Trend2*Trend3,
scalevars = covs, scaleform = ~ Trend1)
```

From a visual assessment of the largest order statistic in Figure 5.4, it is difficult to see trends in either the location or scale parameters. The previous chunk of code creates some covariates - the correct linear trend, labeled ‘Trend1’ and two erroneous covariates, labeled ‘Trend2’ and ‘Trend3’. Then, the non-stationary GEV_r distribution is fit with the full data ($r = 10$) and only the block maxima ($r = 1$), modeling the correct linear trend in both location and scale parameters, a stationary shape parameter, and interaction / main effect terms for the erroneous ‘Trend2’ and ‘Trend3’ parameters in the location.

```
## Show summary of estimates
```

```
fit_full
```

```
## Summary of fit:
```

| ## | Estimate | Std. Error | z value | Pr(> z) |
|---------------------------|-------------|------------|-----------|----------------|
| ## Location (Intercept) | 100.0856115 | 0.2276723 | 439.60378 | 0.0000e+00 *** |
| ## Location Trend1 | 0.0193838 | 0.0042366 | 4.57535 | 4.7543e-06 *** |
| ## Location Trend2 | -0.0716415 | 0.0949454 | -0.75455 | 4.5052e-01 |
| ## Location Trend3 | 0.0031478 | 0.0049866 | 0.63124 | 5.2788e-01 |
| ## Location Trend2:Trend3 | 0.0032205 | 0.0053048 | 0.60710 | 5.4378e-01 |
| ## Scale (Intercept) | 1.0831201 | 0.0922684 | 11.73879 | 8.0627e-32 *** |
| ## Scale Trend1 | 0.0097441 | 0.0016675 | 5.84352 | 5.1108e-09 *** |
| ## Shape (Intercept) | 0.0393603 | 0.0293665 | 1.34031 | 1.8014e-01 |

```
## ---

## Signif. codes:  0 '***' 0.001 '**' 0.01 '*' 0.05 '.' 0.1 ' ' 1

fit_top_only

## Summary of fit:

##              Estimate Std. Error  z value  Pr(>|z|)
## Location (Intercept)  99.5896128  0.4373915 227.68985 0.0000e+00 ***
## Location Trend1       0.0235401  0.0052891   4.45072 8.5582e-06 ***
## Location Trend2      -0.3567545  0.2858703  -1.24796 2.1205e-01
## Location Trend3       0.0170264  0.0170313   0.99971 3.1745e-01
## Location Trend2:Trend3 0.0021764  0.0194109   0.11212 9.1073e-01
## Scale (Intercept)     1.1098238  0.2654124   4.18151 2.8958e-05 ***
## Scale Trend1          0.0036369  0.0042099   0.86390 3.8764e-01
## Shape (Intercept)     0.1375594  0.1063641   1.29329 1.9591e-01

## ---

## Signif. codes:  0 '***' 0.001 '**' 0.01 '*' 0.05 '.' 0.1 ' ' 1
```

From the output, one can see from the fit summary that using $r = 10$, both the correct trend in location and scale are deemed significant. However, using $r = 1$ a test for significance in the scale trend fails.

Next, we fit another two models (using $r = 10$). The first, labeled ‘fit_reduced1’ is a GEV_{10} fit incorporating only the true linear trends as covariates in the location and scale parameters. The second, ‘fit_reduced2’ fits the Gumbel equivalent of this model ($\xi = 0$). Note that ‘fit_reduced1’ is nested within ‘fit_full’ and ‘fit_reduced2’ is further

nested within ‘fit_reduced1’.

```
fit_reduced1 <- gevrFit(data = x, method = "mle",
                        locvars = covs, locform = ~ Trend1,
                        scalevars = covs, scaleform = ~ Trend1)

fit_reduced2 <- gevrFit(data = x, method = "mle",
                        locvars = covs, locform = ~ Trend1,
                        scalevars = covs, scaleform = ~ Trend1, gumbel = TRUE)
```

One way to compare these models is using the Akaike information criterion (AIC) and choose the model with the smallest value. This metric can be extracted by using `AIC(.)` on a `gevrFit` object. By this metric, the chosen model is ‘fit_reduced2’, which agrees with the true model (Gumbel, with linear trends in the location and scale parameters).

```
## Compare AIC of three models
AIC(fit_full)
```

```
## [1] 127.0764
```

```
AIC(fit_reduced1)
```

```
## [1] 120.4856
```

```
AIC(fit_reduced2)
```

```
## [1] 118.4895
```

5.4 Summary

Many of the same options and procedures that are available for the GEV_r distribution are also available for the Generalized Pareto distribution. In particular, functionality is for the most part the same for distribution functions (**r**, **d**, **q**, **p** prefixes), profile likelihood, and model fitting. Model fitting diagnostic plots are the same and include probability, quantile, return level, density, and residual vs. covariates (each provided when appropriate, depending on non-stationarity).

The tests developed in Chapter 2 are implemented via the wrapper function **gevrSeqTests** and those discussed in Chapter 3 can be used through function **gpdSeqTests**, along with a few additional tests. All the tests that require a computational bootstrap approach have the option to be run in parallel, via R package **parallel**. The function **pSeqStop** provides an implementation of the recently developed ForwardStop and StrongStop p-value adjustments derived in G'Sell et al. (2016).

In closing, **eva** attempts to integrate and simplify all aspects of model selection, validation, and analysis of extremes for end users. It does so by introducing new methodology for goodness-of-fit testing in the GEV_r and GP distributions, making model fitting

more straightforward (formula statements, diagnostic plots, and certain class inheritances), and efficient handling of numerical issues known to extremes.

Chapter 6

Conclusion

The research presented here provides new methodology to approach goodness-of-fit testing in extreme value models and alternative estimation procedures in non-stationary regional frequency analysis of extremal data. Chapter 1 presents an overview of extreme value theory and some of the outstanding issues that will be addressed in the following chapters.

In Chapter 2, two goodness-of-fit tests are developed for use in the selection of r in the r largest order statistics model, or GEV_r distribution. The first is a score test. Due to the non-regularity of the GEV_r distribution, a bootstrap approach must be used to obtain critical values for the test statistic. Parametric bootstrap is simple, yet computationally expensive so an alternative multiplier approximation (e.g., Kojadinovic and Yan, 2012) can be used for efficiency. The second, called the entropy difference (ED) test, utilizes the difference in log-likelihood between the GEV_r and GEV_{r-1} and the distribution of the test statistic under the null hypothesis is shown to be asymptotically normal. The properties of the tests are studied and both are found to hold their size and have adequate power to detect deviations from the GEV_r distribution. Recently developed

stopping rules (G'Sell et al., 2016) to control the familywise error rate (FWER) and false discovery rate (FDR) in the ordered, sequential testing setting are studied and applied in our framework. The utility of the tests are shown via applications to extreme sea levels and precipitation.

A similar, but distinct problem is the choice of threshold in the peaks-over-threshold (POT) approach. In Chapter 3, a goodness-of-fit approach is considered for testing a set of predetermined thresholds. Multiple tests are studied for a single, fixed threshold under various misspecification settings and it is found that the Anderson–Darling test is most powerful in the majority of the settings. The same stopping rules used in Chapter 2 are applied in this setting to control the error rate in an ordered, multiple threshold testing situation. The Anderson–Darling test for the Generalized Pareto distribution is studied in detail by Choulakian and Stephens (2001) and they derive the asymptotic distribution of the test statistic, which requires obtaining the eigenvalues of an integral equation. An insightful and generous discussion with one of the authors, Prof. Choulakian, led to development of an approximate, but accurate method to compute p-values in a computationally efficient manner. This provides an automated multiple threshold testing procedure with the Anderson–Darling test that can be scaled in a straightforward manner. Its use is demonstrated by generating a map of precipitation return levels at hundreds of sites in the western United States.

In Chapter 4, two alternative estimation procedures are thoroughly studied and

implemented for modeling extremal data with non-stationary regional frequency analysis (RFA). In stationary RFA, L-moment estimation can be used as an alternative to maximum likelihood (ML). In extremal distributions, L-moment estimation has some desirable properties compared to MLE such as efficiency in small samples and that it only requires existence of the mean (Hosking et al., 1985). However, there is no straightforward extensions to non-stationary RFA and currently MLE is the only available well-studied option. We propose two alternative estimation procedures for the non-stationary setting. The first, is an extension of maximum product spacings (MPS) estimation (Cheng and Amin, 1983) from the one sample case. The second is a hybrid, iterative L-moment / maximum likelihood method. Both have theoretical and/or computational advantages over MLE and they are shown to have better performance (in terms of squared error) via a large scale simulation study of multivariate extremal data fit with a non-stationary RFA model. This improvement is more apparent in simulations with short record length. The three estimation methods are compared in an analysis of daily precipitation extremes in California, fit with a non-stationary flood index RFA model. Interest is in the effect of the El Niño–Southern Oscillation on winter precipitation extremes in this region. Semi-parametric bootstrap procedures (e.g., Heffernan and Tawn, 2004) are used to obtain standard errors in the presence of unspecified spatial dependence.

Most of the methodology developed here has been implemented in the R package `eva`,

which is publicly available on CRAN. In addition, it addresses deficiencies in other software for analyzing extremes. These include efficient handling of numerical instabilities when dealing with small shape parameter values, data generation and density functions for the GEV_r distribution, profile likelihood for stationary return levels and the shape parameter, and more user-friendly functionality for model fitting and diagnostics.

6.1 Future Work

The goodness-of-fit tests developed in Chapter 2 for selection of r in the GEV_r distribution can be extended to allow covariates in the parameters. For example, extremal precipitation in a year may be affected by large scale climate indexes such as the Southern Oscillation Index (SOI), which may be incorporated as a covariate in the location parameter (e.g., Shang et al., 2011). Both tests can be carried out with additional non-stationary covariates in any of the model parameters. However, this introduces additional complexity in performing model selection (i.e., how to choose covariates and select r ?). When the underlying data falls into a rich class of dependence structures (such as time series), this dependence may be incorporated directly instead of using a procedure to achieve approximate independence (e.g. the storm length τ in Section 2.7). For example, take the GEV-GARCH model (Zhao, Scarrott, Oxley, and Reale, 2011) when $r = 1$. It may be extended to the case where $r > 1$ and the tests presented here may be applied to select r under this model assumption.

Threshold selection in the non-stationary GPD, as discussed in Roth, Buishand, Jongbloed, Klein Tank, and van Zanten (2012) and Northrop and Jonathan (2011), is an obvious extension to the automated threshold testing methodology developed in Chapter 3. However, one particular complication that arises is performing model selection (i.e., what covariates to include) while concurrently testing for goodness-of-fit to various thresholds. It is clear that threshold selection will be dependent on the model choice. Another possible extension to this work involves testing for overall goodness-of-fit across sites (one test statistic). In this way, a fixed or quantile regression based threshold may be predetermined and then tested simultaneously across sites. In this setup both spatial and temporal dependence need to be taken into account. Handling this requires some care due to censoring (e.g., Dey and Yan, 2016, Section 2.5.2). In other words, it is not straightforward to capture the temporal dependence as exceedances across sites are not guaranteed to occur at the same points in time.

Future work for estimation in non-stationary regional frequency analysis (RFA) as in Chapter 4, is to study the convergence rate of the estimators presented in terms of the number of sites, m and sample size n at each site. The relationship between m and n for estimator efficiency may be quite complicated and further investigation is needed. Additionally, the methodology can be applied to other heavy-tailed / non-regular distributions such as the Generalized Pareto, Kappa, and Lèvy. Another important, yet not trivial task is to develop a heterogeneity measure in the presence of nonstationarity to determine regional homogeneity. Hosking and Wallis (2005) discuss some metrics

for the stationary case; however this becomes less straightforward when the data are not assumed to be identically distributed. Instead of assuming linear relationships in the covariates, splines can be used to create a smooth curve. This can be quite useful to describe the effect of extremes over a geographic region. Additional care would be needed here to choose the level of smoothness and type of spline used.

It would be desirable to have a mechanism to allow for missing data. Currently, only sites with full and balanced records are used in the analysis. This is a serious drawback, particularly with historical climate records that often exhibit missingness. Assuming data are missing completely at random (MCAR), the initial estimation procedure would not introduce bias and can be handled in a straightforward manner. To generate confidence intervals for the parameters, the semi-parametric bootstrap procedure in Appendix A.3 would need to be adjusted. In the presence of missing data, the cluster size of observations across sites within each year would not necessarily be equal.

On a broader note, variable selection is an important part of any data analysis. As discussed earlier, in extremes often there exists a limited number of observations. This can lead to the number of parameters to be estimated exceeding the number of observations (small n , large p). Even in cases where $n > p$, there is still the very real possibility of over-fitting; such rules of thumb such as the ‘one in ten’ rule states that there must be at least ten observations for each predictor (Harrell, Lee, Califf, Pryor, and Rosati, 1984). For applications of extremes to nature, there are many apparent predictors that one may be interested in for example - linear, quadratic, seasonal, or

cyclic time trends, atmospheric/weather readings, coordinate locations, etc.

Surprisingly, very little work has been done in this area. The only literature that considers regularization is Phatak, Chan, and Kiiveri (2010). They explore the use of RaVE, a sparse variable selection method, and apply it to annual rainfall data with a large number of atmospheric covariates. RaVE is formulated as a Bayesian hierarchical model and can be applied to any model with a well-defined likelihood. Menéndez, Méndez, Izaguirre, Luceño, and Losada (2009) use a modified stepwise selection method to select parameters. Mínguez, Méndez, Izaguirre, Menéndez, and Losada (2010) use modified forward selection, which penalizes based on AIC using a likelihood score perturbation method.

The goal would be to develop a sparse regularization technique for extremes via penalized estimation similar to lasso (Tibshirani, 1996). Implementation of this is not trivial. The GEV distribution is not in the exponential family and thus, some of the nice results in GLM may not be available. Unlike the (usual) case of normal regression with homoscedasticity, when modeling non-stationarity in the GEV distribution often times both the location and scale parameters are assumed to vary with covariates, so shrinkage of both sets of covariates is desired. This would need to be explored; for example, different penalties could be used for each covariate set. Lastly, this regularization can be combined with existing maximum likelihood penalties that ensure the shape parameter ξ can be estimated (Coles and Dixon, 1999).

Appendix A

Appendix

A.1 Data Generation from the GEV_r Distribution

The GEV_r distribution is closely connected to the GEV distribution. Let (Y_1, \dots, Y_r) , $Y_1 > \dots > Y_r$ follow the GEV_r distribution (1.3). It can be shown that the GEV_1 distribution is the GEV distribution with the same parameters, which is the marginal distribution of Y_1 . More interestingly, note that, the conditional distribution of Y_2 given $Y_1 = y_1$ is simply the GEV distribution right truncated by y_1 . In general, given $(Y_1, \dots, Y_k) = (y_1, \dots, y_k)$ for $1 \leq k < r$, the conditional distribution of Y_{k+1} is the GEV distribution righted truncated at y_k . This property can be exploited to generate the r components in a realized GEV_r observation.

The pseudo algorithm to generate a single observation is the following:

- Generate the first value y_1 from the (unconditional) GEV distribution.
- For $i = 2, \dots, r$:
 - Generate y_i from the GEV distribution right truncated by y_{i-1} .

The resulting vector (y_1, \dots, y_r) is a single observation from the GEV_r distribution.

For $\xi \rightarrow 0$, caveat is needed in numerical evaluation. Using function `expm1` for $\exp(1+x)$ for $x \rightarrow 0$ provides much improved accuracy in comparison to a few implementations in existing R packages. For readability, here is a simplified version of the implementation in R package `eva` (Bader and Yan, 2016).

```
## Quantile function of a GEVr(loc, scale, shape)

qgev <- function(p, loc = 0, scale = 1, shape = 0, log.p = FALSE) {

  if (log.p) p <- exp(p)

  if(shape == 0) {

    loc - scale * log(-log(p))

  } else

    loc + scale * expm1(log(-log(p)) * -shape) / shape

}

## Random number generator of GEVr

## Returns a matrix of n rows and r columns, each row a draw from GEVr

rgevr <- function(n, r, loc = 0, scale = 1, shape = 0) {

  umat <- matrix(runif(n * r), n, r)

  if (r > 1) {

    matrix(qgev(t(apply(umat, 1, cumprod))), loc, scale, shape), ncol = r)
```

```

} else {

    qgev(umat, loc, scale, shape)

}

}

```

A.2 Asymptotic Distribution of $T_n^{(r)}(\theta)$

Proof of Theorem 1. Consider a random vector (Y_1, \dots, Y_r) which follows a $\text{GEV}_r(\theta)$ distribution. The following result given by Tawn (1988, pg. 248) will be used:

$$\begin{aligned}
 h(j|\theta, a, b, c) &\equiv E[Z_j^a (1 + \xi Z_j)^{-(\frac{1}{\xi} + b)} \log^c(1 + \xi Z_j)] \\
 &= \frac{(-\xi)^{c-a}}{\Gamma(j)} \sum_{\alpha=0}^a (-1)^\alpha \binom{a}{\alpha} \Gamma^{(c)}(j + b\xi - \alpha\xi + 1)
 \end{aligned} \tag{A.1}$$

where $Z_j = (Y_j - \mu)/\sigma$ and $\Gamma^{(c)}$ is the c th derivative of the gamma function, for $a \in \mathbb{Z}$, $b \in \mathbb{R}$, and $c \in \mathbb{Z}$, such that $(j + b\xi - \alpha\xi + 1) \notin \{0, -1, -2, \dots\}$, $\alpha = 0, 1, \dots, a$.

Assume that $\xi \neq 0$ and $1 + \xi Z_j > 0$ for $j = 1, \dots, r$. The difference in log-likelihoods for a single observation from the $\text{GEV}_r(\theta)$ and $\text{GEV}_{r-1}(\theta)$ distribution, D_{ir} , is given by (2.2) in Section 2.4. Thus, the first moment of D_{ir} is

$$\begin{aligned}
 E[D_{1r}] &= -\log \sigma - h(r|\theta, 0, 0, 0) + h(r-1|\theta, 0, 0, 0) \\
 &\quad - \left(\frac{1}{\xi} + 1 \right) h(r|\theta, 0, -\xi^{-1}, 1)
 \end{aligned}$$

$$= -\log \sigma - 1 + (1 + \xi)\psi(r)$$

where $\psi(x) = \frac{\Gamma^{(1)}(x)}{\Gamma(x)}$.

To prove that the second moment of D_{ir} is finite, note that

$$|D_{1r}| \leq 4 \max \left\{ \left| \log \sigma \right|, \left| (1 + \xi Z_{1r})^{-\frac{1}{\xi}} \right|, \right. \\ \left. \left| (1 + \xi Z_{1r-1})^{-\frac{1}{\xi}} \right|, \left| \left(\frac{1}{\xi} + 1 \right) \log(1 + \xi Z_{1r-1}) \right| \right\},$$

which implies

$$D_{1r}^2 \leq 16 \left(\max \left\{ \left| \log \sigma \right|, \left| (1 + \xi Z_{1r})^{-\frac{1}{\xi}} \right|, \right. \right. \\ \left. \left. \left| (1 + \xi Z_{1r-1})^{-\frac{1}{\xi}} \right|, \left| \left(\frac{1}{\xi} + 1 \right) \log(1 + \xi Z_{1r-1}) \right| \right\} \right)^2.$$

The bound of $E(D_{1r}^2)$ can be established by applying (A.1) to the last three terms in the max operator,

$$E[(1 + \xi Z_{1r})^{-\frac{2}{\xi}}] = h(r|\theta, 0, \xi^{-1}, 0) < \infty,$$

$$E[(1 + \xi Z_{1r-1})^{-\frac{2}{\xi}}] = h(r-1|\theta, 0, \xi^{-1}, 0) < \infty,$$

$$E[\log^2(1 + \xi Z_{1r-1})] = h(r-1|\theta, 0, -\xi^{-1}, 2) < \infty.$$

The desired result then follows from the central limit theorem and Slutsky's theorem.

The case where $\xi = 0$ in Theorem 1 can easily be derived by taking the limit as $\xi \rightarrow 0$ in (2.2) and in (A.1) by the Dominated Convergence Theorem. \square

A.3 Semi-Parametric Bootstrap Resampling in RFA

Described below and borrowed from Heffernan and Tawn (2004) is the iterative procedure used to obtain bootstrapped standard errors for parameters of a regional frequency model in the presence of unspecified spatial dependence.

1. Fit the non-stationary RFA model to the data and obtain parameter estimates.
2. Transform the original GEV distributed data into standard uniform residuals using the estimated parameters from Step 1.
3. Calculate the ranks of the n residuals within each site.
4. Repeat B times, for some large number B :
 - (a) Resample (with replacement) across years from the ranks in Step 3.
 - (b) Generate a new $n \times m$ sample of standard uniform residuals and arrange them (within each site) according to the resampled rankings.¹
 - (c) Transform the new sampled residuals back into GEV margins using the estimated parameters in Step 1.
 - (d) Fit the model again and obtain the estimators.

¹For ties, can use a random assignment process.

Bibliography

An, Y. and M. D. Pandey (2007). The r largest order statistics model for extreme wind speed estimation. *Journal of Wind Engineering and Industrial Aerodynamics* 95(3), 165–182.

Bader, B. and J. Yan (2016). eva: Extreme value analysis with goodness-of-fit testing. R package version 0.2.3.

Balkema, A. A. and L. De Haan (1974). Residual life time at great age. *The Annals of Probability* 2(5), 792–804.

Beirlant, J., P. Vynckier, and J. L. Teugels (1996). Tail index estimation, pareto quantile plots, and regression diagnostics. *Journal of the American Statistical Association* 91(436), 1659–1667.

Benjamini, Y. (2010a). Discovering the false discovery rate. *Journal of the Royal Statistical Society: Series B (Statistical Methodology)* 72(4), 405–416.

Benjamini, Y. (2010b). Simultaneous and selective inference: Current successes and future challenges. *Biometrical Journal* 52(6), 708–721.

Benjamini, Y. and Y. Hochberg (1995). Controlling the false discovery rate: A practical and powerful approach to multiple testing. *Journal of the Royal Statistical Society. Series B* 57(1), 289–300.

Benjamini, Y. and D. Yekutieli (2001). The control of the false discovery rate in multiple testing under dependency. *The Annals of Statistics* 29(4), 1165–1188.

Blanchard, G. and É. Roquain (2009). Adaptive false discovery rate control under independence and dependence. *The Journal of Machine Learning Research* 10, 2837–2871.

Blanchet, J. and M. Lehning (2010). Mapping snow depth return levels: smooth spatial modeling versus station interpolation. *Hydrology and Earth System Sciences* 14(12), 2527–2544.

Buishand, T. (1991). Extreme rainfall estimation by combining data from several sites. *Hydrological Sciences Journal* 36(4), 345–365.

Caeiro, F. and M. I. Gomes (2016). Threshold selection in extreme value analysis. In D. K. Dey and J. Yan (Eds.), *Extreme Value Modeling and Risk Analysis: Methods and Applications*, Chapter 4, pp. 69–82. CRC Press.

- Caires, S. (2009). A comparative simulation study of the annual maxima and the peaks-over-threshold methods. Technical report, SBW-Belastingen: subproject ‘Statistics’. Deltares Report 1200264-002.
- Casella, G. and R. L. Berger (2002). *Statistical Inference* (2 ed.). Duxbury Pacific Grove, CA.
- Chandler, R. E. and S. Bate (2007). Inference for clustered data using the independence loglikelihood. *Biometrika* 94(1), 167–183.
- Cheng, R. C. H. and N. A. K. Amin (1983). Estimating parameters in continuous univariate distributions with a shifted origin. *Journal of the Royal Statistical Society. Series B (Methodological)* 45(3), 394–403.
- Cheng, R. C. H. and M. A. Stephens (1989). A goodness-of-fit test using Moran’s statistic with estimated parameters. *Biometrika* 76(2), 385–392.
- Choulakian, V. and M. Stephens (2001). Goodness-of-fit tests for the generalized Pareto distribution. *Technometrics* 43(4), 478–484.
- Coles, S. (2001). *An Introduction to Statistical Modeling of Extreme Values* (1 ed.). Springer.
- Coles, S. G. and M. J. Dixon (1999). Likelihood-based inference for extreme value models. *Extremes* 2(1), 5–23.
- Danielsson, J., L. de Haan, L. Peng, and C. G. de Vries (2001). Using a bootstrap method to choose the sample fraction in tail index estimation. *Journal of Multivariate Analysis* 76(2), 226–248.
- Davison, A. C., S. Padoan, M. Ribatet, et al. (2012). Statistical modeling of spatial extremes. *Statistical Science* 27(2), 161–186.
- Davison, A. C. and R. L. Smith (1990). Models for exceedances over high thresholds. *Journal of the Royal Statistical Society. Series B (Methodological)* 52(3), 393–442.
- De Haan, L. and A. Ferreira (2007). *Extreme value theory: an introduction*. Springer Science & Business Media.
- Deheuvels, P. (1986). Strong laws for the k th order statistic when $k \leq c \log_2 n$. *Probability Theory and Related Fields* 72(1), 133–154.
- Deheuvels, P. (1989). Strong laws for the k th order statistic when $k \leq c \log_2 n$ (II). In *Extreme Value Theory*, Volume 51, pp. 21–35. Springer.

- Dey, D. K. and J. Yan (2016). *Extreme Value Modeling and Risk Analysis: Methods and Applications*. CRC Press.
- Drees, H., L. De Haan, and S. Resnick (2000). How to make a hill plot. *The Annals of Statistics* 28(1), 254–274.
- DuMouchel, W. H. (1983). Estimating the stable index α in order to measure tail thickness: A critique. *The Annals of Statistics* 11(4), 1019–1031.
- Dupuis, D. (1999). Exceedances over high thresholds: A guide to threshold selection. *Extremes* 1(3), 251–261.
- Dupuis, D. J. (1997). Extreme value theory based on the r largest annual events: A robust approach. *Journal of Hydrology* 200(1), 295–306.
- Dziubdziela, W. (1978). On convergence rates in the limit laws of extreme order statistics. In *Trans. 7th Prague Conference and 1974 European Meeting of Statisticians B*, pp. 119–127.
- El Adlouni, S., T. B. M. J. Ouarda, X. Zhang, R. Roy, and B. Bobée (2007). Generalized maximum likelihood estimators for the nonstationary generalized extreme value model. *Water Resources Research* 43(3), n/a–n/a. W03410.
- Eljabri, S. S. M. (2013). *New Statistical Models for Extreme Values*. Ph. D. thesis, The University of Manchester, Manchester, UK.
- Embrechts, P., C. Klüppelberg, and T. Mikosch (1997). *Modelling Extremal Events*, Volume 33. Springer Science & Business Media.
- Falk, M. (1989). Best attainable rate of joint convergence of extremes. In *Extreme Value Theory*, pp. 1–9. Springer.
- Ferreira, A., L. de Haan, et al. (2015). On the block maxima method in extreme value theory: Pwm estimators. *The Annals of Statistics* 43(1), 276–298.
- Ferreira, A., L. de Haan, and L. Peng (2003). On optimising the estimation of high quantiles of a probability distribution. *Statistics* 37(5), 401–434.
- Ferro, C. A. and J. Segers (2003). Inference for clusters of extreme values. *Journal of the Royal Statistical Society: Series B (Statistical Methodology)* 65(2), 545–556.
- Gilleland, E. (2016). Computing software. In D. K. Dey and J. Yan (Eds.), *Extreme Value Modeling and Risk Analysis: Methods and Applications*, Chapter 25, pp. 505–515. CRC Press.

- Gilleland, E. and R. W. Katz (2011a). New software to analyze how extremes change over time. *Eos* 92(2), 13–14.
- Gilleland, E. and R. W. Katz (2011b). New software to analyze how extremes change over time. *Eos* 92(2), 13–14.
- Gilleland, E., M. Ribatet, and A. G. Stephenson (2013). A software review for extreme value analysis. *Extremes* 16(1), 103–119.
- G'Sell, M. G., S. Wager, A. Chouldechova, and R. Tibshirani (2016). Sequential selection procedures and false discovery rate control. *Journal of the Royal Statistical Society: Series B (Statistical Methodology)* 78(2), 423–444.
- Gudendorf, G. and J. Segers (2010). Extreme-value copulas. In *Copula theory and its applications*, pp. 127–145. Springer.
- Guedes Soares, C. and M. G. Scotto (2004). Application of the r largest-order statistics for long-term predictions of significant wave height. *Coastal Engineering* 51(5), 387–394.
- Hall, P. and S. C. Morton (1993). On the estimation of entropy. *Annals of the Institute of Statistical Mathematics* 45(1), 69–88.
- Hall, P. and I. Weissman (1997). On the estimation of extreme tail probabilities. *The Annals of Statistics* 25(3), 1311–1326.
- Hanel, M., T. A. Buishand, and C. A. T. Ferro (2009). A nonstationary index flood model for precipitation extremes in transient regional climate model simulations. *Journal of Geophysical Research: Atmospheres* 114(D15), n/a–n/a. D15107.
- Harrell, F. E., K. L. Lee, R. M. Califf, D. B. Pryor, and R. A. Rosati (1984). Regression modelling strategies for improved prognostic prediction. *Statistics in medicine* 3(2), 143–152.
- Heffernan, J. E. and H. Southworth (2012). Extreme value modelling of dependent series using r.
- Heffernan, J. E. and A. G. Stephenson (2016). ismev: An introduction to statistical modeling of extreme values. R package version 1.41.
- Heffernan, J. E. and J. A. Tawn (2004). A conditional approach for multivariate extreme values (with discussion). *Journal of the Royal Statistical Society: Series B (Statistical Methodology)* 66(3), 497–546.
- Hill, B. M. (1975). A simple general approach to inference about the tail of a distribution. *The Annals of Statistics* 3(5), 1163–1174.

- Hosking, J. and J. Wallis (1988). The effect of intersite dependence on regional flood frequency analysis. *Water Resources Research* 24(4), 588–600.
- Hosking, J., J. R. Wallis, and E. F. Wood (1985). Estimation of the generalized extreme-value distribution by the method of probability-weighted moments. *Technometrics* 27(3), 251–261.
- Hosking, J. R. M. (1990). L-moments: Analysis and estimation of distributions using linear combinations of order statistics. *Journal of the Royal Statistical Society. Series B (Methodological)* 52(1), 105–124.
- Hosking, J. R. M. and J. R. Wallis (2005). *Regional frequency analysis: an approach based on L-moments*. Cambridge University Press.
- Katz, R. W., M. B. Parlange, and P. Naveau (2002). Statistics of extremes in hydrology. *Advances in Water Resources* 25(8), 1287–1304.
- Khaliq, M., T. Ouarda, J.-C. Ondo, P. Gachon, and B. Bobée (2006). Frequency analysis of a sequence of dependent and/or non-stationary hydro-meteorological observations: A review. *Journal of hydrology* 329(3), 534–552.
- Kharin, V. V., F. Zwiers, X. Zhang, and M. Wehner (2013). Changes in temperature and precipitation extremes in the cmip5 ensemble. *Climatic Change* 119(2), 345–357.
- Kharin, V. V. and F. W. Zwiers (2005). Estimating extremes in transient climate change simulations. *Journal of Climate* 18(8), 1156–1173.
- Kharin, V. V., F. W. Zwiers, X. Zhang, and G. C. Hegerl (2007). Changes in temperature and precipitation extremes in the ipcc ensemble of global coupled model simulations. *Journal of Climate* 20(8), 1419–1444.
- Kjeldsen, T. R., J. Smithers, and R. Schulze (2002). Regional flood frequency analysis in the kwazulu-natal province, south africa, using the index-flood method. *Journal of Hydrology* 255(1), 194–211.
- Kojadinovic, I. and J. Yan (2012). Goodness-of-fit testing based on a weighted bootstrap: A fast large-sample alternative to the parametric bootstrap. *Canadian Journal of Statistics* 40(3), 480–500.
- Kumar, R. and C. Chatterjee (2005). Regional flood frequency analysis using l-moments for north brahmaputra region of india. *Journal of Hydrologic Engineering* 10(1), 1–7.
- Lateltin, O. and C. Bonnard (1999). Hazard assessment and land-use planning in switzerland for snow avalanches, floods and landslides. Technical report, World Meteorological Organization.

- Leadbetter, M. R., G. Lindgren, and H. Rootzén (2012). *Extremes and related properties of random sequences and processes*. Springer Science & Business Media.
- Leclerc, M. and T. B. Ouarda (2007). Non-stationary regional flood frequency analysis at ungauged sites. *Journal of hydrology* 343(3), 254–265.
- López, J. and F. Francés (2013). Non-stationary flood frequency analysis in continental spanish rivers, using climate and reservoir indices as external covariates. *Hydrology and Earth System Sciences Discussions* 17(8), 3103–3142.
- MacDonald, A., C. J. Scarrott, D. Lee, B. Darlow, M. Reale, and G. Russell (2011). A flexible extreme value mixture model. *Computational Statistics & Data Analysis* 55(6), 2137–2157.
- Mächler, M. (2012). Accurately computing $\log(1 - \exp(-a))$ assessed by the rmpfr package.
- Martins, E. S. and J. R. Stedinger (2000). Generalized maximum-likelihood generalized extreme-value quantile estimators for hydrologic data. *Water Resources Research* 36(3), 737–744.
- McNeil, A. J. and T. Saladin (1997). The peaks over thresholds method for estimating high quantiles of loss distributions. In *Proceedings of 28th International ASTIN Colloquium*, pp. 23–43.
- Menéndez, M., F. J. Méndez, C. Izaguirre, A. Luceño, and I. J. Losada (2009). The influence of seasonality on estimating return values of significant wave height. *Coastal Engineering* 56(3), 211–219.
- Menne, M. J., I. Durre, R. S. Vose, B. E. Gleason, and T. G. Houston (2012). An overview of the global historical climatology network-daily database. *Journal of Atmospheric and Oceanic Technology* 29(7), 897–910.
- Mínguez, R., F. Méndez, C. Izaguirre, M. Menéndez, and I. J. Losada (2010). Pseudo-optimal parameter selection of non-stationary generalized extreme value models for environmental variables. *Environmental Modelling & Software* 25(12), 1592–1607.
- Moran, P. A. P. (1953). The random division of an interval-part ii. *Journal of the Royal Statistical Society. Series B (Methodological)* 15(1), 77–80.
- Nadarajah, S. (2005). Extremes of daily rainfall in west central florida. *Climatic change* 69(2-3), 325–342.
- Northrop, P. J. and C. L. Coleman (2014). Improved threshold diagnostic plots for extreme value analyses. *Extremes* 17(2), 289–303.

- Northrop, P. J. and P. Jonathan (2011). Threshold modelling of spatially dependent non-stationary extremes with application to hurricane-induced wave heights. *Environmetrics* 22(7), 799–809.
- Phatak, A., C. Chan, and H. Kiiveri (2010). Fast variable selection for extreme values. In *International Environmental Modelling and Software Society (iEMSs)*.
- Pickands, III, J. (1975). Statistical inference using extreme order statistics. *The Annals of Statistics* 3(1), 119–131.
- Rao, C. R. (2005). Score test: Historical review and recent developments. In N. Balakrishnan, N. Kannan, and H. N. Nagaraja (Eds.), *Advances in Ranking and Selection, Multiple Comparisons, and Reliability*, pp. 3–20. Springer.
- Raoult, J.-P. and R. Worms (2003). Rate of convergence for the generalized pareto approximation of the excesses. *Advances in Applied Probability* 35(4), 1007–1027.
- Renard, B. and M. Lang (2007). Use of a gaussian copula for multivariate extreme value analysis: some case studies in hydrology. *Advances in Water Resources* 30(4), 897–912.
- Ribatet, M. (2009). A users guide to the spatialextremes package.
- Ribatet, M. (2015). Spatialextremes: Modelling spatial extremes. R package version 2.0-2.
- Ribereau, P., A. Guillo, and P. Naveau (2008). Estimating return levels from maxima of non-stationary random sequences using the generalized PWM method. *Nonlinear Processes in Geophysics* 15(6), 1033–1039.
- Roth, M., T. A. Buishand, G. Jongbloed, A. M. G. Klein Tank, and J. H. van Zanten (2012). A regional peaks-over-threshold model in a nonstationary climate. *Water Resources Research* 48(11), n/a–n/a. W11533.
- Scarf, P. A. and P. J. Laycock (1996). Estimation of extremes in corrosion engineering. *Journal of Applied Statistics* 23(6), 621–644.
- Scarrott, C. and A. MacDonald (2012). A review of extreme value threshold estimation and uncertainty quantification. *REVSTAT-Statistical Journal* 10(1), 33–60.
- Schlather, M. (2002). Models for stationary max-stable random fields. *Extremes* 5(1), 33–44.
- Schubert, S. D., Y. Chang, M. J. Suarez, and P. J. Pegion (2008). Enso and wintertime extreme precipitation events over the contiguous united states. *Journal of Climate* 21(1), 22–39.

- Shaffer, J. P. (1995). Multiple hypothesis testing. *Annual Review of Psychology* 46(1), 561–584.
- Shang, H., J. Yan, and X. Zhang (2011). El Niño–Southern Oscillation influence on winter maximum daily precipitation in California in a spatial model. *Water Resources Research* 47, W11507–W11515.
- Shang, H., J. Yan, X. Zhang, et al. (2015). A two-step approach to model precipitation extremes in California based on max-stable and marginal point processes. *The Annals of Applied Statistics* 9(1), 452–473.
- Singh, V. P. (2013). *Entropy Theory and Its Application in Environmental and Water Engineering*. John Wiley & Sons.
- Singo, L. R., P. M. Kundu, J. O. Odiyo, F. I. Mathivha, and T. R. Nkuna (2012). Flood frequency analysis of annual maximum stream flows for Luvuvhu river catchment, Limpopo Province, South Africa. Technical report, University of Venda, Department of Hydrology and Water Resources.
- Smith, R. L. (1985). Maximum likelihood estimation in a class of nonregular cases. *Biometrika* 72(1), 67–90.
- Smith, R. L. (1986). Extreme value theory based on the r largest annual events. *Journal of Hydrology* 86(1), 27–43.
- Smith, R. L. (1990). Max-stable processes and spatial extremes. Unpublished manuscript, University of Surrey.
- Smithers, J. and R. Schulze (2001). A methodology for the estimation of short duration design storms in south africa using a regional approach based on l-moments. *Journal of Hydrology* 241(1), 42–52.
- Southworth, H. and J. E. Heffernan (2013). texmex: Statistical modelling of extreme values. R package version 2.1.
- Stedinger, J. R. (1983). Estimating a regional flood frequency distribution. *Water Resources Research* 19(2), 503–510.
- Tawn, J. A. (1988). An extreme-value theory model for dependent observations. *Journal of Hydrology* 101(1), 227–250.
- Thompson, P., Y. Cai, D. Reeve, and J. Stander (2009). Automated threshold selection methods for extreme wave analysis. *Coastal Engineering* 56(10), 1013–1021.
- Tibshirani, R. (1996). Regression shrinkage and selection via the lasso. *Journal of the Royal Statistical Society. Series B (Methodological)* 58(1), 267–288.

- Tsay, R. S. (2005). *Analysis of Financial Time Series*, Volume 543. John Wiley & Sons.
- Wadsworth, J. L. and J. A. Tawn (2012). Likelihood-based procedures for threshold diagnostics and uncertainty in extreme value modelling. *Journal of the Royal Statistical Society: Series B (Statistical Methodology)* 74(3), 543–567.
- Wang, Z. (2015). Estimating equations for spatial extremes with applications to detection and attribution analysis of changes in climate extremes. <http://digitalcommons.uconn.edu/dissertations/859>.
- Wang, Z., J. Yan, and X. Zhang (2014). Incorporating spatial dependence in regional frequency analysis. *Water resources research* 50(12), 9570–9585.
- Weissman, I. (1978). Estimation of parameters and large quantiles based on the k largest observations. *Journal of the American Statistical Association* 73(364), 812–815.
- Wong, T. S. T. and W. K. Li (2006). A note on the estimation of extreme value distributions using maximum product of spacings. In *Time Series and Related Topics*, pp. 272–283. Institute of Mathematical Statistics.
- Wuertz, D. (2013). fextremes: Rmetrics - extreme financial market data. R package version 3010.81.
- Zhang, X., J. Wang, F. W. Zwiers, and P. Y. Groisman (2010). The influence of large-scale climate variability on winter maximum daily precipitation over north america. *Journal of Climate* 23(11), 2902–2915.
- Zhao, X., C. J. Scarrott, L. Oxley, and M. Reale (2011). GARCH dependence in extreme value models with Bayesian inference. *Mathematics and Computers in Simulation* 81(7), 1430–1440.